Dissertationes Forestales 272

Improving capacity for large-area monitoring of forest disturbance and recovery

Joanne C. White
Department of Forest Sciences
Faculty of Agriculture and Forestry
University of Helsinki

Academic dissertation

To be presented with the permission of the Faculty of Agriculture and Forestry, University of Helsinki, for public criticism in Auditorium XIII of the Main building, Unioninkatu 34, 3rd floor, Helsinki on 31 May, 2019 at 12 o'clock noon.

Title of dissertation: Improving capacity for large-area monitoring of forest disturbance and recovery

Author: Joanne C. White

Dissertationes Forestales 272

https://doi.org/10.14214/df.272

Thesis supervisors:
Professor Markus Holopainen
Department of Forest Sciences, University of Helsinki, Finland

Professor Juha Hyyppä
Finnish Geospatial Research Institute, National Land Survey of Finland, Finland

Associate Professor Mikko Vastaranta
School of Forest Sciences, University of Eastern Finland, Finland

Dr. Michael Wulder, Senior Research Scientist
Natural Resources Canada, Canadian Forest Service, Pacific Forestry Centre, Canada

Pre-examiners:
Professor Håkan Olsson
Department of Forest Resource Management, Swedish University of Agriculture Sciences, Sweden

Associate Professor Miina Rautiainen
Department of the Built Environment, School of Engineering, Aalto University, Finland

Opponent:
Professor Barbara Koch
Department of Remote Sensing and Landscape Information Systems, Albert-Ludwigs-Universität Freiburg, Germany

ISSN 1795-7389 (online)
ISBN 978-951-651-634-2 (pdf)
ISSN 2323-9220 (print)
ISBN 978-951-651-635-9 (paperback)

Publishers:
Finnish Society of Forest Science
Faculty of Agriculture and Forestry at the University of Helsinki
School of Forest Sciences at the University of Eastern Finland

Editorial Office:
Finnish Society of Forest Science, Dissertationes Forestales
Viikinkaari 6, 00790 Helsinki
http://www.dissertationesforestales.fi

White, J.C. (2019). Improving capacity for large-area monitoring of forest disturbance and recovery. Dissertation Forestales 272. 79 p. https://doi.org/10.14214/df.272

ABSTRACT

Information needs associated with forest monitoring have become increasingly complex. Data to support these information needs are required to be systematically generated, spatially exhaustive, spatially explicit, and to capture changes at a spatial and temporal resolution that is commensurate with both natural and anthropogenic impacts. Moreover, reporting obligations impose additional expectations of transparency, repeatability, and data provenance. The overall objective of this dissertation was to address these needs and improve capacity for large-area monitoring of forest disturbance and subsequent recovery. Landsat time series (LTS) enhance opportunities for forest monitoring, particularly for post-disturbance recovery assessments, while best-available pixel (BAP) compositing approaches allow LTS approaches to be applied over large forest extents. In substudies I and IV, forest monitoring information needs were identified and linked to image compositing criteria and data availability in Canada and Finland. In substudy II, methods were developed and demonstrated for generating large-area, gap-filled Landsat BAP image composites that preserve detected changes, generate continuous change metrics, and provide foundational, annual data to support forest monitoring. In substudy III a national monitoring framework was prototyped at scale over the 650 Mha of Canada's forest ecosystems, providing a detailed analysis of areas disturbed by wildfire and harvest for a 25-year period (1985–2010), as well as characterizing short- and long-term recovery. New insights on spectral recovery metrics were provided by substudies V and VI. In substudies V, the utility of spectral measures of recovery were evaluated and confirmed against benchmarks of forest cover and height derived from airborne laser scanning data. In substudy VI the influence of field-measured structure and composition on spectral recovery were examined and quantified. By focusing on four key aspects of forest monitoring systems: information needs, data availability, methods development, and information outcomes, the component studies demonstrated that combining BAP compositing and LTS analysis approaches provides data with the requisite characteristics to support large-area forest monitoring, while also enabling a more comprehensive assessment of forest disturbance and recovery.

Keywords: Landsat, time series, image compositing, change detection, airborne laser scanning, remote sensing

ACKNOWLEDGEMENTS

At its best, science is a collaboration of many diverse and talented individuals and this dissertation is no exception. A sincere thank you to my supervisor Professor Markus Holopainen for this opportunity and to all the members of my supervising committee: Professors Juha Hyppä and Mikko Vastaranta, and Dr. Mike Wulder. Collectively, this supervisory group has a considerable breadth and depth of expertise in remote sensing science and I appreciate their knowledge, support, and encouragement. I have been extremely fortunate in my scientific career to have Dr. Mike Wulder as my mentor, and I am very grateful to him for always being so generous with his time, insights, inspiration, and advice. From Mike I have learned the value of focused scientific inquiry, strong collaborations, and the importance of understanding information needs. Special thanks to Drs. Ninni Saarinen and Mikko Vastaranta for their invaluable assistance, friendship, and tutoring in all things Finnish. Their frequent sojourns at the Pacific Forestry Centre in Victoria were very welcome and kept our collaborations strong, productive, and fun. Thank you Ninni for your invaluable assistance with all the details of the final stages of this process, which are a challenge to tackle from afar. Thank you to all my co-authors for their contributions and collaborations, with special mention to Professor Nicholas Coops, Dr. Txomin Hermosilla, and Geordie Hobart who, along with Mike Wulder, collectively made the NTEMS project a success. Professors Håkan Olsson and Miina Rautiainen reviewed this dissertation and I thank them for their valuable comments and suggestions for improvements. Thank you to Professor Barbara Koch for accepting the invitation to act as the Opponent at my defense. I am also grateful to my employer, the Canadian Forest Service, who supported me in the pursuit of this opportunity, and to the Canadian Space Agency and Academy of Finland, who provided funding for various elements of the research included herein. To my parents, Robert and Viola, my sister Patricia, and my partner John: a very special thank you for all the numerous ways that you have supported and encouraged me. Last but not least, the greatest thanks of all go to Jane for her unlimited supply of hugs and artwork: thank you for bringing so much joy into my life! Jane, I dedicate this work to you and to my mother, Viola. *Femina fortitudinis*!

LIST OF ORIGINAL ARTICLES

This dissertation consists of an introductory review followed by six research articles. Articles I–VI are reprinted with kind permission of the publishers.

I. White, J.C., Wulder, M.A., Hobart, G,W., Luther, J.E., Hermosilla, T., Griffiths, P., Coops, N.C., Hall, R.J., Hostert, P., Dyk, A., Guindon. L. (2014). Pixel-based image compositing for large-area dense time series applications and science. Canadian Journal of Remote Sensing, 40(3): 192-212. https://doi.org/10.1080/07038992.2014.945827

II. Hermosilla, T., Wulder, M.A., White, J. C., Coops, N.C., Hobart, G.W. (2015). An integrated Landsat time series protocol for change detection and generation of annual gap-free surface reflectance composites. Remote Sensing of Environment, 158: 220-234. https://doi.org/10.1016/j.rse.2014.11.005

III. White, J.C., Wulder, M.A., Hermosilla, T., Coops, N.C., Hobart, G.W. (2017). A nationwide annual characterization of 25 years of forest disturbance and recovery for Canada using Landsat time series. Remote Sensing of Environment, 194: 303-321. https://doi.org/10.1016/j.rse.2017.03.035

IV. Saarinen, N., White, J.C., Wulder, M.A., Kangas, A., Tuominen, S., Kankare, V., Holopainen, M., Hyyppä, J., Vastaranta, M. 2018. Landsat archive holdings for Finland: Opportunities for forest monitoring. Silva Fennica, 52(3): id9986. https://doi.org/10.14214/sf.9986

V. White, J.C., Saarinen, N., Kankare, V., Wulder, M.A., Hermosilla, T., Coops, N.C., Pickell, P.D., Holopainen, M., Hyyppä, J., Vastaranta, M. (2018). Confirmation of post-harvest spectral recovery from Landsat time series using measures of forest cover and height derived from airborne laser scanning data. Remote Sensing of Environment, 216: 262–275. https://doi.org/10.1016/j.rse.2018.07.004

VI. White, J.C., Saarinen, N., Wulder, M.A., Kankare, V., Hermosilla, T., Coops, N.C., Holopainen, M., Hyyppä, J., Vastaranta, M. (2019). Assessing spectral measures of post-harvest forest recovery with field plot data. International Journal of Applied Earth Observations and Geoinformation, 80:102–114. https://doi.org/10.1016/j.jag.2019.04.010

AUTHOR CONTRIBUTION

Joanne White was the primary author of articles I, III, V, and VI and was responsible for the main parts of the research design, analyses, and validation, as well as being corresponding author and leading the review process. In article I, Joanne White identified

key information needs and sought input from all co-authors for the articulation of image compositing approaches. In article II, Joanne White contributed to the study design, methods development, analyses, validation, and writing. In article III, Txomin Hermosilla and Geordie Hobart processed the Landsat data. In article IV, Ninni Saarinen and Joanne White processed and analysed the Landsat metadata. In article V, Ville Kankare processed the ALS data, Ninni Saarinen compiled the ancillary geospatial data, and Txomin Hermosilla and Geordie Hobart processed the Landsat data. Ninni Saarinen compiled the field plot data used in article VI. Joanne White analyzed the spectral recovery metrics and derived the ALS benchmarks and field plot attributes used in articles V and VI for recovery assessment. All articles were improved by contributions of the co-authors at various stages of the analysis, writing, and review processes.

TABLE OF CONTENTS

ABBREVIATIONS

ALS Airborne Laser Scanning
ARD Analysis Ready Data
AVHRR Advanced Very High Resolution Radiometer
BAP Best Available Pixel
C2C Composite to Change
CNFDB Canadian National Fire Database
CV Coefficient of Variation
DOS Dark Object Subtraction
DOY Day of Year
EROS Earth Resources Observation and Science
ESPA EROS Science Processing Architecture
ETM+ Enhanced Thematic Mapper Plus
FAO Food and Agriculture Organization
GIS Geographic Information System
L1T Level-1 Terrain Corrected
LaSRC Landsat Surface Reflectance Code
LEDAPS Landsat Ecosystem Disturbance Adaptive Processing System
LGAC Landsat Global Archive Consolidation
LiDAR Light Detection and Ranging
LTS Landsat Time Series
MMU Minimum Mapping Unit
MODIS Moderate Resolution Imaging Spectrometer
MS-NFI Multi-Source National Forest Inventory
MSS Multispectral Scanner
NBR Normalized Burn Ratio
NDVI Normalized Difference Vegetation Index
NFD National Forestry Database
NFI National Forest Inventory
NIR Near Infrared
OLI Orbital Land Imager
RI Recovery Indicator
RMSE Root Mean Square Error
SPOT System Pour Observation de la Terre
SWAB Sliding Window and Bottom-Up
SWIR Shortwave Infrared
TCG Tasselled Cap Greenness
TM Thematic Mapper
TOA Top of Atmosphere
USGS United States Geological Survey
WRS Worldwide Referencing System
Y2R Years to Recovery

INTRODUCTION

Background

The information needs associated with improving the spatial and temporal characterization of forests range across spatial scales, and must address increasing demands on the forest resource for economic, ecological, cultural, and recreational benefit (Corona 2016). Data to support these information needs must be timely, consistent, and spatially exhaustive, and moreover, must be generated in a manner that is transparent and scientifically robust (Pelletier and Goetz 2015). For some jurisdictions, the need to maintain chain of custody information for regulatory or reporting purposes influences how the data is stored and processed (Lewis et al. 2017). In this context, remotely sensed data, available in a range of forms and spatial resolutions, can provide a cost-effective means to improve the characterization and monitoring of forest ecosystems, particularly over very large areas (Banskota et al. 2014; Hirschmugl et al. 2017).

Forest monitoring information needs

Forest disturbance and recovery are important ecological processes that strongly impact regional and global forest carbon budgets (Pan et al. 2010; Hicke et al. 2012). Climate change is anticipated to alter the frequency and intensity of disturbances (Dale et al. 2001), as well as the rate and efficacy of forest regrowth following disturbance (Anderson-Teixeira et al. 2013). Moreover, an increased use in forest biomass to offset the carbon consequences of fossil fuels, may result in shorter harvest rotations and increased harvest levels (Kuuluvainen and Gauthier 2018). In this context, baseline information that characterizes historic trends in forest disturbance and recovery over large areas can be valuable reference information for understanding present and future forest dynamics (Cohen et al. 2016). Time series of remotely sensed data, especially Landsat data, offer opportunities to generate such baseline information on forest disturbance and recovery trends over regions (Kennedy et al. 2012; Griffiths et al. 2014; Potapov et al. 2015), continents (Masek et al. 2008; Lehmann et al. 2012), and the globe (Hansen et al. 2013).

Forest monitoring is particularly challenging in Canada, which has a large forested area, representing approximately 10% of global forests, but much of which is difficult to access (Meijer et al. 2018). Moreover, forest management responsibility is vested primarily with multiple provincial and territorial governments, each with their own standards and systems for forest information (Wulder et al. 2007a). In this context, consistent, nationally synoptic baseline information on forest dynamics is critical. In nations such as Finland, where intensive forest management practices and private forest land ownership prevail (Natural Resources Institute Finland 2017), the capacity for synoptic, spatially-explicit monitoring of forest disturbance and recovery through time, particularly in the context of a complex land use mosaic, is of interest to resource managers and planners (Culotta et al. 2015). Canada has an estimated 347 Mha of forest land, with 226 Mha of managed forest (Natural Resources Canada 2018). By comparison, Finland has 22.8 Mha of forest (Natural Resources Institute Finland 2017), and forest access is not a limiting factor to the establishment of field plots, where the road density (23.3 km/100km^2) is almost double that of Canada (14.1 km/100 km^2; Meijer et al. 2018). In Finland, the National Forest Inventory (NFI) measures more than 10,000 field plots annually (Tomppo et al. 2008a), whereas in

Canada, the NFI measures ~1150 field plots over a 10-year measurement cycle (Gillis et al. 2005).

In the last decade, remote sensing has come to the forefront as a valuable source of information that is well suited to the disparate forest management contexts and information needs of different nations (Banskota et al. 2014). Remotely sensed data is used for 70% of the areas under National Forest Inventories globally (MacDicken et al. 2015). In Canada, national forest monitoring data are needed to support a range of science and program information needs, policy development, and to fulfill national (Natural Resources Canada 2018) and international reporting obligations associated with various international treaties and conventions (Wulder et al. 2004). Ideally, these data should be both spatially exhaustive and spatially explicit, and should enable the assessment of trends over time, as well as characterization of non-timber resources (Gillis 2001). Canada's National Forest Inventory (NFI) program and Carbon Accounting programs are the two most significant stakeholders for this information, particularly for Canada's northern forest areas where there is currently the greatest paucity of forest information (Wulder et al. 2004; Falkowski et al. 2009). Table 1 provides a listing of those core forest attributes that are fundamental to the programmatic information needs of Canada's NFI and Carbon Accounting programs (Gillis et al. 2005; Wulder et al. 2004; Kurz et al. 2009). Some of the attributes presented in Table 1 are readily obtained from remotely sensed data (e.g. land cover, crown closure, and disturbance related attributes), while for others, remotely sensed data can be used to generate a proxy for the attribute of interest (i.e. time since disturbance as a proxy for age (Helmer et al. 2010)). With the aid of an appropriate source of calibration data such as airborne laser scanning (ALS) data, some of the attributes in Table 1, such as volume and biomass can be modeled (e.g. Wulder et al. 2012; Matasci et al. 2018a; 2018b). Of all the attributes listed in Table 1, tree species remains the most difficult to determine reliably over large areas, particularly when using medium resolution remotely sensed data such as Landsat (e.g. van Aardt and Wynne 2001; Thompson et al. 2016), although forest types (e.g., coniferous, deciduous) can be reliably mapped (Wulder et al. 2007b).

Finland is also a signatory to many of the same international treaties and conventions as Canada, and similar to Canada, Finland generates a national annual summary of forest statistics (Natural Resources Institute Finland 2017). The Finnish NFI was established in the 1920s (Tomppo et al. 2010; Kangas et al. 2018) and is based on the statistical sampling of field measurements of standard forest inventory attributes, as well as indicators of forest health and biodiversity.

Table 1. Key attributes for Canada's National Forest Inventory and Carbon Accounting programs

Basic attributes	**Disturbance-related attributes**
Land cover	Pre-disturbance land cover
Crown closure	Post-disturbance land cover
Age	Disturbance agent
Tree species	Disturbance year
Height	Disturbance extent
Volume	Disturbance intensity
Biomass	

National and regional-level strategic forest-planning scenarios for timber procurement, harvests, and silvicultural treatments utilize information from the NFI (e.g. Maltamo et al. 2009; Turtianen et al. 2016; Miina et al. 2018). Likewise, forest carbon budgets and assessments of sustainable forest management practices rely on data from the Finnish NFI (e.g. Härkönen et al. 2011; Majasalmi et al. 2018).

As noted previously, more than 10,000 plots are acquired annually to support the NFI in Finland (Tomppo et al. 2008a). That amounts to ~60,000 plots for a typical NFI 5-year cycle in Finland. The plot density at the national and regional level (i.e. regions > 300,000 ha) is sufficiently high that sampling errors are acceptably low for key variables such as area of land class and volume of growing stock (Tomppo et al. 2013). The size of Finnish forest units (Public Service Units) typically ranges from 800,000 ha to 5 Mha, but these units are divided into smaller sub-areas (referred to as forest management units) for forest planning purposes. Note that operational forest management in Finland is conducted on a much smaller unit, with the average size of forest holdings estimated to be 30 ha (Natural Resources Institute of Finland 2017). Information on the extent and status of the forest resource is required for these smaller units as well; however, the plot density in these smaller units is not sufficient to maintain a low sampling error. Moreover, in the 1980s and 1990s in Finland, there was an increase in forest harvesting, which, combined with changing forest practices and increase in other land uses, created a need for more localized and timely information.

Given this context, in 1989 the multisource-NFI (MS-NFI) was established in Finland as a means to provide estimates of forest characteristics for the areas between the network of established NFI field plots, with the goal of providing estimates for smaller areas than are currently possible based on the field plot data alone (Tomppo et al. 2008b). The MS-NFI uses Landsat data, as well as Sentinel-2 and SPOT data to generate spatially-explicit thematic maps and municipal-level forest statistics. While NFI and MS-NFI estimates are similar at the regional level, prediction error at the individual pixel level is relatively high (Tomppo et al. 2014; Tuominen et al. 2017). Methods for generating the MS-NFI have evolved over time, and the methods used to generate the MS-NFI are under continuous development (Tomppo et al. 2008a). The first national MS-NFI results were published in 1998 (Tomppo et al. 1998), and subsequently in 2006 (Tomppo et al. 2008a), 2009, 2011, 2013, and 2015. As a result of the methodological evolution of the MS-NFI, comparability between MS-NFI output maps generated for different years at a pixel or stand level over time can be challenging.

Forest disturbance and recovery

Combined, disturbance and recovery processes inform forest stand dynamics and influence changes in forest structure over time (Oliver and Larson 1996). Historically, remote sensing science has focused primarily on characterizing forest disturbance, largely because disturbance detection is an application that is well suited to the synoptic nature of remotely sensed data (Coops et al. 2007; Frolking et al. 2009), and because disturbances, particularly stand-replacing disturbances—which are typically spatially and temporally discrete—are readily detected with remotely sensed data (Lu et al. 2004). The opening of the Landsat archive in 2008 (Woodcock et al. 2008) greatly enhanced disturbance detection capacity (Zhu and Woodcock 2014), and renewed interest in the characterization of forest recovery post-disturbance (Banskota et al. 2014). In order to understand forest dynamics, both

disturbance and recovery processes must be characterized and Landsat time series (LTS) data make this possible (White et al. 2011; Gómez et al. 2012; Pflugmacher et al. 2014).

Definitions of forest recovery post-disturbance are not universal (Bartels et al. 2016) and often relate to the return of forest structural characteristics following a particular disturbance type (Frolking et al. 2009), ranging from the initial re-establishment of vegetation to the full return of pre-disturbance forest structure. In reality, forest recovery is a process and not a state; the structure, composition, and function of forests manifest gradually through successional processes that occur following disturbance (Oliver and Larson 1996; Spake et al. 2015). Timing of the various stand development stages and recovery phases post-disturbance (Figure 1) is variable and depends on many factors, including disturbance type and site characteristics. The point in time at which forest recovery is achieved relates to its definition and often depends on whether the information need is related to reclamation (Audet et al. 2014), silviculture (Fagg et al. 2013), carbon (Urbano and Keeton 2017), or ecosystem goods and services (Thompson et al. 2013), among others. Indicators of forest recovery can therefore be compositional, functional, structural, or combinations thereof (Gatica-Saavedra et al. 2017; Chazdon et al. 2016).

In contrast to disturbances, recovery is more of a continuous process, and as such, is particularly well suited to time series analyses (Kennedy et al. 2010). The potential capacity of LTS data to monitor post-disturbance recovery was established some twenty years ago (e.g. Viedma et al. 1997; Lawrence and Ripple 1999); however implementation over large areas was constrained by issues related to both data availability and cost, as well as computational power. Today, the use of LTS data to assess post-disturbance recovery has been greatly facilitated by free and open access to the Landsat archive, as well as by significant advances in computational capacity (Banskota et al. 2014). These factors have enabled assessments of recovery at a spatial resolution that is meaningful for forest monitoring (Kennedy et al. 2014).

Spectral recovery, as measured using a time series of optical satellite data, is not a direct measure of forest recovery (Kennedy et al. 2010; 2012; Griffiths et al. 2014) and must therefore be interpreted within the context of *a priori* expectations of recovery, which are typically derived from ground measurements (Bartels et al. 2016) or ALS data (Magnussen and Wulder 2012; Slesak and Kaebisch 2016). With some rare exceptions (e.g. Hérault et al. 2018), ground-based studies of post-disturbance recovery are typically limited by sample size, and spatial and temporal extent (Bartels et al. 2016), precluding a more comprehensive analysis of recovery across a range of site types, forest types, and disturbance magnitudes. Field plot measurements that are typically used to assess recovery include various structural attributes such as basal area (Bartels et al. 2016), stocking density (Johnstone and Chapin 2006), and combinations of canopy cover and height (Hansen et al. 2013; Chazdon et al. 2016), among others.

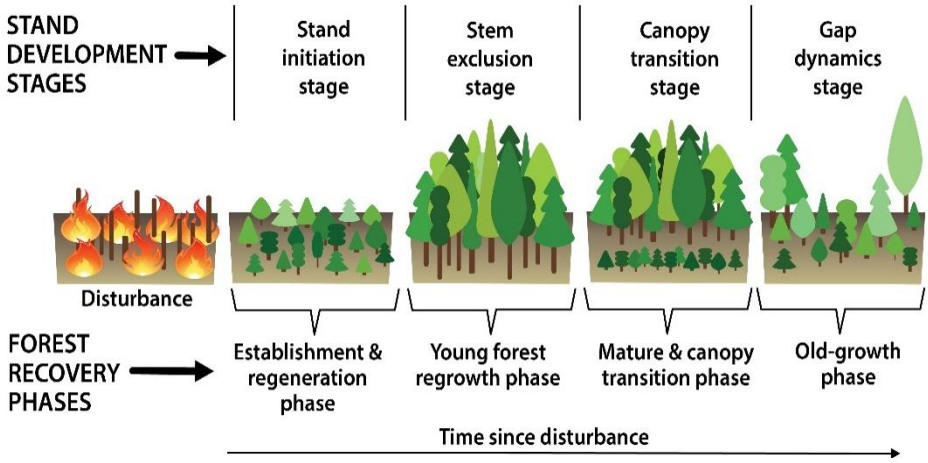

Figure 1. Schematic diagram of the stages of stand development post-disturbance and associated forest recovery phases (adapted from Oliver and Larson, 1996). Stand structure and species composition are known to vary by disturbance type, dominant species, and site conditions.

The Landsat archive has enabled assessments of recovery that are spatially exhaustive and retrospective—providing important baseline data for forest monitoring in an era of climate change. LTS-derived measures of spectral recovery have demonstrated utility for understanding regional (Schroeder et al. 2007; Kennedy et al. 2012), temporal (Frazier et al. 2018), and agent-based (Madoui et al. 2015) variations in forest recovery over large areas. These remotely-sensed assessments can augment ground-based surveys, providing improved understanding of variations in forest return following disturbance (Frolking et al. 2009); however, the linkages between spectral measures of recovery and manifestations of forest structure have not been well understood (Schroeder et al. 2011). Previous studies characterizing national trends in disturbance and recovery in Canada have either focused on wildfire exclusively, using substantially coarser spatial resolution remotely sensed data (i.e., Advanced Very High Resolution Radiometer or AVHRR 1- and 8–km data) (Amiro et al. 2000, Hicke et al. 2003, Goetz et al. 2006), or have been sample-based (Frazier et al. 2015; Pickell et al. 2016). Moreover, previous studies that have used Landsat time series data to characterize annual trends in disturbance and recovery have not distinguished trends by disturbance type (Kennedy et al. 2012, Griffiths et al. 2014).

Vegetation indices and derivatives are the most common methods for assessing post-disturbance recovery with remotely sensed data (Chu and Guo 2014). The Normalized Difference Vegetation Index (NDVI) has been used extensively to evaluate post-fire recovery (e.g., Gitas et al. 2012; Veraverbeke et al. 2012a and 2012b; Vila and Barbosa 2010). Pickell et al. (2016) characterized the relative strengths of commonly used vegetation indices including NDVI, Normalized Burn Ratio (NBR), Tasseled Cap Greenness (TCG), and the shortwave-infrared band (SWIR; Landsat TM/ETM+ band 5). Research on spectral measures of forest recovery have emphasized the use of multiple metrics to provide a comprehensive assessment of recovery (Pickell et al. 2016; Chu et al. 2016), as different metrics characterize different phases of the recovery process (Figure 1). For example, although NDVI and TCG can characterize the initial pulse of vegetation that establishes at a site post-disturbance, these indices also saturate rapidly, and are therefore

less informative on the longer-term return of forest vegetation at a site. (e.g., Buma 2012; Chu et al. 2016). Indices such as NBR, which incorporate the SWIR wavelength, can inform on forest structure (Horler and Ahern 1986; Cohen and Goward 2004) and provide an indication of the longer-term increase in forest structural complexity that is commonly associated with forest regeneration (Frazier et al. 2015; Ireland and Petropolous 2015).

Spectral changes in forests during and following disturbance

The detectability of forest disturbance and subsequent recovery is enabled by changes in the presence, composition, and structure of vegetation, which in turn, influence spectral reflectance properties. The capacity to characterize the spectral properties of forests has advanced markedly, although gaps remain in terms of in situ measurements in the SWIR wavelengths (Rautiainen et al. 2018). While stand-replacing fire and harvest both result in a significant removal of biomass, the magnitude and impacts of these two disturbances and subsequent recovery processes differ (Schroeder et al. 2011). While harvest methods and subsequent regeneration practices are somewhat consistent, particularly in Nordic countries, the impacts of fires are much more variable. Generally, exposed soil will have higher reflectance than vegetation in the visible and SWIR wavelengths, whereas vegetation will have higher reflectance than soil in the NIR (Nilson and Peterson, 1994). Vegetation indices are often designed to take advantage of the different spectral responses of vegetation at different wavelengths (Bannari et al. 1995), and the Normalized Burn Ratio, used extensively in this thesis, measures differences in vegetation response in the SWIR and NIR wavelengths (Key and Benson 1999, 2006). Vegetation moisture will absorb energy in the SWIR wavelengths, resulting in low reflectance in the SWIR for vegetation (White et al. 1996), whereas exposed soil will have higher reflectance in the SWIR (Escuin et al. 2008). Conversely, vegetation has higher reflectance in the NIR than exposed soil. Prior to disturbance, forest canopy will have high reflectance in the NIR and low reflectance in the SWIR. Immediately following disturbance, disturbed areas will have low reflectance in the NIR and high reflectance in the SWIR (Figure 2).

During clearcut harvest most of trees and other vegetation are removed from a site, exposing soil and woody debris. As a result, immediately following harvest, there is a marked increase in reflectance in the visible and SWIR wavelengths and a decrease in NIR reflectance (Horler and Ahern, 1986, Nilson and Peterson, 1994). Over time as green vegetation re-establishes at the site, there will be a gradual decrease in reflectance in the visible wavelengths (particularly in the blue and red wavelengths, which have greater chlorophyll absorption). Reflectance in NIR will increase over time with increasing tree cover. Conversely, reflectance in the SWIR will decrease over time (Horler and Ahern 1986); however, the magnitude of the decrease in SWIR reflectance relative to the variability in spectral response is greatest in this spectral region (i.e. high signal to noise). Horler and Ahern (1986) posited that this characteristic of the SWIR, combined with the fact that SWIR wavelengths are less impacted by atmospheric noise, indicates the potential of the SWIR as a particularly good region for monitoring forest regeneration. Cohen et al. (2018) published a Disturbance Signal to Noise Ratio (DSNR) metric. The NIR band had

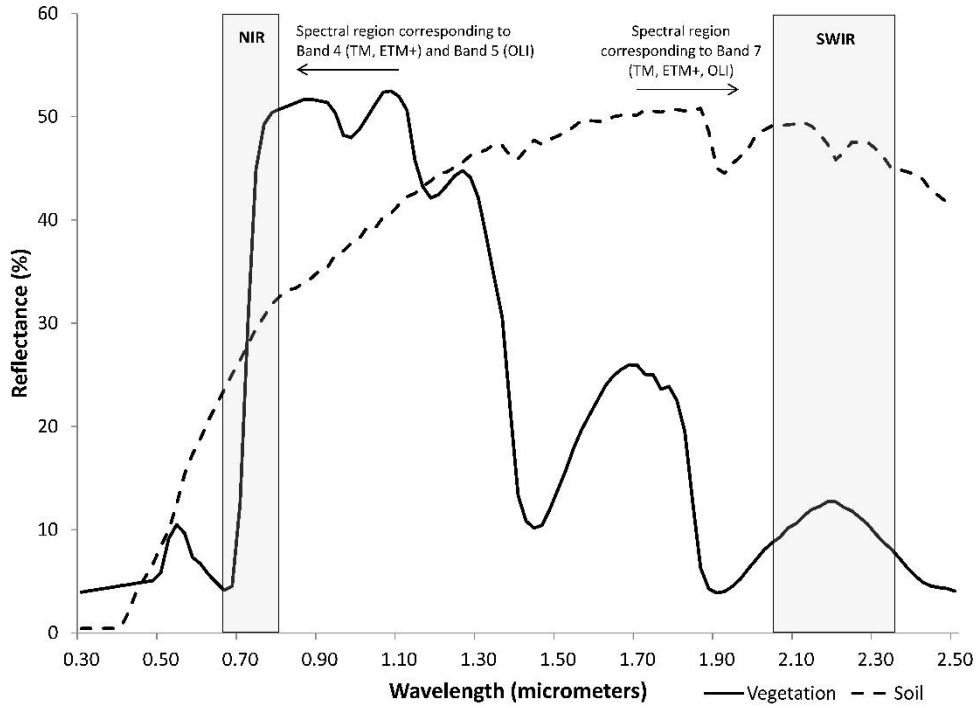

Figure 2. Spectral profiles of vegetation and soil with the near infrared (NIR) and shortwave infrared (SWIR) regions associated with the Landsat bands used in the calculation of the Normalized Burn Ratio (NBR).

the lowest median DSNR value, while SWIR and SWIR-based indices had the highest median DSNR. Of all the spectral indices tested, NBR was found to have the highest median DSNR.

Peterson (1992) acquired in situ spectral measurements in an area of boreal forest in Estonia, similar to the forests of southern Finland analyzed in Studies V and VI. Plots were established in 16 clearcut areas in 1986 prior to the start of the growing season, with the initial conditions dominated by bare soil with some woody debris. Measures were recorded annually for five years post-harvest in the visible and near-infrared wavelengths. Using the Greenness and Brightness indices of Kauth and Thomas (1976), Peterson (1992) described the successional reflectance dynamics in boreal forest communities following clearcutting, identifying two stages of spectral development. The first stage of successional reflectance was characterized by a rapid increase in seasonal greenness associated with a concomitant increase in vegetative cover, primarily from fast growing herbaceous species. Peterson (1992) noted that this effect was more pronounced on sites colonized by vegetation species that were previously light limited under canopy, or when a site was dominated by species of a similar architecture and complete or near-complete ground cover was attained in the first summer following harvest. Under these conditions with relatively uniform vegetation cover, the amount of shadowing was minimal, and therefore maximum seasonal greenness could be achieved within the first growing season post-harvest on more fertile mesic sites,

whereas there was a delay in maximum greenness for less fertile sites. The second stage of successional reflectance is associated with a decrease in seasonal maximum greenness in subsequent years, which results from an increase in shadows as a function of increasing structural complexity in the stand. This decrease in seasonal maximum greenness was found to be correlated with time since disturbance. Moreover, as succession progressed, there was increasing contrast between the visible and near-infrared wavelengths (Peterson 1992)

Image compositing

Pixel-based image compositing approaches were first implemented with low spatial resolution (i.e. > 500m^2) data, including the Advanced Very High Resolution Radiometer (AVHRR; Holben 1986; Cihlar et al. 1994) and MODerate-resolution Imaging Spectrometer (MODIS) (Roy 2000; Justice et al. 2002; Ju et al. 2010), both of which are free and open and provide daily or near-daily global coverage. With abundant observations, compositing approaches using these data have typically used a single characteristic or rule, such as the maximum NDVI or minimum view angle, in order to select the best observation for a given pixel within a specified compositing period (e.g. 16 days) (Wolfe et al. 1998). Landsat compositing approaches have benefitted from experiences gained in methods development for compositing with AVHRR and MODIS data (Roy et al. 2010). Prior to free and open access to the USGS Landsat archive in 2008, cost precluded the application of data-intensive, large-area compositing approaches to Landsat data. Moreover, before the advent of the Landsat Global Acquisition Consolidation (LGAC) project, many areas of the globe would not have had a sufficient density of Landsat observations to support annual, growing-season composites (Wulder et al. 2016).

An early precursor to Landsat image composites were the epochal global Landsat datasets that were generated for the Global Land Survey (GLS) project (Townshend et al. 2012, Gutman et al 2013), which made use of the best single-date image for each Landsat path/row (Tucker et al. 2004). Given the limited availability of cloud-free Landsat data in some areas of the globe, epochal composites have been used extensively to support change detection studies (e.g., Hansen et al. 2008; Potapov et al. 2011). Lindquist et al. (2008) evaluated the potential of the epochal 2000 and 2005 GLS datasets, relative to more data intensive per-pixel compositing approaches (e.g. Hansen et al. 2008), for mapping forest cover change in the tropics. The authors concluded that in order to provide sufficient spatial coverage to support change detection between epochs, Landsat-based image compositing approaches should make use of all available Landsat data for any given path/row. In a similar study, Broich et al. (2011) generated epochal Landsat composites for 2000 and 2005 over Sumatra and Kalimantan, Indonesia and assessed the efficacy of these composites for quantifying forest cover change. The authors found that a time series approach that used "all good land observations" provided more accurate estimates of forest cover change when compared to change maps generated from the epochal composites. For most of the globe, Landsat does not provide data density that is analogous to that of coarser resolution sensors such as MODIS and AVHRR. This low data density combined with the data gaps present in ETM+ data after SLC-off failure therefore require more complex rule-sets for composite generation.

Since the opening of the Landsat archive in 2008, several Landsat compositing approaches have emerged in the literature. Many of the approaches have relied exclusively on Landsat Enhanced Thematic Mapper (ETM**+** data) corrected to TOA reflectance (Roy et al. 2010; Potapov et al. 2011; 2012). The per-pixel compositing approach applied by

Hansen et al. (2008) that was later adapted by Potapov et al. (2011), relies on a MODIS-generated forest/non-forest mask to support radiometric normalization via a dark object subtraction (DOS) method (Chavez 1988). Potapov et al. (2012) further refined this approach, using a 10-year MODIS surface reflectance composite to facilitate band-wise mean bias adjustments with corresponding Landsat bands. For very large areas, the use of coarser spatial resolution data for normalization both increases computational overhead and imposes temporal limitations related to the operational lifetime of a given satellite or sensor (i.e. precludes applicability to the pre-MODIS era in this case) (e.g. Hansen et al. 2013).

Data from TM and ETM+ have been combined via compositing approaches that use data corrected to surface reflectance (Flood 2013; Griffiths et al. 2013) via the Landsat Ecosystem Disturbance Adaptive Processing System (LEDAPS) (Masek et al. 2006; Feng et al. 2013). More recently, OLI data has been integrated into these compositing approaches (Hermosilla et al. 2017; Griffiths et al. 2018). The United States Geological Survey (USGS) now provides Landsat surface reflectance products as a Level-2 Science Product, with data from Landsats 4-7 corrected with LEDAPS (USGS 2012; 2018a), whereas OLI is corrected with Landsat Surface Reflectance Code (LaSRC; USGS 2018b, Vermote et al. 2016). Surface reflectance products are available on-demand for download from the USGS Earth Resources Observation and Science (EROS) Center Science Processing Architecture (ESPA), and the provision of these higher level products further reduces the amount of pre-processing required to enable pixel-based compositing in the same way that the standard Level-1 Terrain Corrected (L1T) products have enabled processing efficiencies (Hansen and Loveland 2012). Analysis Ready Data (ARD) products are now available for the United States, with plans to release such products globally (Elgorov et al. 2018). ARD products are designed specifically to reduce pre-processing requirements and support LTS analysis over large areas. ARD products include cloud and cloud shadow masks and are provided with various levels of correction, including TOA and surface reflectance.

In the context of time series analyses with Landsat data, radiometric correction to surface reflectance is required if models (for change detection, land cover classification, forest structure imputation, etcetera) are to be extrapolated in time or space (Song et al. 2001). While some Landsat compositing approaches use Top-of-Atmosphere (TOA) corrections (e.g. Roy et al. 2010), TOA are bulk corrections typically made to an entire image, not to individual pixels. TOA primarily adjust for sun angle and earth-sun distance; however atmospheric effects can contaminate spectral indices in a manner that is non-linear (Myeni and Asrar; 1994; McDonald et al. 1998), and do not enhance within-scene fidelity (Hansen and Loveland 2012). In contrast, corrections to surface reflectance are typically a per-pixel adjustment that is required when the goal is to achieve a consistent radiometric response within and between images (Song et al. 2001). LEDAPS is the most mature approach for correcting to surface reflectance (Vermote et al. 1997; Masek et al. 2006).

Hansen and Loveland (2012) posit that advances in pixel-based image compositing signal the end of scene-based analysis approaches, making way for progressively more novel opportunities for large-area characterization and monitoring. This shift from a scene-based perspective to a pixel-based perspective for image understanding and processing is key, and certainly mirrors trends and developments in time series analysis approaches (Kennedy et al. 2010). The aforementioned USGS Landsat ARD product provides further opportunity for best-available pixel compositing approaches and the inclusion of data from other sensors, such as Sentinel-2 (Wulder et al. 2016; Zhu et al. 2015; Storey et al. 2016).

Study Objectives

The overall objective of this dissertation was to develop and apply forest monitoring approaches that take advantage of remotely sensed data, particularly LTS data, to improve the capacity to characterize *both* disturbance and recovery over very large areas. To address this objective, the component studies have focused on information needs, data availability, methods development, and information outcomes (Figure 3). Substudies I and II define the information needs in a Canadian context, as well as the rule-base for generating annual, large-area, gap-free and cloud-free surface reflectance image composites from Landsat, which are an important pre-requisite for subsequent monitoring efforts. Substudy III focuses on information outcomes and methods development for characterizing forest recovery over large areas, providing a national assessment of disturbance and subsequent recovery for Canada's 650 Mha of forested ecosystems for 1985 to 2010. Substudies IV–VI explore the adaptation and application of the developed approach in southern Finland, focusing on data availability to support information needs and compositing efforts (IV) and assessing measures of spectral recovery against benchmarks of forest structure and composition measured with airborne laser scanning (ALS; V) and field plot data (VI).

The specific objectives of each substudy are as follows:

(I) Identify and articulate the information needs and target attributes required for large-area forest monitoring in Canada. Subsequently, use these information needs and monitoring requirements as the framework within which to develop and prototype a Landsat best-available pixel (BAP) image compositing approach for generating the required annual source data and information products to meet these information needs and requirements.

(II) Develop and demonstrate a protocol for generating annual change information and BAP composites that have no spatial or temporal gaps (hereafter referred to as proxy composites) and prototype regionally in Canada.

(III) Demonstrate technical capacity for large-area forest monitoring by prototyping at scale (i.e. nationally). Characterize national spatial and temporal trends in stand replacing forest disturbance caused by wildfire and harvest, and subsequent vegetation recovery, for the period 1985–2010 for Canada's forested ecosystems (~650 Mha), using information derived from Landsat time series data.

(IV) Characterize the large-area forest monitoring information needs, as well as the spatial and temporal extent of the USGS Landsat archive holdings for Finland. Document the capacity of the Landsat archive to retrospectively support the generation of baseline data on forest change, and support long-term forest monitoring information needs in Finland.

(V) Improve understanding of the linkages between spectral metrics of forest recovery post-harvest—as derived from LTS data—and manifestations of forest structure (height and cover) as measured from ALS data. The specific objectives of this study were threefold: (i) apply an established image

compositing and change detection approach (Composite2Change or C2C) to an area of managed forest in southern Finland and generate a spatially-explicit dataset characterizing forest change (1984–2012); (ii) validate the detected changes using independent reference data; and (iii) evaluate the utility and appropriateness of the Y2R spectral recovery metric for assessing the return of forest following harvest in a managed, boreal forest context. The assessment of the Y2R metric against measures of forest structure derived from the LTS data is the unique contribution of this work.

(VI) Explore the relationship between spectral recovery metrics and stand conditions in seedling plots that were measured in the year in which the stand was considered spectrally recovered. Using a chronosequence of recovered field plots, characterize stand conditions in the year of spectral recovery and determine those factors that may explain why some sites recover more rapidly than others. The specific objectives were to determine (i) if spectral measures of recovery could be used to accurately predict the plot stand development class assigned by the field crew; (ii) conversely, if seedling plot attributes could be used to predict spectral recovery rates derived from the Landsat times series recovery metrics; and finally determine (iii) what seedling plot characteristics distinguished stands that had rapid (< 5 years) versus slow (> 10 years) rates of spectral recovery.

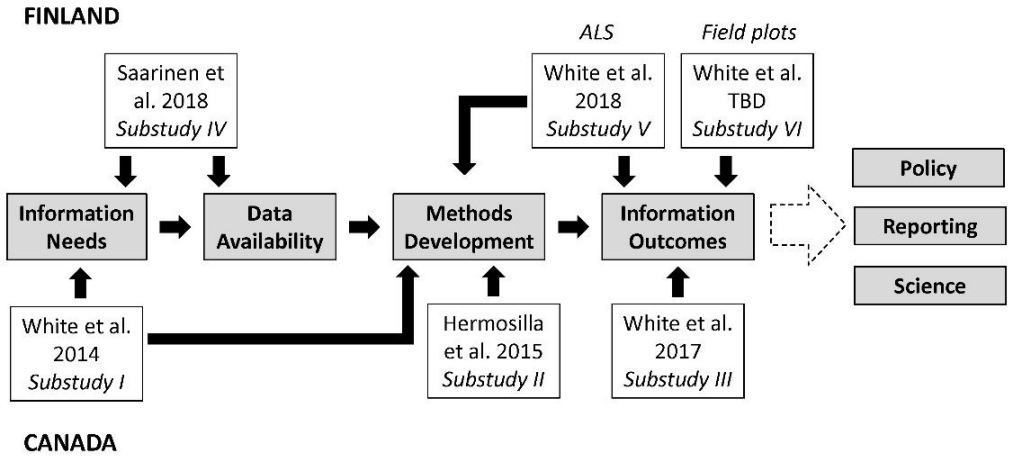

Figure 3. Sub-studies included in this thesis focused on information needs, data availability, methods development, and information outcomes in both Canada and Finland.

MATERIALS

Study areas

Canada

Canada is the second largest nation on earth at nearly 1 billion hectares, with a gradient in ecosystem productivity that is influenced by latitude and precipitation (Hofgaard et al. 1999). Canada's forested ecosystems represent a complex mosaic of treed areas, wetlands, and lakes and cover approximately 65% of Canada's land area (~650 Mha; Wulder et al. 2008). Canada's forests account for approximately 9% of the world's forest and 28% of the world's boreal forest (FAO 2012). The majority of Canada's forests (94%) are publicly owned (Natural Resources Canada 2013) and since the time of Canada's confederation in 1867, resource stewardship responsibilities, including forest management, have been vested with provincial and territorial governments.

In contrast to Nordic countries where intensive forest management is widely practiced, extensive forest management is more common in Canada (Wulder et al. 2007a). Licences to harvest and process wood products are allocated through tenure agreements to the private sector and the total area under some form of tenure amounts to approximately half the forest area of Canada (Natural Resources Canada 2015). This managed forest area implies the existence of inventory data and forest management activity, including fire suppression. Areas outside of this managed forest are typically difficult to access, have lower productivity, are not subject to fire suppression, and are not typically inventoried. Given the large size of Canada's forests and its complex jurisdictional responsibilities for forest stewardship, information needs to characterize forest resources are many and varied and are increasing with cumulative economic, ecological, cultural, and recreational demands on the forest resource. Information is required to support both national and international reporting commitments such as the national annual State of the Forests report, or the United Nations' FAO Forest Resource Assessment program (Wulder et al. 2004).

Substudies I–III were conducted in Canada. In substudy I, compositing approaches were demonstrated nationally for a single year (2010) and regionally on an annual basis for a 15-year period from 1998 to 2012, with detailed analyses of observational capacity for the jurisdictions of Saskatchewan and Newfoundland (Figure 4). Saskatchewan has a highly dynamic disturbance regime, dominated by frequent and large wildfires, whereas Newfoundland is prone to frequent cloud cover. Both of these areas represent unique challenges to compositing algorithms. In substudy II, change detection and proxy infilling of BAP data gaps was prototyped in the province of Saskatchewan (Figure 4). In substudy III, methods developed in substudies I and II were applied nationally (Hermosilla et al. 2016) and information on disturbance and recovery trends for the period 1985–2010 were reported nationally for Canada's forested ecosystems, by ecozone (Figure 5). Ecozones represent broadly defined ecological units characterized by "interactive and adjusting abiotic and biotic factors" (Ecological Stratification Working Group 1996). There are 10 terrestrial ecozones in Canada, two of which (the Boreal and Taiga Shield) have large west-east extents and are often split into their western and eastern components to reflect differences in ecoclimatic conditions between these regions (Stocks et al. 2002, Frazier et al. 2015), resulting in twelve ecozone units for the assessment of national trends in disturbance and recovery.

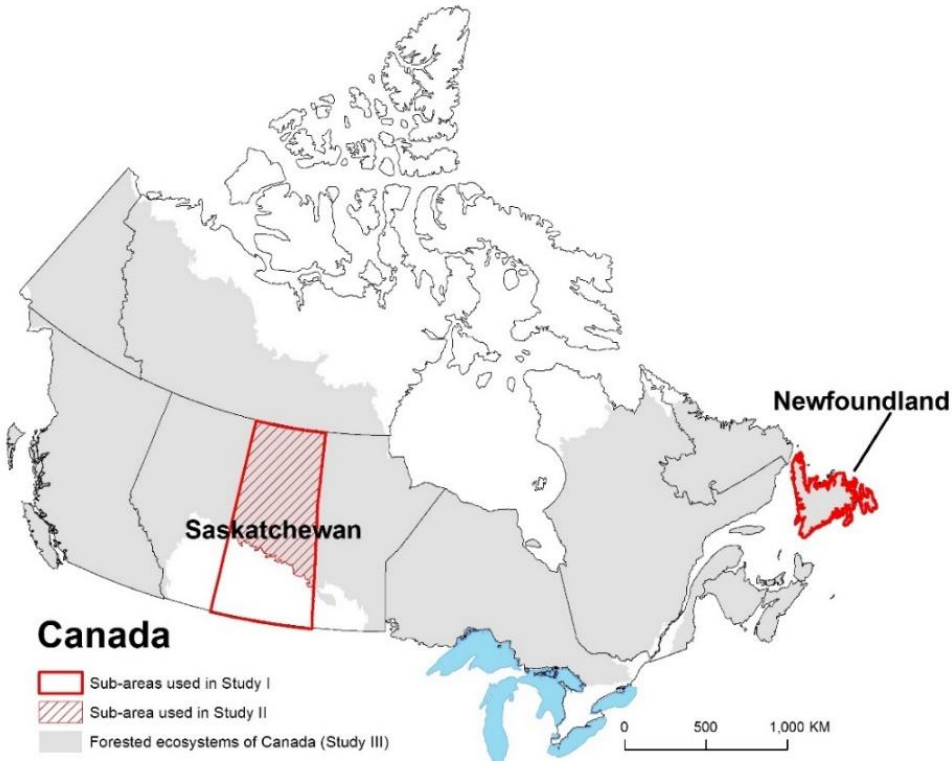

Figure 4. Forested ecosystems of Canada (substudy III) and regional areas used for prototyping of best-available pixel (BAP) compositing methods in subtudies I and II.

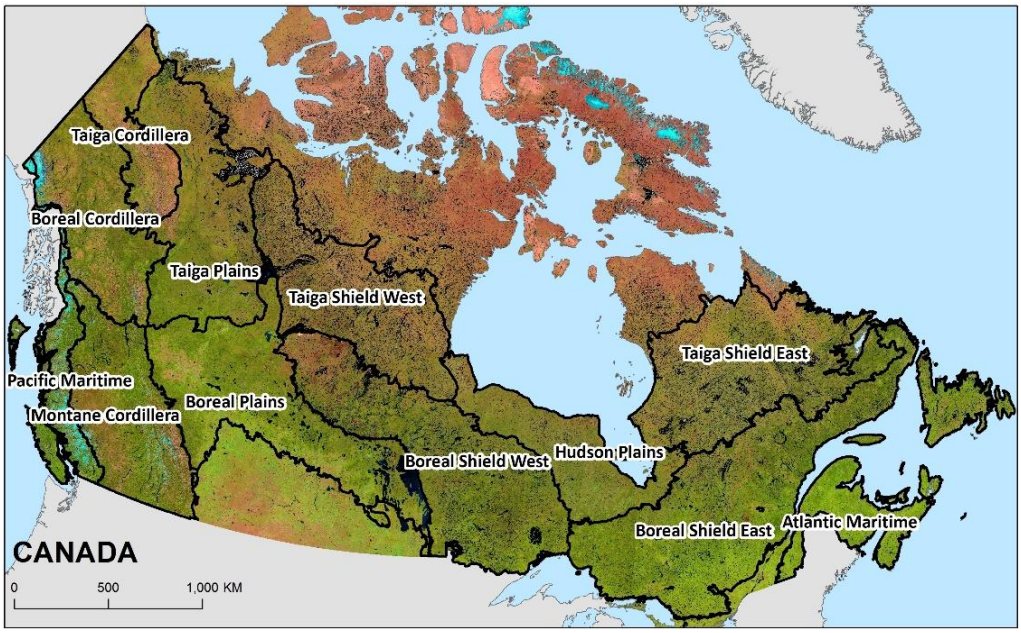

Figure 5. Forested ecozones of Canada used to report results from substudy III.

Finland

In Finland, 22.8 Mha (75%) is considered forest land, representing about 10% of Europe's forest area (Natural Resources Institute Finland 2017). Approximately 60.9% of Finnish forest lands are privately owned; state-owned forests account for 25.4% of Finnish forests and are primarily located in the north of the country. The remainder of forests are owned by private forest companies (8.2%) or other owners (5.4%). Commercial forests in Finland are defined by productivity and productive forest lands are considered those forests where the annual increment is > $1 m^3 ha^{-1} yr^{-1}$.

In substudy IV, the availability of archived Landsat data is summarized by the Public Service Units of the Finnish Forest Centre (Figure 6B). The study area used in substudies IV–VI is approximately 5.3 Mha in size, and represents an intensively managed forest area in southern Finland and a complex landscape mosaic of agricultural, forest, and urban land use (Figure 6A). Approximately 86% of the study area belongs to southern boreal vegetation zone and the majority is considered forest (65% by area). Protected areas, such as national parks, represent 2.3% of the forested area whereas agricultural fields cover approximately 16% of the study area. Forests in this area have a mean stem volume of 146.4 $m3ha^{-1}$ and the main tree species are Norway spruce (Picea abies (L.) Karst.) and Scots pine (Pinus sylvestris L.) contributing 40.2% and 38.5% of the stem volume, respectively. Approximately, 97.5% of the forest area within the study site is considered productive forest, with a growth increment of at least 1 $m3ha^{-1}yr^{-1}$. Site type varies from herb-rich forest to barren heath forest, with the main site type being mesic heath forest covering 49.8% of the forest land within the study area (Natural Resources Institute of Finland 2015).

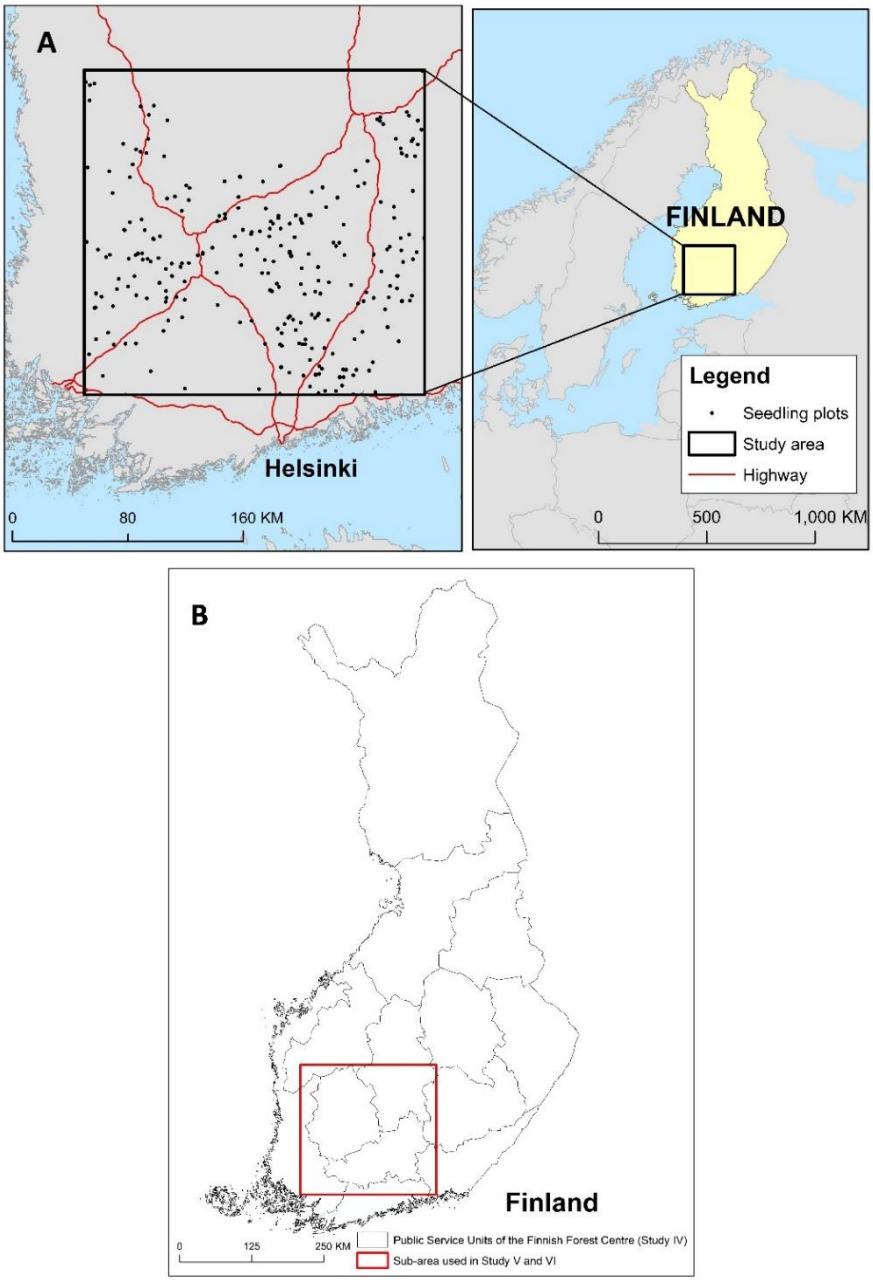

Figure 6. (A) Location of study area used in substudies V and VI. (B) Public Service Units of the Finnish Forest Centre used to summarize Landsat metadata in substudy IV.

Landsat Time Series (LTS) data

All Landsat data used in the component studies were downloaded from the USGS archive in Level-1 Terrain-Corrected (L1T) format. L1T products are systematically corrected for radiometric, geometric, and terrain distortions (Irons et al. 2012). For compositing purposes, a target day of year (DOY) of August 1 (Julian day 213) was selected as being representative within the growing season for the majority of Canada's forested area (McKenney et al. 2006), as well as for the study site in southern Finland (substudy IV). A maximum cloud cover threshold was determined to be 70%; when cloud cover exceeds 70%, potential ground control points may be obscured and images are more difficult to geometrically correct (White and Wulder 2013). For substudies I–III, annual BAP image composites were generated by considering as potential candidates all Landsat Thematic Mapper (TM) and Enhanced Thematic Mapper Plus (ETM+) images acquired within ± 30 days of August 1 (1984–2012) that have less than 70% cloud cover. For Canada, which is represented by 1285 unique Landsat Worldwide Referencing System (WRS-2) scenes (path/row combinations), a total of 81,000 images meeting these criteria were downloaded from the USGS Landsat archive (Hermosilla et al. 2016). Landsat metadata used in substudy IV included 30,076 images available for Finland from the USGS archive (1972–2017 inclusive). For substudy V in southern Finland, which is represented by 11 unique WRS-2 scenes, 554 images that met the aforementioned compositing criteria were downloaded from the USGS archive in L1T format for the period 1984–2012. For substudy VI, the 1984–2012 time series used in substudy V was extended to 2017 following the approach outlined in Hermosilla et al. (2017), and included data from Landsat-8 OLI. An additional 143 images were downloaded from the USGS archive.

Airborne laser scanning data

In 2008, the National Land Survey of Finland began acquiring ALS data in order to generate a new national-level digital terrain model (DTM) with a 2-m resolution. The NLS and the Finnish Forest Centre have outlined a plan to cover the entire area of Finland by the end of 2019; free and open access to the ALS data provided by the NLS data services. The ALS data have been acquired for production areas of varying sizes. The ALS data used in substudy V were acquired between 2008 and 2016 for production areas that ranged from 43,200 ha and 417,600 ha in size. Target parameters set by the NLS for ALS data acquisitions were a minimum point density of 0.5 pts/m^2; and a point height error less than 15 cm. Flying altitude of all acquisition campaigns was approximately 2000 m above sea level, a scan angle of ± 20 degrees with a footprint size of < 60 cm. The utility of these national ALS data for characterizing the vertical distribution of vegetation has been demonstrated (e.g. Kankare et al. 2015; Kotivuori et al. 2016). ALS data used in substudy V were downloaded from the NLS data services in 3 x 3 km tiles, with ground and non-ground points classified by the NLS.

Field plot data

Data for seedling stand plots used in substudy VI were obtained from the Finnish Forestry Centre. Seedling stands are considered to be those stands with a mean height < 7 m for

coniferous-dominated, or < 9 m for deciduous-dominated stands, respectively (Äijälä et al. 2014). Seedling stands are further divided into young (< 1.3 m) and advanced (1.3–7 or 9 m) seedling stands. Seedling plots were selected for analysis based on two criteria: (i) the plots were located within change events identified from our C2C time series and were more than 20 m from the nearest stand boundary; and (ii) the plots were measured in the same year in which spectral recovery was indicated by the Y2R metric. The application of these criteria yielded a total of 284 plots measured from 271 different seedling stands in the summers of 2010 to 2017. Time since disturbance for the seedling plots ranged from 1 to 15 years. Plots had a radius of 9 m, and the location of plot centroids were measured with < 1 m accuracy. In northern European forests, the regeneration stage is characterized as that period of time between clearcutting and when the main tree species established at a site has attained an average height of 1.3 m (Nilsson et al. 2010). Approximately 82% of the selected seedling plots had attained or exceeded this threshold. Additionally, the target stem density for regenerated stands is a minimum of 1800-2500 stems per ha, and although this target is frequently not met (Nilsson et al. 2010), 95% of the selected seedling plots had met this target. The selected plots were therefore considered representative of successfully regenerated stand conditions post-harvest. Time since disturbance for the plots ranged from 1 to 15 years. Measured plot attributes included species-level mean height and number of stems per ha for up to seven unique species-strata in each plot. Using the stratum-wise data we calculated the mean, median, maximum, and coefficient of variation (CV) of plot height, as well as the weighted mean height, whereby the number of stems in each stratum were used as weights. We also calculated the mean, median, total, and CV of stems per ha, percentage of total stems in the plot that were deciduous species (hereafter referred to as percent deciduous), and the ratio of the mean deciduous height to mean coniferous height in each plot (hereafter referred to as height ratio). Information on dominant tree species, site type, and drainage class were also recorded as categorical variables for each plot (Table 2).

METHODOLOGY

Characterizing Landsat archive holdings for forest monitoring in Finland

The spatial and temporal availability of the images in the Landsat archive directly influences the successful generation of annual BAP image composites that are useful for forest monitoring. The extent of archive holdings for Canada have previously been summarized by White and Wulder (2013), and more recently, globally (Wulder et al. 2016). In substudy IV, the metadata for all Landsat images acquired for Finland between the inception of the Landsat program in 1972 and December 31st, 2017 were analyzed to assess their spatial and temporal variability, and suitability for image compositing. Finland is covered by 66 unique WRS-2 scenes. The number of images acquired for each scene is analogous to the number of observations for each scene. The total number of archived images was summarized by year of acquisition, day of year, and Landsat sensor (MSS, TM, ETM+, OLI). Images were interrogated for their suitability for pixel compositing, as defined in substudy I, and were likewise summarized by sensor, by year of acquisition, and spatially, according to the Public Service Units of the Finnish Forest Centre (Figure 6B). Overlap between WRS-2 scenes increases the theoretical observation yield for compositing. Following the approach developed in substudies I and II, BAP image composites were

generated for a 5.3 Mha study area in southern Finland (corresponding to 11 WRS-2 frames) to demonstrate the realized potential of the archive and overlap areas for image compositing.

Table 2. Summary of seedling plot attributes.

Plot attribute	Summary and class codes					
	Mean	***Min***	***Max***	***Lower Quartile***	***Upper Quartile***	***Std. Dev.***
Mean height (m)	1.98	0.20	6.10	1.16	2.59	1.14
Weighted mean height (m)	0.86	0.05	4.00	0.41	1.08	0.70
Median height (m)	1.94	0.20	6.10	1.15	2.50	1.13
Maximum height (m)	2.52	0.20	8.40	1.50	3.50	1.45
CV height (%)	28.88	0.00	118.11	14.43	40.11	19.87
Mean stems per ha	3151	367	25000	1417	3750	2842
Median stems per ha	2667	100	25000	1100	3150	2824
Maximum stems per ha	5705	500	38000	2350	7300	5190
Total stems per ha	8227	1100	38200	3850	11250	6041
CV stems per ha (%)	78.51	0.00	181.67	50.91	108.73	41.31
Percent deciduous	60.35	0.00	100.00	35.00	85.25	30.37
D height: C height (Height ratio)	1.29	0.00	6.67	0.81	1.67	0.85
Dominant species	1. Scots pine (*Pinus sylvesteris* L.; n = 83) 2. Norway spruce (*Picea abies* L. Kars; n = 149) 3. Deciduous (primarily birches, *Betula* spp. L; n = 52)					
Site type	1. Heath with rich grass-herb vegetation and corresponding natural and ditched peatland (n = 66) 2. Mesic heath forest, and corresponding natural and drained peatland (n = 159) 3. Sub-xeric heath forest, and corresponding natural and drained peatland (n = 44) 4. Xeric heath forest, and corresponding natural and drained peatland (n = 15)					
Drainage class	1.Undrained mineral soil (default) (n = 244) 2. Swampy mineral soil (n = 7) 3. Drained mineral soil (n = 21) 4. Forested drained peatland (n = 12)					
Stand development class	T1. Young seedling stand, dominant height of the dominant species is < 1.3 m (n = 89); T2. Advanced seedling stand, dominant height of the dominant species is > 1.3 m (n = 195)					

Best-available pixel (BAP) image composites

Pixel-based image compositing of Landsat data aims to make use of the best observation for each available pixel within a defined acquisition period. The ultimate goal of BAP image compositing is to generate cloud-free, gap-free surface reflectance data products to support forest monitoring applications. As the annual BAP may have data gaps and likely also noise, additional processing of the annual BAPs is required to filter noise, fill data gaps, and generate a gap-free surface reflectance product, also known as a proxy BAP.

Generation of annual BAP composites

The analysis-ready L1T format, and the consistency of the Landsat calibrated data record (Markham and Helder 2012) greatly reduces the amount of additional pre-processing required. In 2018, the USGS further refined its analysis-ready data products through the provision of data collections; however, the studies described herein pre-date the release of these more mature products. For the Landsat data used in substudies I–VI, downloaded L1T images were subjected to cloud screening and converted to surface reflectance. Cloud screening was performed using the Function of mask (Fmask version 2.1; Zhu and Woodcock 2012). Fmask is an object-based algorithm designed to identify clouds and cloud shadows, as well as clear land pixels, clear water pixels, snow, and areas of no data. The water pixels identified by Fmask were also used to generate a water mask that was used to exclude water features from further processing (Lunetta et al. 2004; Hermosilla et al. 2016). LEDAPS was used to correct the data to surface reflectance (version 1.3.0; Schmidt et al. 2013). LEDAPS generates a TOA reflectance from Landsat digital numbers (DN) and applies atmospheric corrections to then generate a surface reflectance product (Masek et al. 2006). LEDAPS corrections are based on the Second Simulation of a Satellite Signal in the Solar Spectrum (6S) radiative transfer model (Vermote et al. 1997). LEDAPS was applied to the six Landsat optical bands (i.e. bands 1–5 and 7).

After pre-processing, all pixels in each candidate image are assigned scores for four factors: sensor, day of year, distance to cloud or cloud shadow, and opacity. Composite scores are based on the approach described in Griffiths et al. (2013). Sensor and DOY scores are assigned at the image level, so all pixels within the same image are assigned the same score. The distance to cloud or cloud shadow score and the opacity score are unique to every pixel. The characteristics of these four scores are summarized in Table 3. Note that for subsequent studies, some alterations were made to the original scoring protocol described in substudy I. The scoring rules outlined in Table 3 are the definitive, final version of the scoring protocol used in the subsequent studies.

Table 3. Summary of best-available pixel compositing scores.

	Score	Equation and scoring details
IMAGE SCORE	**Sensor**	Landsat TM = 1 Landsat ETM+ pre-SLC-off (< 2003) = 1 Landsat ETM+ post-SLC-off (≥ 2003) = -0.7 (as per Hermosilla et al. 2016)
	DOY	$Score_{DOY} = \frac{1}{\sigma\sqrt{2\pi}} e^{-\frac{1}{2}\left(\frac{x_i-\mu}{\sigma}\right)^2}$ (T1.1) where μ and σ denote the mean and standard deviation respectively of all the image DOYs, and x_i is the DOY for the image being assessed • μ force to the target DOY (August 1; Julian day 213); σ = 38 • DOY score calculated using Equation T1.1 and then scaled to a value between 0 and 1, by dividing by the maximum score.
PIXEL SCORE	**Distance to cloud or cloud shadow score**	$Score_{CloudDistance} = \frac{1}{1+e^{\left(-0.2\left(min(D_i, Dreq) - \left(\frac{Dreq-Dmin}{2}\right)\right)\right)}}$ (T1.2) where D_i is the pixel's distance to cloud or cloud shadow, D_{req} is the minimum required distance (i.e., 50 pixels), and D_{min} is the minimum distance of the given pixel observations (i.e., 0 pixels). • Pixels identified as clouds or cloud shadows are assigned a "no data" value • Pixels located at a distance greater than 50 pixels from an identified cloud or cloud shadow pixel are assigned a score of 1. • Pixels that are not identified as clouds or cloud shadows, and that are less than 50 pixels away from clouds and cloud shadows are assigned a score between 0 and 1 using Equation T1.2.
	Opacity	$Score_{Opacity} = 1 - \left(\frac{1}{1+e^{\left(-0.2\left(min(O_i, O_{max}) - \left(\frac{O_{max}-O_{min}}{2}\right)\right)\right)}}\right)$ (T1.3) where O_i is the pixel's opacity value, O_{max} is the maximum opacity value (i.e., 0.3), and O_{min} is the minimum opacity value (i.e., 0.2). • Pixels with an opacity value < 0.2, score = 1 • Pixels with an opacity value > 0.3 were labelled as "no data". • Pixels with opacity values ≥ 0.2 and ≤ 0.3 were assigned a score between 0 and 1 using the opacity score Equation T1.3 above.

The four scores are generated for each pixel, as described in Table 3, and summed. The best observation for any given pixel location is determined as being the pixel that has the highest summed score. The final annual BAP composite is populated with the surface reflectance value corresponding to the best observation for that pixel. Not all pixels will have an observation, so "no data" gaps are possible in the final annual BAP composites.

Generation of proxy best-available pixel composites and change detection

The Composite-to-Change or C2C protocol is an approach optimized for generating gap-filled BAP composites over very large areas. The approach builds on the temporal segmentation algorithm of Kennedy et al. (2007; 2010). An overview of the C2C protocol is provided in Figure 7.

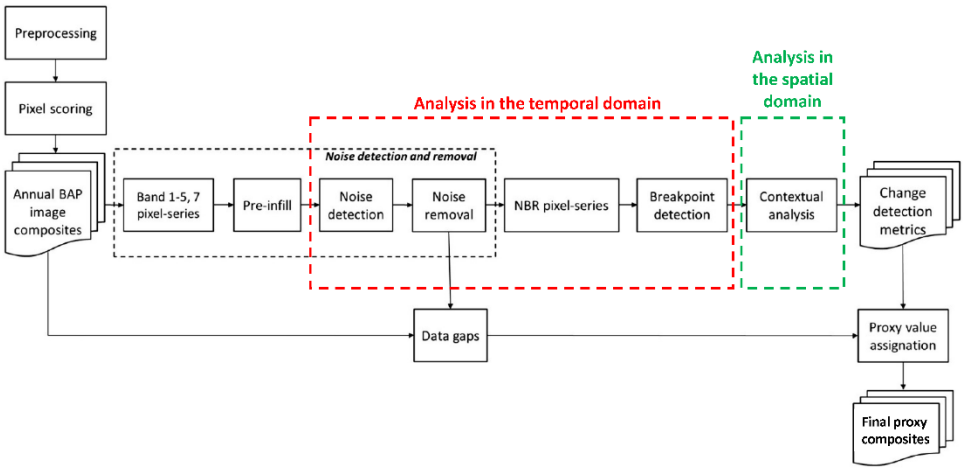

Figure 7. Overview of the Composite-2-Change (C2C) protocol used for generating gap-free BAP composites.

The full temporal trajectory of surface reflectance values for a given pixel (hereafter referred to as a pixel series) are used to define a range of expectation for spectral values. While minor variation in spectral values through time is expected, anomalous values are likely indicative of clouds/cloud shadows that were missed by the Fmask algorithm, or by other factors such as haze or smoke (Figure 8). Such anomalous values in the pixel series must be identified and distinguished from more marked variation in spectral values that result from real change. First, the outlier filtering method of Kennedy et al. (2010) was applied. Using this method, a pixel's surface reflectance value for any given year is compared to its surface reflectance value in the year immediately preceding and immediately following. This outlier filtering is applied to each of the six Landsat optical bands independently. If a pixel is detected as an outlier *and* the difference between the pixel's surface reflectance value and the average of the reflectance values in the previous and subsequent year exceeds a pre-defined threshold in 3 of the 6 Landsat optical bands, the pixel is flagged as noise and is set to a no data value. These no data pixels further add to existing data gaps in the original annual BAPs (Figure 7).

The next step is to temporally segment each pixel series to identify change. However, in order to enable change detection and to avoid interpolation across potential breakpoints that are indicative of change events, a preliminary infill of pixel values was undertaken (Figure 7). These preliminary proxy values are determined by examining each year within a pixel series. A year with no data in the pixel series is assigned the spectral value of either the preceding year or the subsequent year, depending on which is lower: the standard deviation of the surface reflectance values for two years preceding or the two years following.

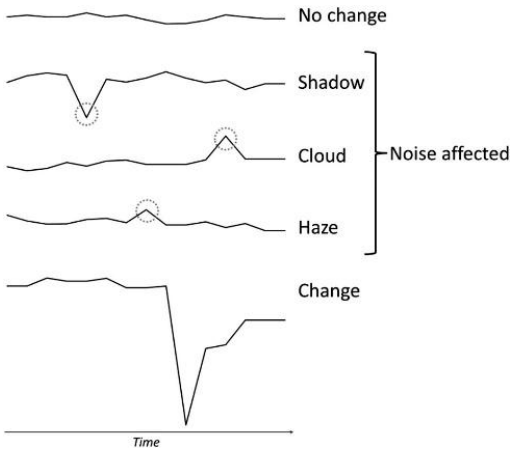

Figure 8. Schematic of pixel series illustrating differences between the various forms of noise and actual change.

Following the pre-infilling of spectral values, temporal segmentation or breakpoint detection is undertaken. The accurate identification of breakpoints is critical to the assignment of final proxy values and to ensure that changes are detected in the correct year. In the C2C approach, breakpoint detection is undertaken using the Normalized Burn Ratio (NBR; Key and Benson 2006) pixel series. The bottom-up/sliding window (SWAB) breakpoint detection algorithm of Keogh et al. (2001) was applied and consisted of four steps. Initially, *n*-1 segments are created in a pixel series composed of *n* values. Thus, for a pixel series of 30 years with 30 reflectance values, 29 segments would be generated initially. Second, the cost of merging each pair of adjacent segments is calculated using root mean square error (RMSE). Third, the pair of segments with the lowest cost is merged. Finally, the cost of merging the remaining segments is recalculated and the process is repeated until the stopping criteria are fulfilled. Two stopping criteria are used by C2C: the maximum number of segments, and the maximum allowable merging cost. During the iteration of segment merging, the maximum allowable merging cost can be dynamically altered to ensure enforcement of the maximum segment criterion. The maximum number of segments for the 1984-2012 time series was set to 5 and the maximum allowable cost was set to 0.125 (Hermosilla et al. 2015; 2016). When the time series were extended to 2016 in substudy VI, an additional segment was used, for a total of 6 segments, while the maximum allowable cost remained unchanged (Hermosilla et al. 2017).

Once the breakpoints are detected, four distinct types of trends are computed: (i) monotonic trends with no breakpoints (i.e. single segment); (ii) trends with multiple breakpoints, with all segments having positive slopes; (iii) trends with a single breakpoint and a negative-sloped segment; and, (iv) trends consisting of multiple breakpoints, with at least one negative slope. The latter represent change events and subsequent activity (i.e., forest recovery, change in land use) that are of interest for forest monitoring applications. From the aforementioned trends, segments, and breakpoints, a set of descriptive metrics are generated that enable the characterization of change events, as well as pre- and post-change

conditions. Metrics include change year, magnitude, persistence, and rate (Table 4; Hermosilla et al. 2015; 2016).

Once spectral changes are detected in the temporal domain, a subsequent process analyzes the change events in the spatial domain to improve the consistency and spatial homogeneity of change detection. The aforementioned preliminary infill of pixel values may result in spatially discordant change events having an incorrect change year. From a monitoring perspective, the key is that change events are labelled to the correct year and that they have spatial cohesion with surrounding pixels within the same event. This is achieved by ranking the reliability of the change detection according to number of missing years of observations in a pixel series. In this context, an inverse relationship is assumed between the ability to detect the change in the correct year and the number of missing observations in the pixel series. Data availability in the years before, during, and after the change event therefore determines the reliability of the change detection.

Detected change events are aggregated into spatial segments based on date of change and persistence. Spatial segments that are missing less than 50% of their observations in a given year are deemed more reliable than segments that are missing more than 50% of observations. Lower-ranked segments that are spatially adjacent to a higher ranked segment within one year are assigned the change year of their more reliable neighbour. This spatial analysis also imposes a minimum mapping unit (MMU) of 0.5 ha, or approximately 5 pixels, for detected changes. Change events that have a size less than the MMU (0.5 ha) are removed. As per Kennedy et al. (2012), this MMU is small enough to capture most forest management activities, while also being sufficiently large to enable validation—which is most often enabled through visual interpretation of the LTS (Cohen et al. 2010).

Table 4. Summary of Composite-2-Change (C2C) change metrics.

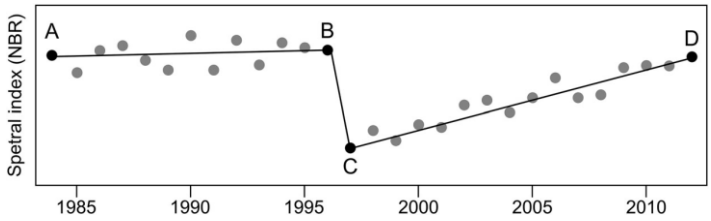

	Metric	Description
Pre-change[1]	Magnitude	Difference between NBR values at the start (A) and end (B) points of the pre-change segment.
	Persistence	Number of years between the start (A) and end (B) points of the pre-change segment.
	Rate	Ratio of pre-change magnitude variation to pre-change persistence.
Change (negative segments)	Greatest Change Year	Year in which breakpoint occurs (C). For pixel series with multiple change events, this is the year in which the greatest change event occurs (greatest magnitude change). The breakpoint separates the pre-change and change segments.
	Magnitude	Difference between NBR values at the start (B) and end (C) points of the change segment.
	Persistence	Number of years between start (B) and end (C) points of the change segment.
	Rate	Ratio of change magnitude to persistence.
	First change year	For pixel series with multiple change events, this is the year of the first change event (first breakpoint).
	First change persistence	For pixel series with multiple change events, this is the persistence of the first change event (first breakpoint).
	Last change year	For pixel series with multiple change events, this is the year of the last change event (last breakpoint).
	Last change persistence	For pixel series with multiple change events, this is the persistence of the last change event (last breakpoint).
Post-change[1]	Magnitude	Difference between NBR values at the start (C) and end (D) points of the post-change segment.
	Persistence	Number of years with no negative segments years following a change event.
	Rate	Ratio of post-change magnitude variation to post-change persistence.

[1]*Pre- and post-change metrics are calculated for the change event with the greatest magnitude in the pixel series.*

The final step is then to assign the final proxy values to those pixels with no observations. Proxy values are computed using piecewise linear interpolation from the temporal segments in which breakpoints and trends have been identified and characterized, as follows:

$$x_t = x_{t-1} + (x_{t+1} - x_{t-1}) \times \frac{t-(t-1)}{(t+1)-(t-1)} \quad (1)$$

Where x_t is the proxy value assigned to pixels with no observation in the year *t*, and x_{t-1} and x_{t+1} are the spectral values in years with observations before (t-1) and after (t+1) the no data observation respectively. For no data values located at the extremes of the temporal segments in a pixel series, pixel values are assigned using extrapolation, as follows:

$$x_t = x_{k-1} + (x_k - x_{k-1}) \times \frac{t-(k-1)}{(k)-(k-1)} \quad (2)$$

Where x_k and x_{k-1} are the spectral values of the two nearest years, *k* and *k-1*, with observations. With this approach, the proxy value assigned to a data gap is uniquely a function of the spectral values within the temporal segment where the gap is located. This approach avoids interpolation across temporal segments, and the combination of trend information from different trend components, preserving the change events in the time series. The outputs from the combined spatial and temporal processing are gap-free, surface reflectance proxy image composites at a 30 m resolution, annual change detection information, and a series of change metrics characterizing the detected changes (including pre- and post-change conditions).

Observation yield and radiometric consistency

In substudy I, the observation yield (the number of pixels with BAP observations from the target date range of August 1 ± 30 days) and the number of consecutive years with observations were assessed. In substudy II, the observation yield was also evaluated, however the origin of the gaps were also tracked according to whether the data gaps resulted from the scoring mechanism or from the noise removal step (Figure 7).

In substudy I, the radiometric consistency of the annual BAP composites was assessed using reference data (i.e. selecting a single WRS-2 path/row scene, identifying a target year, and withholding the most cloud-free image). Annual BAP were generated from remaining images and samples of pixels (n = 500) were randomly selected from areas of dense forest cover and surface reflectance values for these sample pixels were extracted from the annual BAP and reference data and compared using the coefficient of determination (R^2).

In substudy II, the assigned proxy values were evaluated by artificially generating gaps in each annual composite using a random sample of 0.005% of pixels (n = 116,000). The C2C protocol to generate proxy BAPs was applied and the generated proxy values were evaluated against the reference data. Values were compared using the Pearson correlation coefficient (*r*; to determine the degree of association between the reference and the proxy values), root mean square error (RMSE; to determine the average difference between the

reference and the proxy values; Equation 3), bias (to determine if proxy values are typically higher or lower than references values; Equation 4), and coefficient of variation (CV; for comparing between disturbed and undisturbed pixel groups within any given spectral band, but not for comparisons between bands; Equation 5).

$$Bias_b = \frac{1}{n} \sum_{i=1}^{n} \left(Reference_{b,i} - Proxy_{b,i} \right) \quad (3)$$

$$RMSE_b = \sqrt{\frac{1}{n} \sum_{i=1}^{n} \left(Reference_{b,i} - Proxy_{b,i} \right)^2} \quad (4)$$

$$CV_b = \frac{RMSE}{\overline{X}_{Reference_b}} \times 100 \quad (5)$$

where $Reference_{b,i}$ and $Proxy_{b,i}$ are, respectively, the reference and proxy values for each pixel in band b, n is the number of samples, and $\overline{X}_{Reference_b}$ is the mean spectral value for band b. Values for *r*, *RMSE*, *Bias*, and *CV* were calculated for all six spectral bands, and were also generated for three strata: all pixels, pixels without change events, and pixels with change events. The impacts of an increasing number of data gaps, as well as consecutive numbers of data gaps, on the quality of the proxy value assignment, were also assessed.

Composite-to-change (C2C) outputs

Forest disturbances: Canada (wildfire and harvest)

Detected changes were attributed to a change type according to the change hierarchy and methods described in Hermosilla et al. (2015; 2016), with both stand-replacing and non-stand replacing disturbances being identified. The four change types identified were wildfire, harvesting, road, and non-stand replacing change. Non-stand replacing changes relate to temporary variations in vegetation condition (Vogelmann et al. 2016) such as defoliating insects, or longer-term gradual changes in vegetation condition (Cohen et al. 2016) such as water stress. Changes were attributed at the object-level using spectral, temporal, and geometrical characteristics of the change objects, and a random forest classifier (Breiman 2001).

Forest disturbances: Finland (harvest)

In substudies V and VI, the objective was to assess post-harvest recovery, hence it was necessary to identify C2C changes that represented clearcutting (i.e. final felling). Clearcutting describes an even-aged silvicultural system that removes an entire stand of trees from an area in a single harvesting operation. In Finland, forest certification currently requires that at least 10 retention trees are left for every hectare of clearcut (Forest Stewardship Council Finland 2010, PEFC Finland 2014). In order to correctly identify these clearcuts, a forest mask was applied to constrain the analysis area (Saksa et al. 2003).

The forest mask was generated using information from the national base map of Finland (i.e. agricultural fields, non-forest land, lakes, rivers wider than 125 m, urban areas, highways, railways, power lines, main roads and other roads). For C2C changes located within this forest mask, the size (>2 ha) and magnitude (< -0.4) of the changes were used to aid in identifying clearcuts. The appropriate change magnitude threshold was determined using visual interpretation of high resolution imagery available from Google Earth™. Stratifying by change magnitude ensured that other management activities, such as pre-commercial thinnings, were not included as areas identified as harvest. Lastly, a 30-m (equivalent to 1 Landsat pixel) buffer was applied to the interior of these change events to account for stand edge effects, particularly with the ALS data, and excluded these pixels from further analysis. The 2-ha minimum change event size therefore ensured that there were sufficient pixels for analysis remaining within each event after the 1-pixel internal buffer is applied.

Spectral recovery metrics

Recovery metrics were derived using the Normalized Burn Ratio (NBR), a spectral index that was initially designed by Key and Benson (1999, 2006) to map burn severity. NBR is calculated using near-infrared (NIR; Band 4 for TM/ETM+ and Band 5 for OLI) and SWIR wavelengths (Band 7 for TM/ETM+/OLI) as follows:

$$NBR = \frac{NIR - SWIR}{NIR + SWIR} \quad (6)$$

The NBR takes advantage of the different spectral responses that disturbed and undisturbed areas will have in the NIR and SWIR wavelengths (Kennedy et al. 2010). NBR values range from -1 to 1, with positive values for pixels dominated by vegetation, and negative values for pixels dominated by bare soil (Escuin et al. 2008).

Recovery metrics used in all sub-studies are developed using trend-fitted NBR values from C2C time-series analysis (i.e., from the proxy surface reflectance BAP composites), to which a despiking approach was applied similar to that of Kennedy et al. (2010) and Bolton et al. (2015), where noisy observations are detected by examining them in relation to their previous and subsequent spectral values in the time series (substudy II). Schroeder et al. (2007) identified that year-to-year differences that result from phenology or atmospheric effects such as haze would be minimized by a fitted trajectory curve.

In substudy III, the objective was to characterize national spatial and temporal patterns in both short- and long-term post-disturbance vegetation recovery. Recovery in this context was defined as both the initial establishment of vegetation post-disturbance, and the longer-term, sustained regeneration of forests at a site (Johnstone et al. 2004), hence recovery metrics that captured both short and long-term recovery were applied (Pickell et al. 2016, Chu et al. 2016).

The first short-term metric was an absolute measure of post-disturbance regrowth considered as a spectral proxy for recovery (Griffiths et al. 2014). As defined by Kennedy et al. (2012), this metric indicates the change in NBR at five years following disturbance:

$$\Delta NBR_{regrowth} = NBR_{fitted,\,y5} - NBR_{fitted,\,y} \quad (7)$$

where $NBR_{fitted,y5}$ is the fitted NBR value 5-years post-disturbance and $NBR_{fitted,y}$ is the fitted NBR value in the year of disturbance. Effectively, this metric indicates how much the NBR value for a given pixel has changed over the 5-year period following disturbance (Figure 9).

The second short-term metric provides a relative measure of post-disturbance regrowth. Previous studies have demonstrated the importance of conditioning spectral measures of vegetation recovery on pre-disturbance characteristics (Bolton et al. 2015, DeVries et al. 2015, Pickell et al. 2016); and therefore a relative measure of vegetation recovery was also included. Kennedy et al. (2012) defined the Recovery Indicator (RI), which scaled the post-disturbance regrowth ($\Delta NBR_{regrowth}$) metric by the magnitude of the disturbance segment:

$$RI = \frac{\Delta NBR_{regrowth}}{\Delta NBR_{disturbance}} \quad (8)$$

where $\Delta NBR_{regrowth}$ is defined in Equation 7 and $\Delta NBR_{disturbance}$ is defined in Equation 9 below. While Kennedy et al. (2012) defined magnitude as a percent change in vegetative cover, with NBR values calibrated to cover estimates, herein the Recovery Indicator was adapted, defining the denominator, $\Delta NBR_{disturbance}$, as the change in NBR during the disturbance segment (Figure 9):

$$\Delta NBR_{disturbance} = NBR_{y-1} - NBR_{y} \quad (9)$$

where NBR_{y-1} is the NBR value at the beginning of the disturbance segment and NBR_y is the NBR value at the end of the disturbance segment. By scaling $\Delta NBR_{regrowth}$ by change magnitude, it is possible to account for vegetated areas with lower NBR at the time of disturbance, and for lower magnitude disturbances, which may leave more residual vegetation at a site (Kennedy et al. 2012), thereby influencing recovery (Figure 9).

A long-term spectral metric of recovery was adapted from the approach of Pickell et al. (2016) and determined the length of time it took, in years, for a given pixel to reach 80% of its pre-disturbance NBR value (Years to Recovery or Y2R;Figure 9). The pre-disturbance NBR value was defined as the average NBR value of the two years prior to the disturbance segment, calculated as follows:

$$NBR_{pre-disturbance} = \frac{NBR_{y-2} + NBR_{y-1}}{2} \quad (10)$$

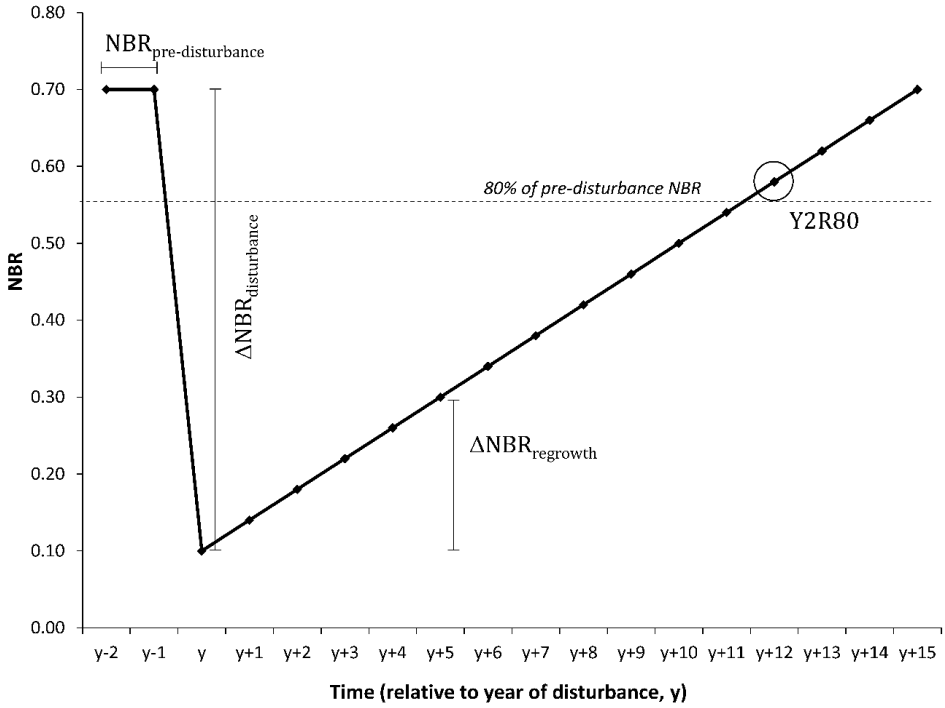

Figure 9. A schematic of a spectral NBR pixel series illustrating the short-term spectral recovery absolute (NBRregrowth) and relative (Recovery Indicator, RI) metrics and the long-term spectral recovery metric, Y2R.

In substudy V, different Y2R thresholds were applied to define recovery: 60%, 80%, and 100%. In addition, a probabilistic threshold was applied to define when a pixel was no longer statistically significantly different from $NBR_{pre\text{-}disturbance}$ (Figure 10).

Validation of change outcomes

Canada

Substudy III relies on information outputs generated in Hermosilla et al. (2015; 2016). The accuracy of the change detection, the year of change, and the attribution of change were evaluated using independent reference data. The methods used to assess those change products are described briefly here. A stratified random sampling strategy was applied to select evaluation samples for the change detection and attribution processes following the approach described in Olofsson et al. (2014) and guided by Hermosilla et al. (2015b). Change/no change were evaluated by allocating the total number of sample points (n = 1200) equally to change and no change strata. Change attribution (i.e. wildfire, harvest,

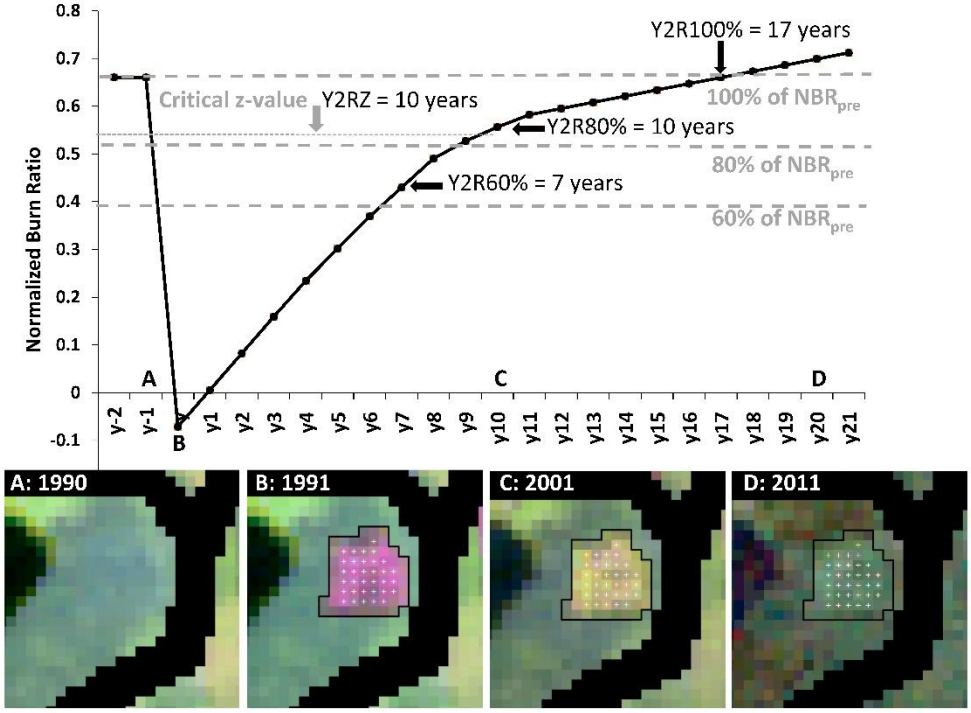

Figure 10. Illustration of the different Y2R thresholds tested in Study V: 60%, 80%, 100%, and a probabilistic threshold (critical z-value).

road, non-stand replacing changes) were evaluated by allocating the 600 samples within the change strata equally to each of the four change types (n = 150). Lastly, in order to report the frequency with which change events were detected within the correct year, the 600 samples within the change strata were also allocated equally among the 25 years. Each sample was manually interpreted by the same interpreter who was trained to visually recognize the four change types, and was given reference examples to use as a guide. Interpretations were then checked by a second, independent interpreter to ensure consistency. The annual BAP images composites and high spatial resolution imagery from Google Earth™ were the main reference data sources. Other ancillary data were used to support interpretation, including the Canadian National Fire Database (Burton et al. 2008) and regional spatial coverages depicting the locations of insect damages. Samples were identified as either change or no-change; in the case of change, the year and change type were also recorded. A confusion matrix was generated based on estimated class area proportions, from which overall user's and producer's accuracies per class were computed to assess the commission and omission errors as well as error bounds (Olofsson et al. 2014). The temporal accuracy of the change detection was also evaluated by comparing the change year with the reference year. The temporal accuracy of detected changes occurring within three years of the reference events was assessed. Changes detected with a difference of four or more years from the reference data were directly flagged as detection errors. A

confusion matrix based on estimated class area proportions was also used to evaluate the accuracy on the attribution of the change agent (Hermosilla et al. 2015).

Finland

Information outputs generated for Finland in substudy V and subsequently used for analyses in substudies V and VI were evaluated using independent reference data, following the same approach as described for Canada. A stratified random sample of points was selected to evaluate the change detection outputs following the approach described in Olofsson et al. (2014) and similar to that implemented in Hermosilla et al. (2015; 2016). An overall sample size of 400 points was allocated equally to the change and no change strata. To assess the attribution of changes to the correct year, samples in the change strata (n = 200) were allocated approximately equally to each year in which changes were detected. Similar to methods outlined in Hermosilla et al. (2016), each sample was manually interpreted from the LTS as per Cohen et al. (2010), augmented by interpretation of high resolution Digital Globe imagery in Google Earth™, when available. The spatial support region for interpretation of each validation point was considered as the area corresponding to a 30 m Landsat pixel surrounding the point. An interpreter visually examined each sample and identified whether the pixel at the sample location was considered "changed" or "not changed", and in what year the change occurred. Results were summarized using a confusion matrix, with associated measures (e.g. producer's, user's, and overall accuracy) calculated using estimated area proportions of change and no change, as per Olofsson et al. (2014).

Airborne laser scanning data processing

In substudy V, ALS data processing was done independently for each production area to ensure metadata concerning data origin (i.e. data provider, sensor, and year of acquisition) was maintained. A rough skypoint classification (single points above the canopy height level) was conducted using Terrascan (Terrasolid Ltd) with a threshold value of 40 m to remove outliers. Ground and vegetation points were exported into new (.las) files for further processing. ALS elevation data were normalized to heights above ground and a spatial index for each 3 x 3 km tile was created to facilitate processing. A tessellation of 30 x 30 m grid cells identical to the footprint and orientation of Landsat pixels was then created and used to clip and generate metrics from the normalized ALS data. ALS metrics used in the analysis included the mean and standard deviation of ALS heights, ALS height percentiles (1%, 5%, 10%, 25%, 50%, 75%, 90%, 95%, 99%; referenced as p01, p05, p10, etcetera), and the percentage of ALS returns within specified height intervals relative to the total number of returns (1, 2, 3, 4, 5, 6, 7, 8, 9, 10, 15, 20, and 25 m; referenced as d00 for 0–1 m, d01 for 1–2 m, etcetera). Following on the recommendations of Ørka et al. (2016) and Korhonen et al. (2013), who studied the use of ALS data to characterize regenerating forests, no minimum height threshold (e.g. 2 m) was applied, and only first returns were used when calculating ALS metrics.

In substudy V, ALS data were used to assess the Years to Recovery or Y2R spectral metric of recovery. Forest structural benchmarks were established following the FAO definition of forest (FAO 2012), whereby canopy cover must exceed 10% and height must exceed 5 m. ALS data were used to determine whether the spectrally recovered pixel had

achieved these structural benchmarks. Canopy cover was measured using the sum of ALS point densities > 2 m, and height was assessed using the 99th height percentile.

Modeling stand development class and spectral recovery rates

In substudy VI, the LTS recovery metrics ($\Delta NBR_{regrowth}$, RI, and Y2R) were used to predict the stand development class, and seedling plot data were used to predict spectral recovery rates. In both cases, an ensemble regression tree algorithm (Breiman 2001) was used for classification. Correlation analysis was used to aid in screening candidate predictors. Random forests was implemented using the R packages *caret* (Kuhn 2018; Liaw and Weiner 2002; 2018) and the *cforest* function in the package *party* (Hothorn et al. 2006; Strobl et al. 2007; 2008; 2009). The number of trees to grow (*ntree*) was set to 1000, and the number of variables to use at each split (*mtry*) was optimized within caret. Finally, to determine those field-measured characteristics associated with plots that have slow and fast rates of spectral recovery we analyzed the variance in continuous seedling plot attributes by recovery group, and for the categorical seedling plot attributes (i.e., species, site type, and drainage), we analyzed the variance in Y2R.

RESULTS AND DISCUSSION

Information needs and their linkages to image compositing criteria (I)

Linking compositing approaches to information needs in a Canadian context (substudy I) indicated that a target DOY that corresponded to the growing season for the majority of the forested area of Canada (August 1), combined with a relatively narrow temporal window (± 30 days), resulted in a suitable data yield to support a broad range of forest monitoring information needs, while limiting phenological variation that may be detrimental to some applications. In this substudy, a BAP compositing approach was developed and prototyped both nationally for a single year (2010) and regionally on an annual basis for the period 1998–2012. A prototype national 2010 composite was generated for Canada using the aforementioned compositing rules. Approximately 17% of pixels nationally did not have a best observation for 2010 within ± 30 days of August 1. Expanding the compositing window to ± 45 days or ± 62 days reduced the percentage of pixels with no observations to 4% and < 1% respectively. To complete a 2010 national BAP composite, areas of no data in 2010 were populated with BAP observations from 2009 and 2011.

Annual composites were prototyped for sub-areas of Saskatchewan and Newfoundland for the period 1998 to 2012 (Figure 11). In Saskatchewan, 29% of pixels had BAP observations within ± 30 days of August 1 for all 15 years considered, and 74% of pixels had ≥ 13 years of observations. All pixels in Saskatchewan had at least 7 years of observations. For time series analyses and monitoring, consecutive years of missing data may be problematic, as they can reduce the accuracy with which disturbances can be attributed to the correct year (or can obscure the detection of non-stand replacing disturbances). In Saskatchewan, 14% of pixels had consecutive years of missing data, while 11% had just two consecutive years of missing observations. Consecutive years of missing data increased after the Landsat-7 ETM+ SLC-off failure in 2003, as SLC-off gaps recur

spatially. Compared to Saskatchewan, the BAP observation yield in Newfoundland for the 1998–2012 period was markedly lower, with <1% of pixels in Newfoundland having observations within ± 30 days of August 1 for all 14 years. However, 52% of pixels had ≥ 10 years of observations. All pixels in Newfoundland had ≥ 3 years of observations and 18% had no consecutive data gaps. Overall, 82% of pixels in Newfoundland were missing ≥ 2 consecutive years of observations, with consecutive data gaps increasing after 2003 (Figure 11).

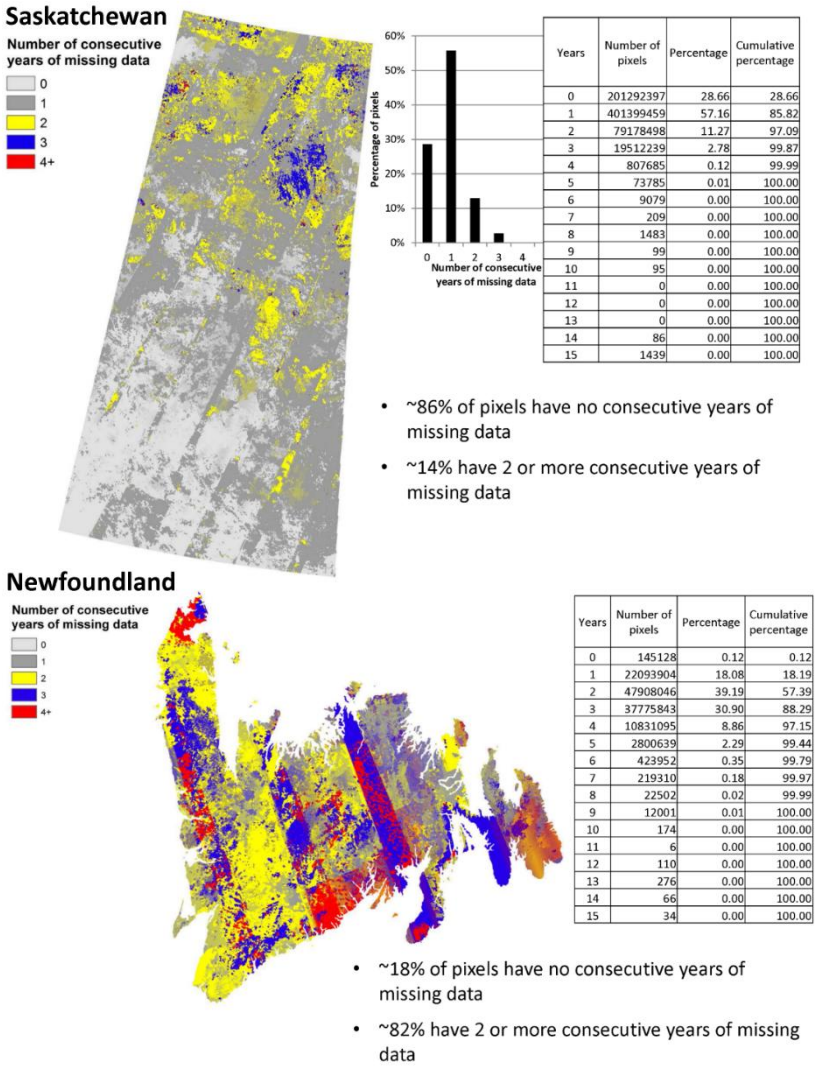

Years	Number of pixels	Percentage	Cumulative percentage
0	201292397	28.66	28.66
1	401399459	57.16	85.82
2	79178498	11.27	97.09
3	19512239	2.78	99.87
4	807685	0.12	99.99
5	73785	0.01	100.00
6	9079	0.00	100.00
7	209	0.00	100.00
8	1483	0.00	100.00
9	99	0.00	100.00
10	95	0.00	100.00
11	0	0.00	100.00
12	0	0.00	100.00
13	0	0.00	100.00
14	86	0.00	100.00
15	1439	0.00	100.00

Years	Number of pixels	Percentage	Cumulative percentage
0	145128	0.12	0.12
1	22093904	18.08	18.19
2	47908046	39.19	57.39
3	37775843	30.90	88.29
4	10831095	8.86	97.15
5	2800639	2.29	99.44
6	423952	0.35	99.79
7	219310	0.18	99.97
8	22502	0.02	99.99
9	12001	0.01	100.00
10	174	0.00	100.00
11	6	0.00	100.00
12	110	0.00	100.00
13	276	0.00	100.00
14	66	0.00	100.00
15	34	0.00	100.00

Figure 11. Consecutive data gaps in annual BAP composites for 1998–2012 (substudy I). Data gaps represent those pixels with no best available observation, resulting from clouds, cloud shadows, and ETM+ SLC-off data.

Correspondence between annual BAP and reference data were greatest in the near- and SWIR wavelengths (TM and ETM+ bands 4, 5 and 7) with $R^2 > 0.79$. Atmospheric effects were more prevalent in the visible wavelengths and correspondence between the BAP and the reference data was lower, with R^2 ranging from 0.60 to 0.75. These results indicate the regional variability in data yield for BAP compositing, highlighting issues for cloud-prone areas such as Newfoundland, as well as the opportunities for data yield in other areas such as Saskatchewan. In both regions, the temporal compositing window (August 1 ± 30 years) provided a sufficient data yield and is a reasonable trade-off against increased phenological variation that would result from expanding the temporal compositing window. The regional and national prototypes generated in this study demonstrate that annual BAP compositing is possible in a Canadian context, but that data gaps are an important limitation.

Methods for generating gap-free image composites over large areas (II)

Substudy II sought to address the limitations of the annual BAP compositing identified in substudy I by developing methods to fill data gaps with synthetic values. The protocol developed in substudy II (hereafter referred to as the Composite-to-Change, or C2C approach) takes advantage of the spatial and temporal context of the data gap. As a starting point, this study used the annual BAP composites generated in substudy I for Saskatchewan for 1998 to 2012 (Figure 12). On average 15% of pixels in each annual composite were missing a best observation (as a result of applying the scoring functions from substudy I). A noise detection approach was developed and applied in substudy II (Figure 7), resulting in an additional 7.5% of pixels on average for each annual composite being identified as noise (ranging from 5.8% to 9.6%), thereby creating additional data gaps. Overall, more than 50% of pixels had ≤ 3 years of missing observations. Noise detection was useful for mitigating residual clouds, haze, and smoke from wildfires (Figure 8). Contextual analysis in the spatial domain was useful for ensuring that the correct date was assigned to pixels, enabling reconstruction of the spectral response of the disturbance event (Figure 7).

Results of substudy II indicated that it was more difficult to generate an accurate proxy value when change events and data gaps were present in the pixel series. On average, pixel series with change events had a lower correlation between proxy and reference values (r = 0.76 versus 0.85 for no change pixels), a higher RMSE (0.019 versus 0.012), a greater bias (0.0005 versus 0.0002), and a larger CV (23.23 versus 17.09). Moreover, cumulative data gaps (years with missing observations) also had a negative impact on the generation of accurate proxy values. Correlation, RMSE, and CV were found to be relatively stable until there were 5 or more consecutive years of data gaps in the pixel series. Several years of consecutive data gaps may be a concern in areas that are very dynamic (i.e. that have a large amount of change annually), and where persistent, extensive cloud cover limits the availability of suitable imagery. In such circumstances, using spatial interpolation techniques to fill in data gaps may be considered as a complement to the lack of spectral information in the time series.

The C2C protocol as applied to the annual BAP composites from substudy I, resulting in the gap-free proxy BAP composites shown in Figure 12. The average annual area of change in Saskatchewan for the period 2000–2010 was highly variable, with a mean of 393,600 ha

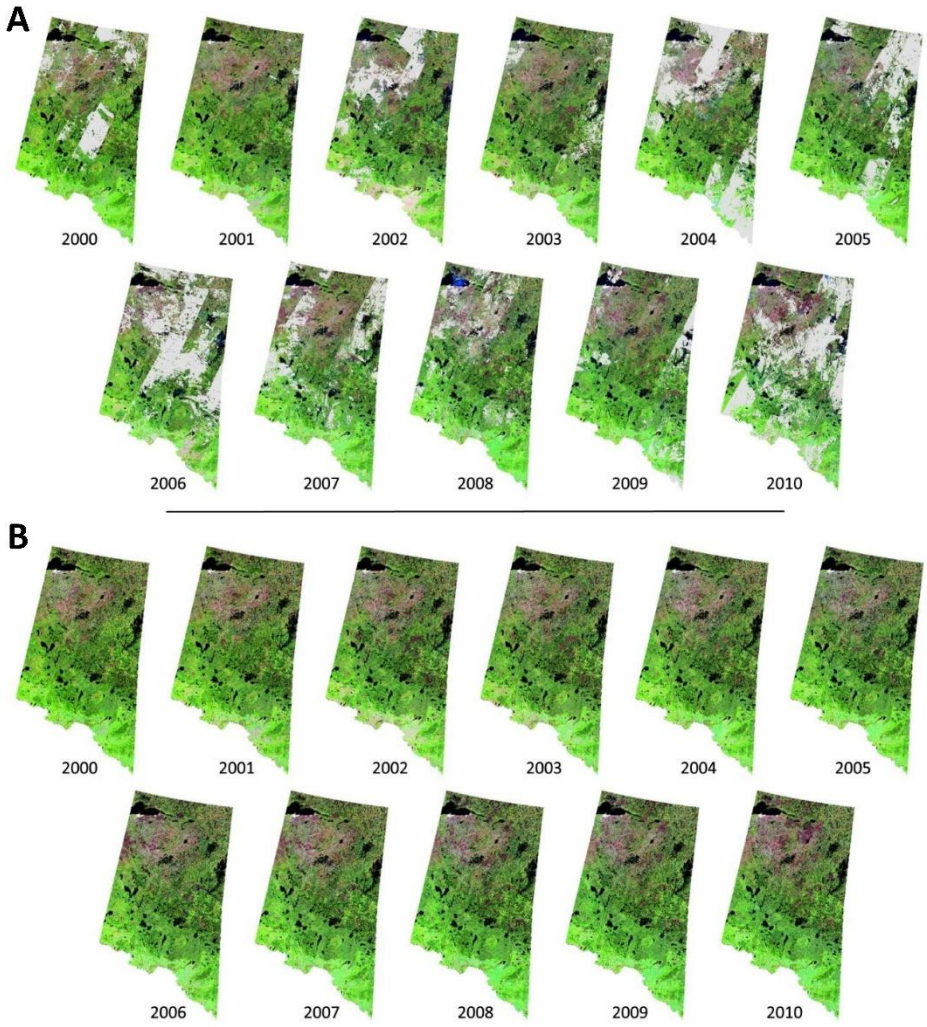

Figure 12. (A) Annual BAP composites for forested area of Saskatchewan, Canada (2000–2010). Data gaps (grey) result from a lack of observations (as a function of cloud, cloud shadows, ETM+ SLC-off), as well as from the noise removal process applied in the C2C protocol (see also Figures 5 and 6); (B) Gap-filled proxy BAP surface reflectance composites generated using the C2C protocol.

and a large standard deviation (292,000 ha). Change metrics generated by the C2C protocol (Table 4) enable the attribution of change types, as demonstrated in Hermosilla et al. (2015). In the north of Saskatchewan, change events were large and of a high magnitude, with a shorter persistence (wildfire), whereas in the south, change events were smaller and generally persisted for > 1 year (harvesting).

Information outcomes: a national 25-year summary of disturbance and recovery (III)

Substudy III made use of national change products for Canada generated using the C2C protocol of substudy II and subsequently deployed nationally (Hermosilla et al. 2016). Detected changes were attributed to change type (wildfire, harvest, non-stand-replacing change) following the approach described in Hermosilla et al. (2015). The accuracy of the change outcomes that were used in substudy III were assessed and reported in Hermosilla et al. (2016). Overall change detection accuracy was 89%, with 89.3% of changes labelled to the correct year and 97.7% labelled to within ± 1 year. User's and producer's accuracies for wildfire were 98% and 93%, respectively. For harvest, user's and producer's accuracies were both 88%.

Over the period 1985 to 2010, approximately 57.5 Mha or 10.75% of Canada's net ecosystem area (exclusive of water) were disturbed by wildfire and harvest (Figure 13). This represents an annual rate of disturbance of 0.43%. Wildfire was by far the dominant stand replacing disturbance, accounting for 2.5 times more area than harvesting. On average, wildfire in Canada's forested ecosystems impacted 1.6 Mha annually but was highly variable from year to year (standard deviation = 1.1 Mha), while harvesting impacted 0.65 Mha (standard deviation = 0.1 Mha). By ecozone (Figure 5), the Boreal Shield West had the greatest amount of stand replacing disturbance for this 25-year period (12.6 Mha), while the Pacific Maritime had the least (0.8 Mha). Wildfire was also the dominant change in the majority of ecozones, with the exception of the Atlantic Maritime, Pacific Maritime, Montane Cordillera, and Boreal Shield East where harvesting accounted for more disturbed area.

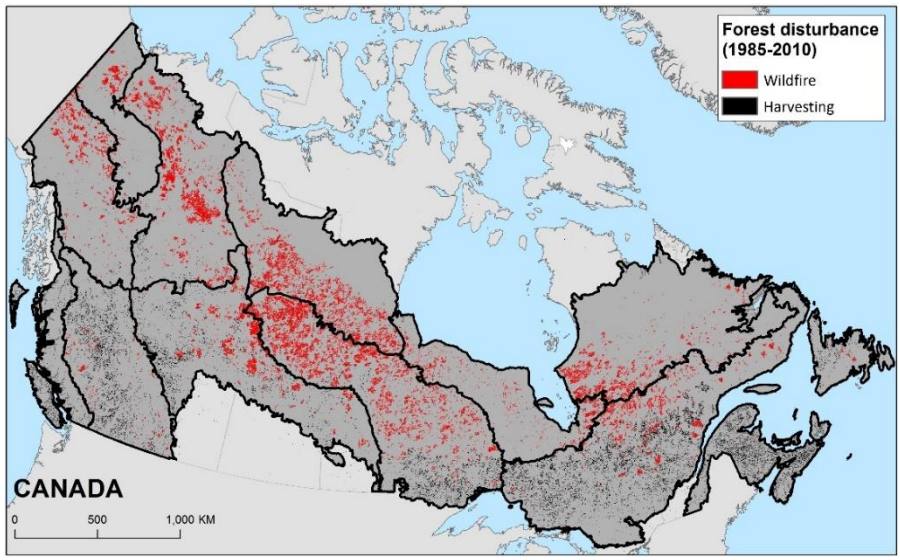

Figure 13. Area disturbed by wildfire and harvest in Canada's forested ecosystems (1985–2010).

C2C outcomes were compared to other national disturbance datasets. Canada currently has no national, spatially-explicit record of forest harvest and while some jurisdictions in Canada do maintain spatial records, these records are not spatially or temporally consistent. As the use of geographic information systems (GIS) have become more common in forest management agencies, spatial records of forest harvesting are increasingly common (Leckie and Gillis 1995). The Canadian Forest Service maintains the National Forestry Database (NFD; http://nfdp.ccfm.org/), which is a compendium of national forest statistics. The area harvested is reported annually by each jurisdiction in Canada. The NFD data do not report harvesting on private land. On public lands, all forms of harvesting are reported, including partial or selective harvests (harvesting is distinguished by type: partial or clearcut). Harvesting is sometimes reported from operational plans, which may not represent the actual areas harvested in any given year; reporting methods have varied by jurisdiction and over time. Furthermore, the reporting period for government agencies typically is from April 1 of the calendar year to March 31 of the following calendar year, and for years pre-1990, the NFD contains harvest numbers that were estimated by the Canadian Forest Service (i.e. not reported by jurisdictions). Lastly, the NFD reports harvest by jurisdiction, not by ecozone, and while C2C estimates of harvest are restricted to forest dominated ecosystems, the NFD includes harvest data from outside this area (which is expected to represent a small area). Given these caveats, differences in total area reported as harvest are expected between the C2C spatial output and the NFD aspatial estimates. The NFD estimated the average annual area clearcut in Canada (1985–2010) was 0.82 Mha. C2C estimated the average annual area at 0.65 Mha. The NFD shows a somewhat consistent trend in area harvested over time; however, C2C shows an increasing trend in area harvested over time, from 415,000 ha in 1985 to 866,000 ha in 2005. Differences in trends over time between C2C and NFD may be explained by the factors noted above. While the C2C outputs were vetted through two independent accuracy assessments, the numbers reported in the NFD are have not been similarly vetted. Of note, Masek et al. (2011) identified an increasing trend in harvest levels in certain jurisdictions and this is reflected in the NFD data for those jurisdictions. Interestingly, correspondence between C2C and NFD has increased over time with the advent of GIS systems in forest management agencies and these data are used as the source of the jurisdictional estimates in the NFD.

For wildfire, comparisons with the C2C outcomes were undertaken between the NFD, and the Canadian National Fire Database (CNFDB). The NFD and CNFDB estimate the annual area impacted by wildfire at 2.3 Mha, whereas C2C estimates 1.6 Mha. Differences are greatest in the years with the greatest amount of wildfire, and the amount of wildfire in a given year explained a significant proportion of the variance in the absolute difference between the C2C and CNFDB estimates of wildfire area (R^2 = 0.692). The largest fires for the time period were examined (the N largest fires that accounted for > 50% of wildfire area). On average, C2C identified 61% of these areas as being disturbed by wildfire, highlighting the refined detection and mapping of wildfires using Landsat data, and the importance of excluding unburned islands and water bodies from fire perimeters (Stinson et al. 2011).

Short- and long-term measures of recovery revealed different recovery trends for areas impacted by wildfire and harvest. Using an absolute measure of recovery at 5 years ($\Delta NBR_{regrowth}$), 86.8% of areas impacted by wildfire and 85.8% of areas impacted by harvest had positive $\Delta NBR_{regrowth}$ values indicative of spectral recovery. The average $\Delta NBR_{regrowth}$ values were 0.36 for wildfire (σ = 0.22) and 0.26 for harvest (σ = 0.14). Ecozone-level trends were consistent with those found nationally. Using a relative measure

of recovery at 5 years (Recovery Indicator or RI), 95.7% of wildfire areas and 93.9% of harvested areas had positive spectral recovery. Accounting for the magnitude of disturbance in the RI resulted in harvested areas generally having greater spectral recovery than wildfire areas. These two short-term metrics provide an initial assessment of recovery that is influenced by residual vegetation, as well as herbaceous and shrub vegetation. These metrics are therefore indicative of a greening or return of vegetation to a site, but not necessarily the return of forest structure.

The Y2R metric assesses longer-term spectral recovery and relates how many years it takes for a pixel to return to 80% of its pre-disturbance NBR value (Figure 9). Results of substudy III indicate that 68.4% of wildfire areas and 92.5% of harvest areas attained the 80% benchmark by the end of the time series in 2010 (Figure 14). Considering only those disturbances that occurred prior to 1990, 86.3% of wildfire and 98.4% of harvest areas achieved the Y2R benchmark, indicating that given sufficient time, forests will return to their pre-disturbance spectral characteristics. The national Y2R average value was 10.6 years (σ = 5.6 years) for wildfire and 6.6 years (σ = 3.9 years) for harvest areas. Nationally, 35.5% of wildfire areas and 78.5% of harvested areas had a Y2R value that was $\leq$ 10 years.

Generally, the relative percentage of pixels that were non-recovered was small: < 1% of areas disturbed by wildfire and harvest were considered as non-recovering by all three measures of spectral recovery, whilst 77.4% of harvest and 57.4% of areas disturbed by wildfire were considered as spectrally recovered by all 3 metrics. By the end of the time series in 2010, 15% of areas disturbed by wildfire and harvest that were identified as non-recovering by the short term metrics, were recovered by 2010.

Trends in non-recovery were not consistent among disturbance types. For example, 28.7% of areas disturbed by wildfire that were identified as recovering by the short-term metrics had not yet recovered using the Y2R by the end of the time series in 2010. Approximately 50% of these pixels were disturbed prior to 2000, and 6.8% were disturbed prior to 1990. For harvested areas, only 6.7% of the area identified as recovering by the short-term metrics had not yet recovered by 2010. Approximately 21% of this area was harvested prior to 2000, and only 3.2% prior to 1990. Over the longer-term therefore, areas impacted by harvesting are recovering more consistently than areas impacted by harvesting.

The C2C data provides an unprecedented opportunity to characterize variability in post-disturbance vegetation recovery in Canada's forested ecosystems in a consistent and systematic fashion by ecozone and disturbance type. Also critical to understanding vegetation recovery post-disturbance is the variability in recovery trends across forested ecosystems, which for a country like Canada with such a large and diverse range of forest conditions, is difficult to quantify on the basis of a small number of field plots alone (Bartels et al. 2016).

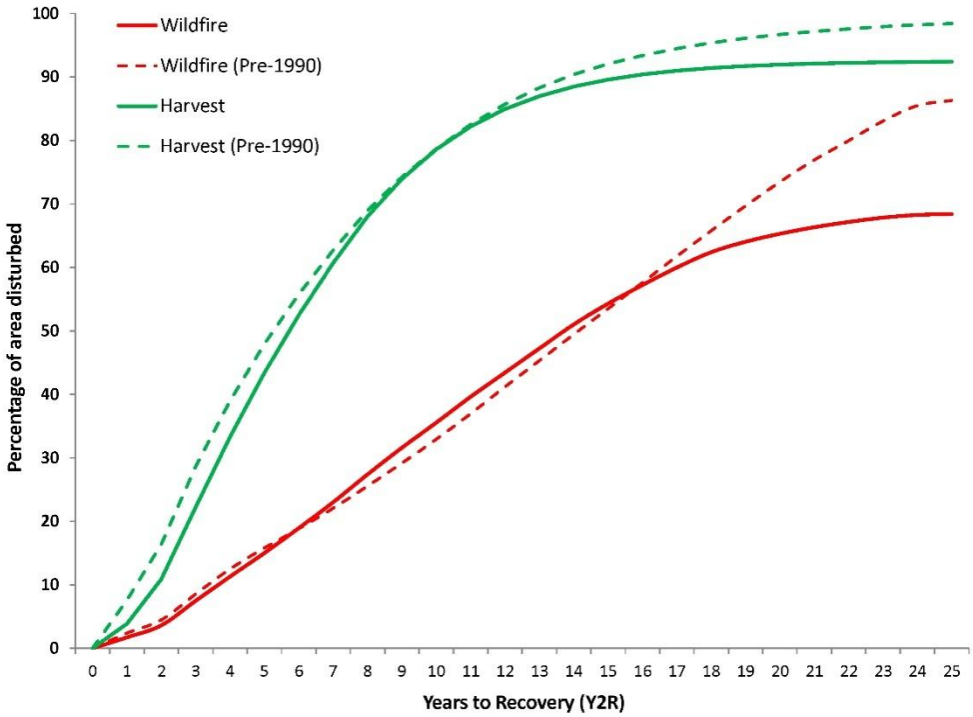

Figure 14. A summary of Years to Recovery (Y2R) for areas impacted by wildfire and harvest in Canada's forested ecosystems.

Finnish context: Information needs and data availability for forest monitoring (IV)

There were a total of 30,076 images for Finland in the USGS Landsat archive. The bulk of these images were acquired with TM (42.8%) and ETM+ (31.8%; Figure 15). In Canada, the distribution of pre-OLI data (1984-2012) was 57% TM and 26% ETM+ (White and Wulder 2013). The temporal distribution of archive Landsat images for Finland reflect inconsistencies in program administration over time with little data available prior to 1984, and between 1991 and 1993, and likewise between 1995 and 1997 (Goward et al. 2017). Overall, more than two-thirds (68.5%) of the available archived data for Finland were acquired after the launch of Landsat-7 (ETM+), primarily as a result of the implementation of a systematic, long-term acquisition plan (Arvidson et al. 2001). Of note, data from OLI accounted for 19.1% of available archived images even though OLI has only been acquiring data since 2013. Moreover, the rate at which OLI is acquiring data for Finland is almost double that at which TM and ETM+ data were acquired. For BAP compositing, 16.3% of total archive holdings were considered suitable according to the criteria of substudy I, and approximately 72.3% of land area has sufficient data. Landsat data density was greater in

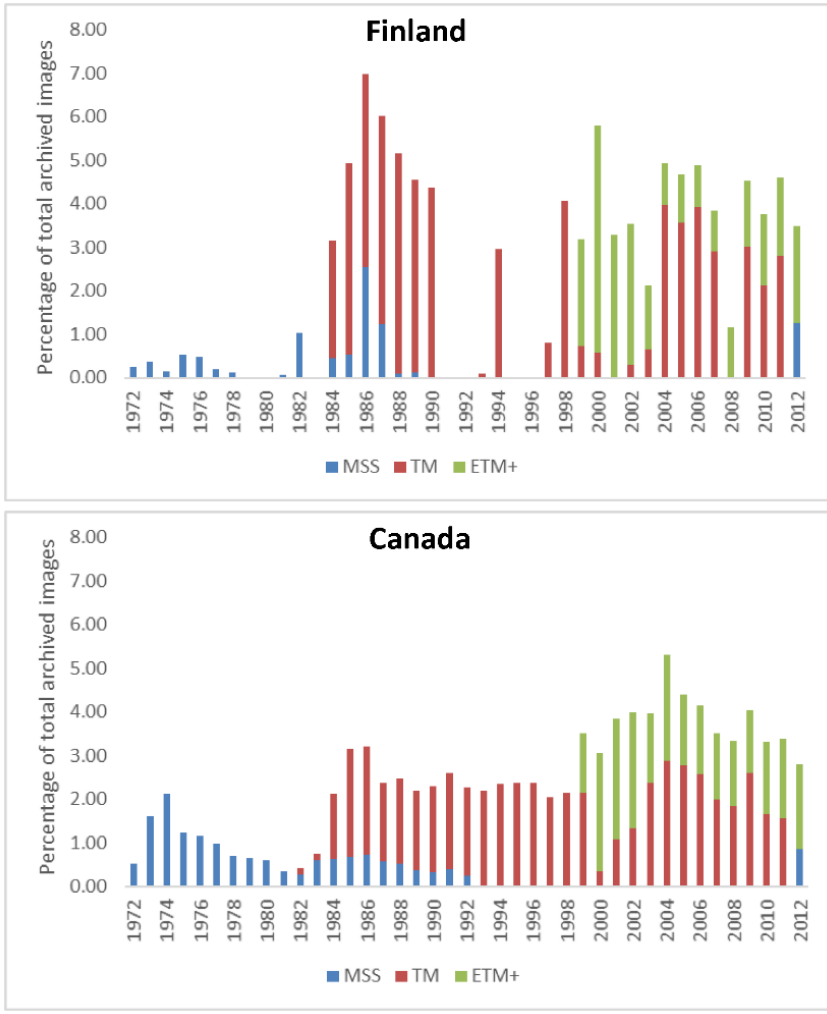

Figure 15. A comparison of the temporal distribution of USGS Landsat archive images for Finland and Canada (1972–2012).

southern Finland with overlap areas between WRS-2 scenes providing increased observational density to support image compositing.

Finland has a long-standing history of incorporating Landsat data into national forest information products through the MS-NFI. Tomppo et al. (2008a) suggested that one potential means of enhancing the MS-NFI would be to incorporate historical data as a source of additional information on the age and development of forests. The MS-NFI was first introduced during the eighth NFI for which the field measurements were carried out between 1986 and 1994. During this period, the coverage of the USGS Landsat archive in Finland is very limited, particularly for 1991–1997 (with the exception of 1994). The 1980s

and 1990s represented a period of instability in the Landsat program, with Landsat data priced for cost recovery by NOAA, and programmatic control of Landsats 4 and 5 (and development of Landsat 6) transferred from the United States government (NOAA) to the private sector (EOSAT) from 1985 until 2001. During this commercialization period, costs for Landsat data increased dramatically and demand fell. The global Landsat archive holdings suffered most significantly during this time. In the absence of a long-term acquisition plan, and faced with substantial data downlink costs, acquisitions became increasingly US-centric and were demand-driven (Goward et al. 2017). In particular, acquisitions were very limited between 1985 and 1992. EOSAT had to pay NASA for data downlink from Landsat 4 via the Tracking and Data Relay Satellite System (TDRSS) and transmissions decreased to two scenes daily in 1991 and ended in 1993 with the failure of onboard relay capacity. By 1992, Landsat 5 only had X-band downlink functionality, meaning the only way to download data from the satellite was via X-band, when the satellite was within proximity of a ground stations. Although International Cooperators continued to downlink data, they were also applying the same cost-recovery model as EOSAT, with a similar data pricing structure. Moreover, few International Cooperators had data reciprocity agreements with EOSAT. The Kiruna ground station in Sweden was one of the few International Cooperators sending data back to EOSAT (1993–1997; Goward et al. 2017). Faced with significant funding shortfalls from the US Government, EOSAT ceased processing Landsat data by the end of 1992 and did not resume processing until 1994. Other relevant events during this time included the passing of the Land Remote Sensing Policy Act of 1992 in the United States, which transferred control of the Landsat program back to the US Government with the development of Landsat 7, and the failure of the Landsat 6 launch in 1993. EOSAT (and later Space Imaging) continued to control the operation of Landsat 5 until 2001 when satellite operations were turned over to the USGS.

Through the Landsat Global Archive Consolidation project, which saw the repatriation of Landsat data from International Cooperators' holdings back to the USGS (Wulder et al. 2016), it was discovered that approximately 250,000 TM images that were downloaded from Landsats 4 and 5 had no Payload Correction Data (PCD). PCD contains information required to correct for geometric disturbances that occur during image acquisition. Without PCD, the TM images cannot be corrected to the level required for ingestion into the archive. As of February 2018, the USGS has developed a method to correct these data and bring them into the archive. For Finland, it is estimated that there are approximately 786 TM images that are lacking PCD, and the vast majority of these (614) were acquired in 1997 (Shaw and Loveland, 2017). The suitability of these images for compositing remains to be determined; however, regardless, these images do not provide substantial additional data for those years with the greatest paucity of observations.

Confirmation of post-harvest spectral recovery using ALS data (V)

At the study site in southern Finland, a total of 117,901 change events were detected within the area of the forest mask (1991–2011), with a mean change event size of 1.85 ha. Changes were detected with an overall accuracy of 89%, with 85.88% of changes attributed to the correct year, and 94% to ± 1 year. Approximately 33,164 changes were identified as clearcuts, with a mean size of 3.83 ha. In order to assess longer-term post-harvest recovery, only change events that occurred in 1991 (3697 events; 40,365 pixels) were further analyzed.

In substudy V, varying thresholds were applied to the Y2R metric: 60%, 80%, 100%, and a probabilistic threshold indicating when a pixel was no longer statistically significantly different from its pre-disturbance value (Figure 10). As the spectral threshold indicative of recovery increases from 60% to 100%, the number of years required for a harvested pixel to attain this threshold also increases (Figure 16). For the Y2R60% and Y2R80% recovery scenarios, all pixels in all recovery groups were considered spectrally recovered by the end of the time series. The Y2R80% and Y2RZ scenarios had similar distributions of pixels among the different recovery groups, but the Y2RZ identified 1.67% of pixels as not recovered. Conversely, the Y2R100% scenario resulted in 31% of pixels identified as not recovered.

Differences in ALS metrics between the different recovery groups were compared for each recovery scenario. In terms of ALS metrics examined, the largest significant differences between recovery groups were for the density metric d00 (the density of ALS returns within 0–1 m of the ground surface), and the 99th percentile of ALS heights. Generally, differences in ALS metrics between groups decreased with the increasing spectral threshold used to define recovery. For example, the maximum difference among recovery groups for d00 was 28.61% for Y2R60%, compared to only 4.275% for Y2R100%. Likewise, the maximum difference for p99 was 4.68 m for the Y2R60% scenario, compared to only 1.03 m for the Y2R100% scenario. Generally, pixels that were considered as spectrally recovered within 10 or fewer years (recovery group 1) had larger median values for ALS height percentiles p75, p90, p95, p99, relative to pixels that took longer to recover. Therefore, pixels that recovered rapidly were taller on average at the time of ALS measurement, than pixels that took longer to recover. This relationship with ALS-measured forest structure confirms the utility and appropriateness of the Y2R metric as an indicator of forest recovery in the boreal forest environment studied. Regardless of the Y2R threshold used herein, pixels that recovered rapidly had larger median values for the upper ALS height percentiles; conversely, pixels that took longer to recover had smaller median values for height percentiles.

For the Y2R100% scenario, a subset of pixels were analyzed in which the year of spectral recovery was the same as the year of ALS acquisition. Within this subset, the Y2R ranged from 17 to 22 years (i.e. all pixels were within this recovery group). Of note, differences in mean values for the ALS metrics were markedly lower among the Y2R within this single recovery group than between recovery groups.

Pixels were assessed according to benchmarks of cover and height derived from the ALS data. The relative distribution of pixels among the benchmark categories within recovery groups was relatively consistent across all four scenarios: benchmarks of height were more commonly achieved than benchmarks of cover, while achieving benchmarks of both cover and height was most common overall. Other studies have similarly reported that height growth post-disturbance is more rapid than the return of canopy cover (Bartels et al. 2016; Bolton et al. 2017).

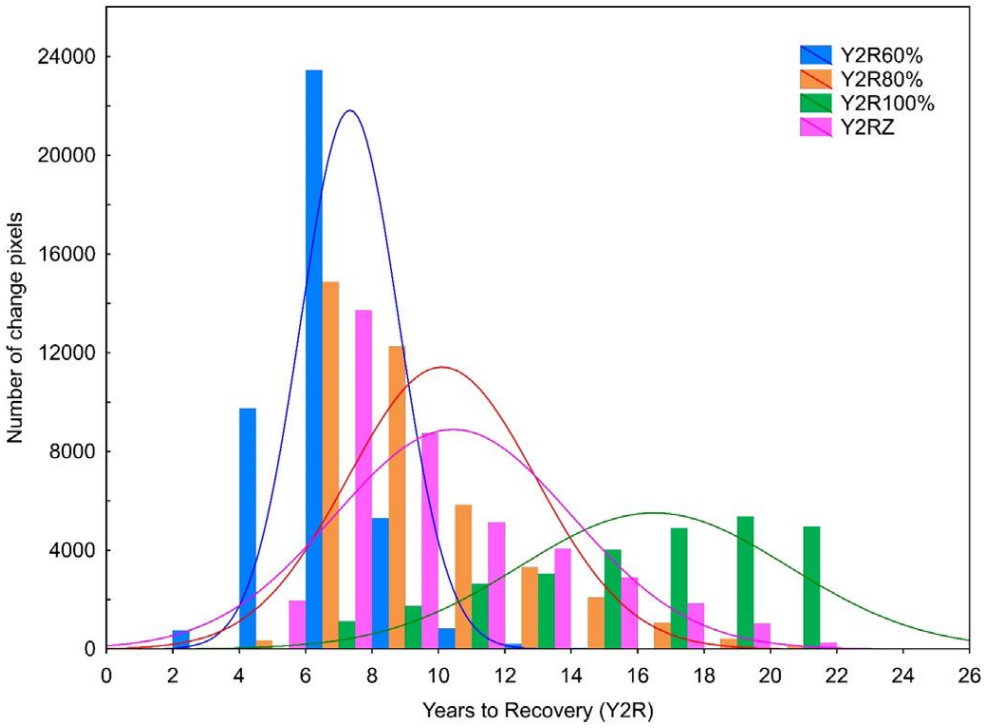

Figure 16. Relative distribution of pixels by Y2R scenario. Lines represent the fitted normal distribution.

Differences between recovery groups decreased with an increasing spectral threshold for recovery, indicating that with the longer recovery times required to achieve a higher target spectral threshold (i.e. 100%), forest structural conditions in terms of height and cover, begin to converge. The 60% spectral threshold was found to provide an overly optimistic scenario of forest recovery, with pixels able to attain spectral recovery rapidly, before attaining benchmarks of forest structure. For example, only about half of pixels that the Y2R60% scenario indicated as spectrally recovered in 14–17 years had achieved the benchmarks for both cover and height, compared to approximately 80% of Y2R80% pixels in that same recovery group (Table 5). Furthermore, under the Y2R60% scenario, 2.5 times as many pixels that were spectrally recovered in <10 years had not yet achieved the structure benchmarks, compared to the Y2R80% scenario. Likewise, the Y2R100% may be an excessively pessimistic threshold, with more than 86% of pixels that were considered as not yet spectrally recovered by the end of the time series having already attained the benchmark values of cover and height (Table 5). As noted by Pickell et al. (2016), it may be unrealistic to assume that a pixel will return to 100% of its pre-disturbance value within the temporal window of the LTS, particularly if the forest was mature prior to disturbance (as in our study) or there was a change in dominant species or management practices post disturbance that would alter the density and configuration of the canopy, and thereby also the reflectance properties of the stand. As noted by Song et al. (2002), successional reflectance trajectories are noisy and are driven by a myriad of factors.

Table 5. Percentage of pixels within each of the recovery groups that achieved the indicated benchmarks of cover (> 10%), height (> 5 m), both cover and height, or neither benchmarks, by recovery scenario.

Benchmarks of recovery	***Recovered***					***Not recovered***
	<10 years	**11–13 years**	**14–17 years**	**>17 years**	**Total**	
Y2R60%						
cover	1.29	0.22	0	0	1.52	0
height	5.08	0.41	0.06	0	5.55	0
cover & height	84.2	4.51	0.17	0	88.88	0
none	3.38	0.58	0.09	0	4.05	0
TOTAL	**93.96**	**5.72**	**0.32**	**0**		**0**
Y2R80%						
cover	0.47	0.69	0.31	0.05	1.52	0
height	2.71	1.81	0.75	0.28	5.55	0
cover & height	50.75	27.58	8.73	1.82	88.88	0
none	1.39	1.52	0.83	0.3	4.05	0
TOTAL	**55.32**	**31.6**	**10.63**	**2.45**		**0**
Y2R100%						
cover	0.05	0.14	0.32	0.58	1.09	0.42
height	0.2	0.5	0.82	1.79	3.3	2.25
cover & height	4.43	11.34	18.35	27.92	62.04	26.84
none	0.13	0.29	0.54	1.62	2.58	1.48
TOTAL	**4.8**	**12.27**	**20.03**	**31.91**		**30.99**
Y2RZ						
cover	0.47	0.57	0.34	0.09	1.48	0.04
height	2.42	1.56	0.9	0.49	5.37	0.18
cover & height	45.92	25	12.48	4.14	87.54	1.34
none	1.33	1.27	0.9	0.44	3.94	0.11
TOTAL	**50.14**	**28.41**	**14.62**	**5.17**		**1.67**

The results of substudy V demonstrate that LTS-derived spectral measures of recovery, specifically the Y2R or number of years required for a pixel to return to a certain percentage of its pre-disturbance NBR value, relate to measures of forest cover and height derived from ALS data. For post-harvest scenarios in managed boreal forests of southern Finland, the Y2R80% scenario provided the most realistic assessment of recovery. Using the 80% threshold, the majority of pixels identified as spectrally recovered had attained the benchmarks of cover and height, as derived from the ALS data. Moreover, with the 80% threshold, false positives (spectral recovery attained, structural benchmarks not attained), and false negatives (spectral recovery not attained, structural benchmarks attained) were minimized. False positives were more common for the Y2R60% scenario, while false negatives accounted for 26.84% of pixels under the Y2R100% scenario. Under the Y2R80% scenario, all pixels were considered recovered within the time period assessed, and sites that recovered rapidly (< 10 years) had forest structural properties at the time of ALS measurement that were distinct from sites that took longer (i.e. >17 years) to recover.

Assessing post-harvest spectral recovery with field plot data (VI)

Substudy VI builds on the results of substudy V and seeks to further increase understanding of spectral measures of recovery through the use of field plot data. Seedling plots were measured in the year the plot was considered spectrally recovered by the Y2R metric (using an 80% threshold). Short and long-term LTS spectral recovery metrics discriminated the young and advanced seedling stand development classes with an overall accuracy of 73.59% ± 5.11% (Table 6Table 6).

Table 6. Confusion matrix for classification of stand development class. T1 = young seedling stand; T2 = advanced seedling stand.

	Observed				
Predicted	**T1**	**T2**	**Total**	**User's accuracy**	**Commission error**
T1	45	31	**75**	59.25%	40.75%
T2	44	164	**208**	78.75%	21.25%
Total	**89**	**195**	**209**		
Producer's accuracy	50.16%	84.26%		**Overall accuracy**	**Margin of error**
Omission error	49.84%	15.74%		**73.59%**	**± 5.11%**

Seedling plot attributes were then used to discriminate the three spectral recovery groups with an overall accuracy of 61.06% (± 5.67%; Table 7). Producer's accuracy was high for recovery groups 1 and 3 (70.51% and 68.69% respectively), but was low for recovery group 2 (43.64%). Likewise user's accuracies were comparable for recovery groups 1 and 3 (~66%), and lower for recovery group 2 (48.95%). Confusion was greater between recovery groups 1 and 2. Conversely, there was relatively minor confusion between recovery groups 1 and 3. The most important predictors were mean height, dominant species, percent deciduous, height ratio, site type, and coefficient of variation of stem density. Examples of the three recovery groups at mesic and xeric sites are shown in Figure 17.

Table 7. Confusion matrix for 5-year spectral recovery groups. RG1 = spectral recovery in 1–5 years, RG2 = 6–10 years, RG3 = 11–15 years.

	Observed					
Predicted	**RG1**	**RG2**	**RG3**	**Total**	**User's accuracy**	**Commission error**
RG1	71	33	3	**107**	66.40%	33.60%
RG2	19	41	24	**84**	48.95%	51.35%
RG3	11	20	61	**92**	66.15%	33.85%
Total	**101**	**94**	**89**	**173**		
Producer's accuracy	70.51%	43.64%	68.69%		**Overall accuracy**	**Margin of error**
Omission error	29.49%	56.36%	31.31%		61.06%	± 5.67%

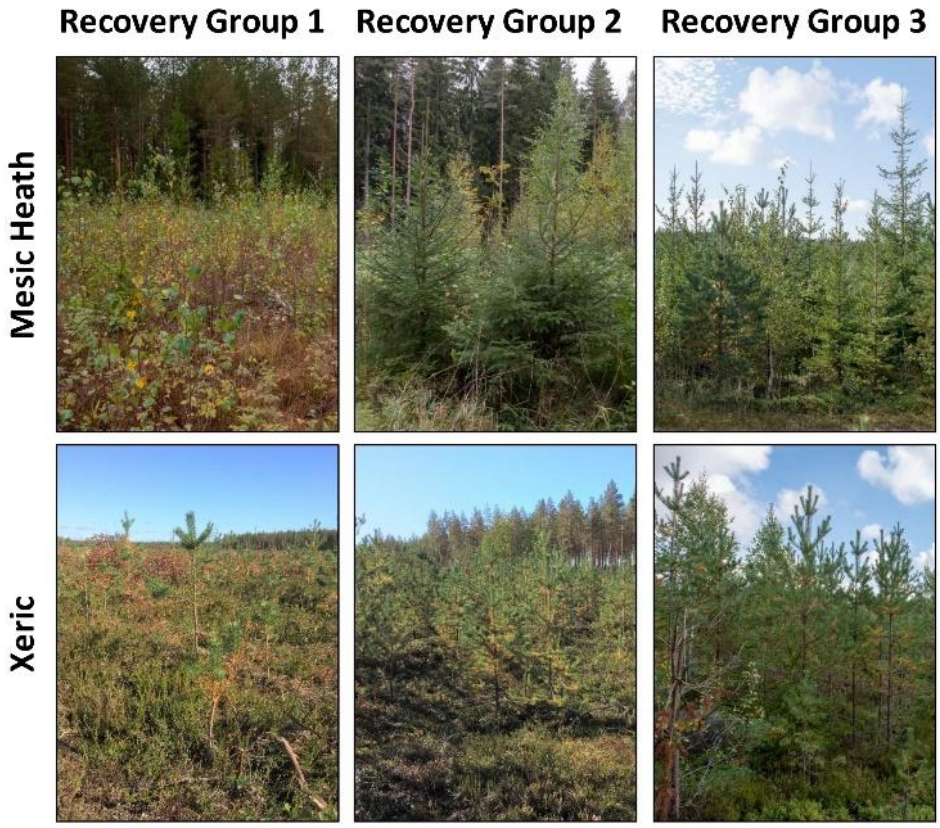

Figure 17. Examples of the three recovery groups (1: recovery in < 5 years; 2: 5–10 years, and 3: 10–15 years) for the mesic heath and xeric sites.

One-way ANOVAs indicated significant differences in mean height among spectral recovery groups ($F_{(2,281)}$ = 50.96, p = 0.00), and post-hoc Tukey tests indicated that there were significant differences in mean height amongst all three recovery groups (Figure 18). The average mean height for recovery group 1 was 1.4 m, compared to 3.29 m for recovery group 3. There were also significant differences in percent deciduous ($F_{(2,281)}$ = 7.29, p = 0.00) by recovery group, and post-hoc Tukey tests indicated significant differences between recovery groups 1 and 3, and groups 2 and 3, but not between groups 1 and 2 (Figure 18). The average percentage of stems that were deciduous in recovery group 1 was 69%, compared to 49% for group 3. No thinnings or treatments had been applied to any of the seedling plots. No significant differences were found between recovery groups for coefficient of variation in stem density ($F_{(2,281)}$ = 0.329, p = 0.72) (Figure 18); however, there were significant differences in total stem density ($F_{(2,281)}$ = 3.74, p = 0.02) between groups 1 (mean = 9322 stems) and 3 (mean = 6264 stems).

Height was consistently the most important predictor of spectral recovery rates. The trend in the seedling plot data whereby height increased with increasing Y2R80 (Figure 18) is

typical of spectral trends associated with increasing time since disturbance (Horler and Ahern 1986, Nilson and Peterson 1994, Olsson 2009). Height is used as an indicator of recovery (Bartels et al. 2016; substudy V) and is fundamental to many definitions of forests (Chazdon et al. 2016). The relationship between height and Y2R80 was moderate (r = 0.55) for the seedling plot data used in substudy VI. Seedling plots were measured in the year in which spectral recovery was achieved, and it was observed that stands that recovered rapidly (i.e. < 5 years), were on average shorter in the year they recovered than stands that took longer to recover. This finding aligns with knowledge of stand development post-disturbance (Oliver and Larson 1996), and the fact that the seedling plots represent a chronosequence of time since disturbance. These results should be considered in the context of the results reported in substudy V. Therein, the heights of stands that were harvested in 1991 at the same study site in southern Finland as used herein, were assessed against benchmarks of cover and height derived from the ALS data. In substudy V, pixels that had rapid spectral recovery (i.e. < 10 years) had significantly larger median values for ALS height percentiles (75th, 90th, 95th, and 99th) relative to pixels that took longer to recover. Therefore, pixels that recovered rapidly were taller on average at the time of ALS measurement, than pixels that took longer to recover. Results indicated that there is marked variability in heights in regenerating forests, particularly within 10 years post-disturbance and that while height may be a useful indicator of recovery, height is also the structural manifestation of other site factors that influence the recovery process. Even in northern Finland though, natural regeneration was found to effectively restock stands to required density and heights within 13–15 years post-disturbance (Valkonen and Siitonen 2016). In southern Finland, mean stand height at 10 years of age typically ranges from 2.4–2.7 m (Valkonen et al. 2011).

Variability in spectral recovery was also influenced by species and site factors, including the amount of deciduous tree species that establish at a site, as well as the heights of those deciduous species relative to the coniferous stems present at the site. As indicated in Figure 18, an abundance of deciduous species in a plot influences the rate of spectral recovery.

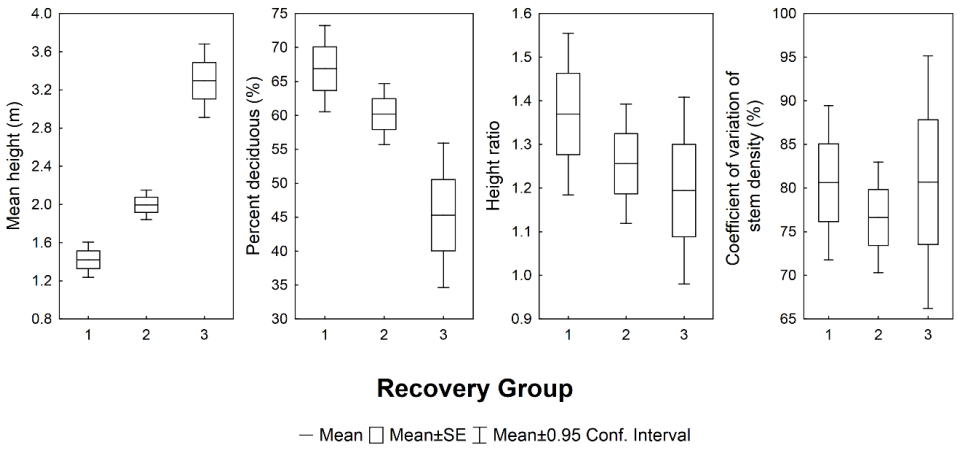

Figure 18. Seedling plot characteristics, by recovery group.

On average, seedling plots in recovery group 1 had a higher percentage of deciduous stems (66%), than recovery group 3 (45%). As noted by Bartels et al. (2016), regeneration by remnant species at a site can influence recovery, with deciduous species that can regenerate vegetatively establishing much more quickly at a site than species that regenerate from seed. In turn, these deciduous species can grow rapidly on productive sites, further influencing assessments of recovery rates that use height thresholds as an indicator of recovery. For example, Valkonen and Ruuska (2003) found that the average height of naturally emerged birches was consistently 1 m greater that of planted pines at the age of 6–13 years in southern Finland.

A one-way ANOVA indicated significant differences in mean Y2R values among dominant species ($F_{(2,283)} = 12.91$, $p = 0.00$). Post-hoc Tukey tests revealed that there were significant differences ($p < 0.05$) in Y2R between Scots pine (mean = 8.4 years, sd = 3.6 years) and both Norway spruce (mean = 6.2 years, sd = 2.7 years) and deciduous species (mean = 6.7 years, sd = 3.1 years), but not between Norway Spruce and deciduous dominated plots (Figure 19). Likewise, we found significant differences in Y2R among site types ($F_{(3,282)} = 6.77$, $p = 0.00$), with a post-hoc Tukey test indicating significant differences ($p < 0.05$) in Y2R between heath (mean = 6.1 years, sd = 2.6 years) / mesic heath (mean = 6.7 years, sd = 3.3 years) site types, and the sub xeric (mean = 8.3 years, sd = 3.2 years)/xeric (mean = 9.2 years, sd = 3.4 years) site types. There was no significant difference in Y2R among soil drainage classes ($F_{(3,282)} = 1.75$, $p = 0.16$).

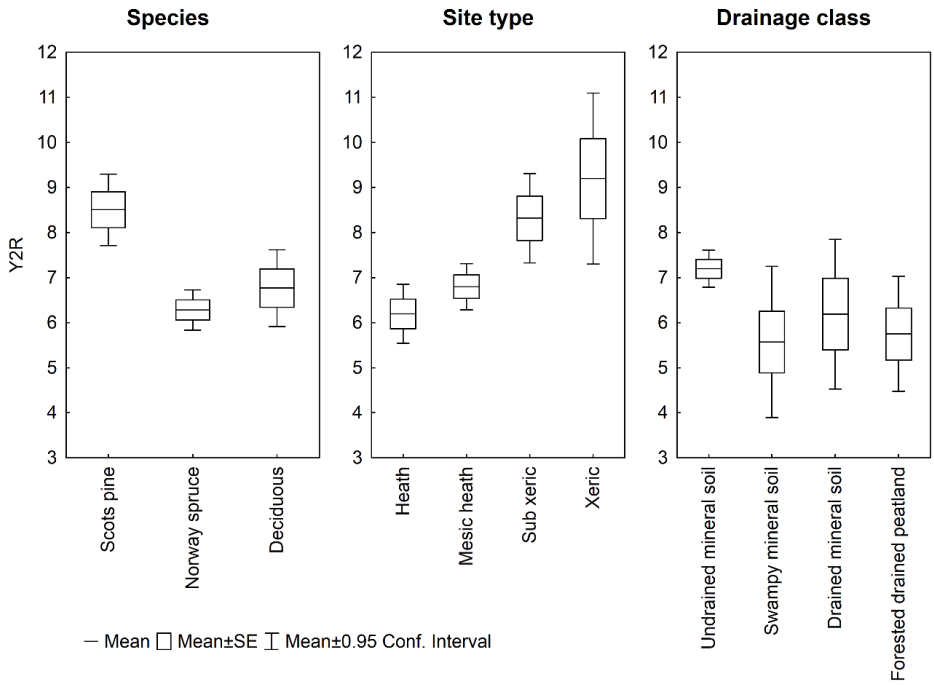

Figure 19. Difference in average Y2R metric for species, site type, and drainage class.

Uncertainty in monitoring the successional trajectories of forests post-disturbance with Landsat data are driven by factors such as topography, atmosphere, phenology, and sun and view angles (Song et al. 2000; Song and Woodcock 2003; Song et al. 2007). While it is possible to model successional reflectance trajectories (e.g. Nilson and Peterson 1994; Song et al. 2007), real successional trajectories are noisy and often non-linear (Song et al. 2002).

Future prospects for monitoring forest disturbance and recovery over large areas

Landsat-established baselines and subsequent trends provide a framework to augment and integrate existing information, including ground measurements. Such baseline information is important for identifying spatial and temporal trends regarding forest disturbance and recovery that can be used to inform and bound questions related to forest management and climate change. Moreover, the combination of BAP compositing methods with time series analyses overcomes some of the key limitations of using remotely sensed data for forest monitoring: namely consistent, cloud-free observations (Kimes et al. 2008, Püssa et al. 2005). Future prospects for implementing and refining these approaches are promising. New satellite missions that augment the Landsat satellite archive through purposeful harmonization (i.e. Sentinel-2), further increase capacity for cloud-free observations and enable virtual constellations of operational satellite programs (Wulder et al. 2015). Increased within-year observations expand BAP compositing options (substudy I), have demonstrated utility for land cover mapping applications (Griffiths et a. 2019), and improve capacity to monitor non-stand replacing disturbances (Cohen et al. 2016). Both the Landsat-8 and Sentinel-2 programs are considered operational programs, with measurement continuity as a key program objective. Free and open data policies, are also a critical component of these programs (Zhu et al. 2019). This operational capacity and commitment to measurement continuity (Wulder et al. 2016) is particularly useful for the design and implementation of national, large-area forest monitoring programs.

Globally, an increased commitment and interest in forest regeneration and reforestation will require spatially-explicit information to guide investments, evaluate outcomes, and support policy development (Gellrich et al. 2007, Holl and Aide 2011). For the study of forest recovery, integration of temporal information from optical satellites with characterizations of vertical structure from LIDAR takes advantage of the relative strengths of these two data sources (Hudak et al. 2002). The integration of LIDAR to corroborate spectral measures of recovery and support further investigations of LTS recovery metrics under a broad range of forest types and management scenarios will be key to improving and operationalizing these measures (substudy V). Systematic national ALS acquisitions are increasingly common (e.g. Stoker et al. 2008, Kotivuori et al. 2016) and the recent launch of two spaceborne lidars, the Advanced Topographic Laser Altimeter System (ATLAS) instrument onboard IceSat-2 (Popescu et al. 2018, Neuenschwander and Pitts 2019), and the Global Ecosystem Dynamics Investigations (GEDI) full waveform light detection and ranging (lidar) onboard the International Space Station (Qi et al. 2016, 2019) provide additional opportunities to characterize forest structure and support retrospective analyses of recovery. Likewise, other opportunities to characterize vegetation height from Polarimetric Synthetic Aperture Interferometry (TanDEM-X and TerraSAR-X; Koch 2010) further expand data options for integrated forest recovery assessments.

Advances in computational capacity and availability of free and open data support development of national forest monitoring programs and the operationalization of the approaches and methods described herein. However, these advances also provide unprecedented opportunities for the generation of information products by a multitude of

stakeholders (Gorelick et al. 2017). In the near future then, a potential challenge will undoubtedly be a proliferation of information products and a need to establish authoritative data sources for national reporting and accounting purposes. While governments are typically constrained by issues related to transparency, chain of custody, and data provenance, other stakeholders may not have such limitations (Lewis et al. 2017).

CONCLUSIONS

Information needs associated with forest monitoring have evolved, becoming increasing complex over time. Data to support these information needs are required to be spatially exhaustive, spatially explicit, and to capture changes at a spatial resolution that is commensurate with both natural and anthropogenic impacts. Bi- or multi-temporal remotely sensed data have previously enabled spatially detailed characterizations of forest disturbance. However, Landsat time series data support more detailed accounts of forest change through time, allowing both disturbance and the subsequent return of vegetation to be characterized. When combined with image compositing approaches, LTS enable the generation of large-area, gap-filled best-available-pixel image composites that preserve detected changes and provide continuous change metrics, resulting in foundational, annual data to support forest monitoring.

The overall goal of this dissertation was to improve the capacity to monitor forest disturbance and recovery over large areas. Component studies focused on four key areas: information needs, data availability, methods development, and information outcomes. Through the six different substudies (I-VI):

- forest monitoring information needs were identified and linked to image compositing criteria and data availability;
- methods were developed and demonstrated for generating gap-filled best-available pixel composites that preserve detected changes, generate continuous change metrics, and provide foundational annual data to support forest monitoring;
- a national monitoring framework was prototyped at scale over the 650 Mha that comprise Canada's forest ecosystems, providing a detailed analysis of areas disturbed by wildfire and harvest over a 25-year period (1985–2010) and their subsequent short- and long-term recovery;
- Landsat image compositing methods were ported and adapted to a different forest environment and management context and successfully applied;
- the utility of spectral measures of recovery were evaluated and confirmed against benchmarks of forest cover and height derived from ALS data; and
- the influence of forest structure and composition on spectral recovery was assessed and quantified using field plot data.

Information needs should ultimately drive the selection of the most appropriate data source for forest monitoring efforts, defining the desired spatial and temporal characteristics of the data. Substudies I and IV focused on defining forest monitoring information needs for Canada and Finland respectively, as well as linking these needs to compositing approaches and data availability. For Canada, the goal was to create gap-free image composite products

that could expand the current sample-based NFI monitoring approach and provide spatially-explicit information on forest dynamics for carbon accounting as well as a myriad of other forest information needs in Canada that would benefit from wall-to-wall image and data products with an annual time step. For Finland, the opportunity exists to incorporate LTS data into existing Landsat forest information products such as the MS-NFI and to support retrospective analyses of changing land use in support of greenhouse gas reporting. Such retrospective analyses also contribute to an improved understanding of the impacts of disturbances and management activities on Finnish forests through time, and can provide baseline data on the potential natural regeneration capacity of different management areas.

The opening of the Landsat archive and the adaptation of image compositing approaches to Landsat data have caused a processing shift in remote sensing science. No longer constrained by the best-available Landsat image, the use of the best-available observation for any given pixel has provided improved opportunities to take advantage of Landsat time series data over large areas. Substudies I and II developed a rule-base for compositing that was tied to information needs for forest monitoring. Substudy I demonstrated that the scoring mechanism for compositing can be adapted to a wide range of information needs; however data availability, both spatially and temporally, will dictate observation yield. The persistence of cloud cover, topography, phenology, availability of Landsat data, and dynamism of landscape processes are all important considerations when applying compositing processes. Trade-offs in compositing rules are often required; however, desired composite characteristics for the majority of forest monitoring applications include consistent phenology, maximum observation yield, and minimization of consecutive data gaps. An important limitation for the application of annual BAP products to derive forest ecosystem information products (i.e. land cover, land cover change, and forest structure) is missing data, that is, pixels with no observations due to clouds, cloud shadows, smoke, haze, sensor issues (SLC-off), or a restricted acquisition period. Substudy I demonstrated the potential for variability in observation yield in different regions of Canada, whereas substudy IV demonstrated analogous insights for Finland.

By leveraging the full temporal information in the pixel series along with the disturbance history, substudy II developed methods that enable the generation of gap-free proxy BAP composites. These proxy surface reflectance composites, whereby synthetic surface reflectance values are generated to fill data gaps while also preserving disturbance information, provide the foundation for forest monitoring efforts over large areas. As an important precursor to proxy value assignment, the method presented analyzes the spectral reflectance values of the pixels through time and generates a set of change metrics that characterize the year, persistence, rates of change, severity, recovery, rates of recovery, as well as the pre- and post-change metrics (Table 4). These proxy composites, together with the derived change metrics, provide valuable independent information for systematically mapping, monitoring, and reporting physical characteristics of land cover, land-cover changes, and related forest dynamics over large areas, for extended time periods at regional or national levels.

Landsat time series data have allowed for a more holistic assessment of forest dynamics: it is now possible to characterize both disturbance and recovery on an annual time step, which was previously not feasible with bi-temporal or multi-temporal epochal image data. Substudy III focused on information outputs, by prototyping at scale a national assessment of disturbance and recovery for Canada's forested ecosystems. Annual, spatially-explicit information on stand replacing disturbances provides refined information outputs, including heretofore unavailable information in the case of a national, spatially-

explicit record of forest harvesting for Canada. Previous assessments of post-disturbance recovery in Canada have either been sample-based or have used coarse spatial resolution data. LTS enable assessments of recovery that are spatially exhaustive and retrospective, with sufficient spatial resolution to capture and attribute anthropogenic impacts, providing important baseline data for forest monitoring efforts. A spatially-explicit assessment of recovery at a 30 m spatial resolution provides a framework for integration with field plot data to enable further insights into recovery processes in different regions and forest types. In substudy III, differentiation of short- and long-term trends in recovery was informative, as was the capacity to distinguish recovery trends independently for areas impacted by wildfire and harvesting. For example, at 5-years post-disturbance, areas impacted by wildfire and harvest had relatively similar recovery trends; however by the end of the time series, harvested areas had recovered more rapidly than areas impacted by wildfire. Likewise, 15% of areas disturbed by wildfire and harvest that were identified as non-recovering at 5-years post-disturbance were spectrally recovered by the end of the time series.

Much remains to be understood concerning the linkages between spectral measures of recovery and manifestations of forest structure. While, Landsat data provides useful information on the presence and horizontal distribution of vegetation, ALS provides useful information on the vertical distribution of that vegetation, indicative of forest structure. Combined, the integration of these data enable the characterization of the return of vegetation and trees post-disturbance. Substudy V demonstrated the utility of national ALS acquisitions for providing data to corroborate spectral measures of recovery and improve our understanding of the linkage between forest structural development and spectral measures of recovery. Benchmarks of forest cover and height, generated from ALS data provide an objective measure of recovery, against which spectral measures can be evaluated. In the boreal forests of southern Finland, post-harvest measures of spectral recovery realistically captured and related structural development of forests post-harvest.

As a process, forest recovery is highly variable, and monitoring efforts require definitions of recovery that are tied to the information need and the management context, as well as clear linkages between spectral recovery metrics and measurable indicators of forest structure, composition, or function. In substudy VI, field plot measurements were related to spectral measures of recovery and provided insights on those forest structural or compositional factors that influence the rate of spectral recovery within the first 15 years of stand development post-harvest in the boreal forests of southern Finland. Of the field plot attributes assessed, height was the most important predictor of forest spectral recovery, thereby linking structural development with spectral indicators of recovery. However, other factors, such as dominant species, and the percentage of stems that were deciduous were also useful for discriminating different recovery rates. Results of this study demonstrated that recovery, whether it be measured spectrally or in the field, is highly variable within the first 10-years of stand establishment and therefore, attempting to discriminate amongst different spectral recovery rates for stands < 10 years in this forest environment may not be informative for management.

In this dissertation, methods and approaches to improve the capacity for monitoring forest disturbances and subsequent recovery over large areas were developed and demonstrated. LTS greatly enhance opportunities for forest monitoring, particularly for post-disturbance recovery assessments, while BAP compositing approaches allow LTS analyses to be applied over large forest extents. As forest monitoring systems continue to evolve, they are no longer theoretically constrained by data availability or computational capacity. In reality however, many national forest monitoring programs are challenged by decreasing budgets and increasing expectations. Remotely sensed data have an increasingly

important role to play in meeting these challenges. The approaches presented herein are readily operationalized and are capable of providing the requisite baseline data to support science and programmatic information needs, as well as reporting requirements, policy development, and monitoring.

REFERENCES

Äijälä, O., Koistinen, A., Sved, J., Vanhatalo, K., Väisänen, P. (toim.) (2014). Metsänhoidon suositukset. Metsätalouden kehittämiskeskus Tapion julkaisuja. https://www.metsanhoitosuositukset.fi/wp-content/uploads/2016/08/Metsanhoidon_suositukset_Tapio_2014.pdf. [Cited August 16, 2018]

Amiro, B.D., Chen, M., Liu, J. (2000). Net primary productivity following forest fire for Canadian ecoregions. Canadian Journal of Forest Research, 30, 939–947. https://doi.org/10.1139/x00-025

Anderson-Teixeira, K.J., Miller, A.D., Mohan, J.E., Hudiburg, T.W., Duval, B.D., DeLucia, E.H. (2013). Altered dynamics of forest recovery under a changing climate. Global Change Biology, 19: 2001–2021. https://doi.org/10.1111/gcb.12194

Arvidson T., Gasch J., Goward S.N. (2001). Landsat 7's long-term acquisition plan – an innovative approach to building a global imagery archive. Remote Sensing of Environment 78(1–2): 13–26. https://doi.org/10.1016/S0034-4257(01)00263-2

Audet, P, Pinno, B.D., Thiffault, E. (2014). Reclamation of boreal forest after oil sands mining: Anticipating novel challenges in novel environments. Canadian Journal of Forest Research, 45: 364–371. https://doi.org/10.1139/cjfr-2014-0330

Bannari, A., Morin, D., Bonn, F., Huete, A.(1995). A review of vegetation indices. Remote Sensing Reviews, 13(1): 95–120. https://doi.org/10.1080/02757259509532298

Banskota, A., Kayastha, N., Falkowski, M.J., Wulder, M.A., Froese, R.E., White, J.C. (2014). Forest monitoring using Landsat time series data: a review. Canadian Journal of Remote Sensing, 40(5): 362–384. https://doi.org/10.1080/07038992.2014.987376

Bartels, S.F., Chen, H.Y.H., Wulder, M.A., White, J.C. (2016). Trends in post-disturbance recovery rates of Canada's forests following wildfire and harvest. Forest Ecology and Management, 361: 194–207. https://doi.org/10.1016/j.foreco.2015.11.015

Bolton, D.K., Coops, N.C., Wulder, M.A. (2015). Characterizing residual structure and forest recovery following high-severity fire in the western boreal of Canada using Landsat time-series and airborne LiDAR data. Remote Sensing of Environment, 163: 48–60. https://doi.org/10.1016/j.rse.2015.03.004

Bolton, D.K., Coops, N.C., Hermosilla, T., Wulder, M.A., White, J.C. (2017). Assessing variability in post-fire forest structure along gradients of productivity in the Canadian boreal using multi-source remote sensing. Journal of Biogeography: 44, 1294–1305. https://doi.org/10.1111/jbi.12947

Breiman, L. (2001). Random Forests. Machine Learning, 45: 5–32. https://doi.org/10.1023/A:1010933404324

Broich, M., Hansen, M. C., Potapov, P., Adusei, B., Lindquist, E., Stehman, S.V. (2011). Time series analysis of multi-resolution optical imagery for quantifying forest cover loss in Sumatra and Kalimantan, Indonesia. International Journal of Applied Earth Observation and Geoinformation, 13: 277–291. https://doi.org/10.1016/j.jag.2010.11.004

Buma, B. (2012). Evaluating the utility and seasonality of NDVI values for assessing post-disturbance recovery in a subalpine forest. Environmental Monitoring and Assessment, 184: 3849–3860. https://doi.org/10.1007/s10661-011-2228-y

Burton, P.J.; Parisien, M.-A.; Hicke, J.A.; Hall, R.J.; Freeburn, J.T. (2008). Large fires as agents of ecological diversity in the North American boreal forest. International Journal of Wildland Fire 17(6): 754-767. https://doi.org.10.1071/WF07149

Chavez, P.S. (1988). An improved dark-object subtraction technique for atmospheric scattering correction of multispectral data. Remote Sensing of Environment, 24: 459–479. https://doi.org/10.1016/0034-4257(88)90019-3

Chazdon, R.L., Brancalion, P.H.S., Laestadius, L., Bennett-Curry, A., Buckingham, K., Kumar, C., Moll-Rocek, J., Guimarães Vieira, I.C., Wilson, S.J. (2016). When is a forest a forest? Forest concepts and definitions in the error of forest and landscape restoration. Ambio, 45: 538–550. https://doi.org/10.1007/s13280-016-0772-y

Chu, T., Guo, X. (2014). Remote sensing techniques in monitoring post-fire effects and patterns of forest recovery in boreal forest regions: A review. Remote Sensing, 6, 470–520. https://doi.org/10.3390/rs6010470

Chu, T., Guo, X., Takeda, K. (2016). Remote sensing approach to detect post-fire vegetation regrowth in Siberian boreal larch forest. Ecological Indicators, 62: 32–46. https://doi.org/10.1016/j.ecolind.2015.11.026

Cihlar, J., Manak, D., and D'Iorio, M. (1994). Evaluation of compositing algorithms for AVHRR data over land. IEEE Transactions on Geoscience and Remote Sensing, 32: 427–436. https://doi.org/10.1109/36.295057

Cohen,W.B., Goward, S.N. (2004). Landsat's role in ecological applications of remote sensing. Bioscience 54, 535–545. https://doi.org/10.1641/0006-3568(2004)054[0535:LRIEAO]2.0.CO;2

Cohen, W.B., Yang, Z., Kennedy, R. (2010). Detecting trends in forest disturbance and recovery using yearly Landsat time series: 2. TimeSync — Tools for calibration and

validation. Remote Sensing of Environment, 114: 2911–2924. https://doi.org/10.1016/j.rse.2010.07.010

Cohen, W.B., Yang, Z., Stehman, S.V., Schroeder, T.A., Bell, D.M., Masek, J.G., Huang, C., Meigs, G.W. (2016). Forest disturbance across the conterminous United States from 1985–2012: the emerging dominance of forest decline. Forest Ecology and Management, 360: 242–252. https://doi.org/10.1016/j.foreco.2015.10.042
Cohen, W.B., Yang, Z., Healey, S.P., Kennedy, R.E., Gorelick, N. (2018) A LandTrendr multispectral ensemble for forest disturbance detection. Remote Sensing of Environment, 205: 131–140. https://doi.org/10.1016/j.rse.2017.11.015

Coops, N.C., Wulder, M.A., White, J.C. (2007). Identifying and Describing Forest Disturbance and Spatial Pattern: Data Selection Issues and Methodological Implications. Chapter 2, pages 31–61 in Wulder, M.A., Franklin, S.E. (editors). Forest Disturbance and Spatial Pattern: Remote Sensing and GIS Approaches. (Boca Raton: CRC Press). https://doi.org/10.1201/9781420005189.ch2

Corona, P. (2016). Consolidating new paradigms in large-scale monitoring and assessment of forest ecosystems. Environmental Research, 144(B): 8–14. https://doi.org/10.1016/j.envres.2015.10.017

Culotta, S., Boncina, A., Carvalho-Ribeiro, S.M., Chauvin, C., Farcy, C., Kurttila, M., Maetzke, F.G. (2015). Forest planning across Europe: the spatial scale, tools, and intersectoral integration in land-use planning. Journal of Environmental Planning and Management, 58(8): 1384–1411. https://doi.org/10.1080/09640568.2014.927754

Dale, V.H., Joyce, L.A., McNulty, S., Neilson, R.P., Ayres, M.P., Flannigan, M.D., Hanson, P.J., Irland, L.C., Lugo, A.E., Peterson, C.J., Simberloff, D., Swanson, F.J., Stocks, B.J., Wotton, B.M. (2001). Climate change and forest disturbances. Bioscience, 51: 723–734. https://doi.org/10.1641/0006-3568(2001)051[0723:CCAFD]2.0.CO;2

DeVries, B., Decuyper, M., Verbesselt, J., Zeileis, A., Herold, M., Joseph, S. (2015). Tracking disturbance-regrowth dynamics in tropical forests using structural change detection and Landsat time series. Remote Sensing of Environment, 169: 320–334. https://doi.org/10.1016/j.rse.2015.08.020

Ecological Stratification Working Group. (1995). A National Ecological Framework for Canada. http://sis.agr.gc.ca/cansis/publications/ecostrat/cad_report.pdf [Cited November 9, 2018].

Elgorov, A.V., Roy, D.P., Zhang, H.K., Hansen, M.A., Kommareddy, A. (2018). Demonstration of percent tree cover mapping using Landsat Analysis Ready Data (ARD) and sensitivity with respect to Landsat ARD processing level. Remote Sensing, 10(2): 209. https://doi.org/10.3390/rs10020209

Escuin, S., Navarro, R., Fernández, P. (2008). Fire severity assessment by using NBR (Normalized Burn Ratio) and NDVI (Normalized Difference Vegetation Index) derived

from Landsat TM/ETM+ images. International Journal of Remote Sensing, 29: 1053–1073. https://doi.org/10.1080/01431160701281072

Falkowski, M.J., Wulder, M.A., White, J.C., Gillis, M.D. (2009). Supporting large-area, sample-based forest inventories with very high spatial resolution satellite imagery. Progress in Physical Geography, 33(3): 403–423. https://doi.org/10.1177/0309133309342643

Fagg, P., Lutze, M., Slijkerman, C., Ryan, M. Bassett, O. (2013). Silvicultural recovery in ash forests following three recent large bushfires in Victoria. Australian Forestry, 76(3-4): 140-155. https://doi.org/10.1080/00049158.2013.848610

FAO (2012). FRA 2015: Terms and definitions. In: Forest Resource Assessment Working Paper 180. Food and Agriculture Organization of the United Nations, Rome, Italy. http://www.fao.org/docrep/017/ap862e/ap862e00.pdf, [Cited January 5, 2018].

Feng, M., Sexton, J.O., Huang, C., Masek, J.G., Vermote, E.F., Gao, F., Narasimhan, R., Channan, S.,Wolfe, R.E., Townshend, J. R. (2013). Global surface reflectance products from Landsat: Assessment using coincident MODIS observations. Remote Sensing of Environment, 134: 276–293. https://doi.org/10.1016/j.rse.2013.02.031

Flood, N. (2013). Seasonal composite Landsat TM/ETM +images using the Medoid (a multi-dimensional median). Remote Sensing, 5(12): 6481–6500. https://doi.org/10.3390/rs5126481

Forest Stewardship Council Finland. (2010). FSC standard for Finland. FSC-SECR-0160. https://fi.fsc.org/preview.fsc-standard-for-finland-v1-1-approved-210111.a-84.pdf. [Cited: May 8, 2018].

Frazier, R.J., Coops, N.C., Wulder, M.A. (2015). Boreal shield forest disturbance and recovery trends using Landsat time series. Remote Sensing of Environment, 170: 317–327. https://doi.org/10.1016/j.rse.2015.09.015

Frazier, R.J., Coops, N.C., Wulder, M.A., Hermosilla, T., White, J.C. (2018). Analyzing spatial and temporal variability in short-term rates of post-fire vegetation return from Landsat time series. Remote Sensing of Environment, 205: 32–45. https://doi.org/10.1016/j.rse.2017.11.007

Frolking, S., Palace, M.W., Clark, D.B., Chambers, J.Q., Shugart, H.H., Hurtt, G.C. (2009). Forest disturbance and recovery: A general review in the context of spaceborne remote sensing of impacts on aboveground biomass and canopy structure. Journal of Geophysical Research: Biogeosciences 114: G00E02. https://doi.org/10.1029/2008JG000911

Gatica-Saavedra, P., Echeverria, C., Nelson, C.R. (2017). Ecological indicators for assessing ecological success of forest restoration: a world review. Restoration Ecology, 25(6): 850–857. https://doi.org/10.1111/rec.12586

Gellrich, M., Baur, P., Koch, B., Zimmerman, N.E. (2007). Agricultural land abandonment and natural forest re-growth in the Swiss mountains: A spatially explicit economic analysis.

Agriculture, Ecosystems and Environment, 118: 93–108. https://doi.org/10.1016/j.agee.2006.05.001

Gillis, M.D. (2001). Canada's National Forest Inventory (responding to current information needs). Environmental Monitoring and Assessment, 67: 121–129. https://doi.org/10.1023/A:1006405820244

Gillis, M., Omule, A., Brierley, T. (2005). Monitoring Canada' s forests: The National Forest Inventory. The Forestry Chronicle, 81: 214–221. https://doi.org/10.5558/tfc81214-2

Gitas, I.Z., Mitri, G., Veraverbeke, S., Polychronaki, A. (2012). Advances in remote sensing of post-fire vegetation recovery monitoring—a review. Chapter 7. In: Fatoyinbo, L. (Ed.), Remote Sensing of Biomass - Principles and Applications. InTech. https://dx.doi.org/10.5772/20571

Gorelick, N., Hancher, M., Dixon, M., Ilyushchenko, S., Thau, D., Moore, R. (2017). Google Earth Engine: planetary-scale geospatial analysis for everyone. Remote Sensing of Environment, 202: 18–27. https://dx.doi.org/10.1016/j.rse.2017.06.031

Goetz, S., Fiske, G.J., Bunn, A.G. (2006). Using satellite time-series data sets to analyze fire disturbance and forest recovery across Canada. Remote Sensing of Environment, 101: 352–365. https://doi.org/10.1016/j.rse.2006.01.011

Gómez, C., Wulder, M.A., White, J.C., Montes, F., Delgado, J.A. (2012). Characterizing 25 years of change in the area, distribution, and carbon stock of Mediterranean pines in Central Spain. International Journal of Remote Sensing, 33: 5546–5573. https://doi.org/10.1080/01431161.2012.663115

Goward S.M., Williams D.L., Arvidson T., Rochchio L.E.P., Irons J.R., Russel C.A., Johnston S.S. (2017). Landsat's enduring legacy: pioneering global land observations from space. American Society for Photogrammetry and Remote Sensing, Bethesda, Maryland. 586 p.

Griffiths, P., van der Linden, S., Kuemmerle, T., and Hostert, P. (2013). A pixel-based Landsat compositing algorithm for large area land cover mapping. Journal of Selected Topics in Applied Earth Observations and Remote Sensing, 6(5): 2088–2101. https://doi.org/10.1109/JSTARS.2012.2228167

Griffiths, P., Kuemmerle, T., Baumann, M., Radeloff, V.C., Abrudan, I.V., Lieskovsky, J., Munteanu, C., Ostapowicz, K., Hostert, P. (2014). Forest disturbances, forest recovery, and changes in forest types across the Carpathian ecoregion from 1985 to 2010 based on Landsat image composites. Remote Sensing of Environment, 151: 72–88. https://doi.org/10.1016/j.rse.2013.04.022

Griffiths, P., Jakimow, B., Hostert, P. (2018). Reconstructing long term annual deforestation dynamics in Pará and Mato Grosso using the Landsat archive. Remote Sensing of Environment, 216: 497–513. https://doi.org/10.1016/j.rse.2018.07.010

Griffiths, P., Nendel, C., Hostert, P. (2019). Intra-annual reflectance composites from Sentinel-2 and Landsat for national-scale crop and land cover mapping. Remote Sensing of Environment, 220: 135–151. https://doi.org/10.1016/j.rse.2018.10.031

Gutman, G., Huang, C., Chander, G., Noojipady, P., and Masek, J.G. (2013). Assessment of the NASA-USGS Global Land Survey (GLS) datasets. Remote Sensing of Environment, Vol. 134: pp. 249–265. https://doi.org/10.1016/j.rse.2013.02.026

Hansen, M.C., Roy, D.P., Lindquist, E., Adusei, B., Justice, C.O., Alstatt, A. (2008). A method for integrating MODIS and Landsat data for systematic monitoring of forest cover and change in the Congo Basin. Remote Sensing of Environment, 112(5): 2495–2513. https://doi.org/10.1016/j.rse.2007.11.012

Hansen, M.C., Loveland, T.R. (2012). A review of large area monitoring of land cover change using Landsat data. Remote Sensing of Environment, 122, 66–74. https://doi.org/10.1016/j.rse.2011.08.024

Hansen, M.C., Potapov, P. V., Moore, R., Hancher, M., Turubanova, S.A., Tyukavina, A., Thau, D., Stehman, S.V., Goetz, S.J., Loveland, T.R., Kommareddy, A., Egorov, A., Chini, L., Justice, C.O., Townshend, J.R.G. (2013). High-resolution global maps of 21st-century forest cover change. Science, 342: 850–853. https://doi.org/10.1126/science.1244693

Härkönen, S., Lehtonen, A., Eerikäinen, K., Peltoniemi, M., Mäkelä, A. (2011). Estimating forest carbon fluxes for large regions based on process-based modelling, NFI data, and Landsat satellite images. Forest Ecology and Management, 262(12): 2364–2377. https://doi.org/10.1016/j.foreco.2011.08.035

Helmer, E. H., Ruzycki, T. S., Wunderle, J. M., Vogesser, S., Ruefenacht, C., Kwit, C., Brandeis, T. J., and Ewert, D. N. (2010). Mapping tropical dry forest height, foliage height profiles and disturbance type and age with a time series of cloud-cleared Landsat and ALI image mosaics to characterize avian habitat. Remote Sensing of Environment, 114: 2457–2473. https://doi.org/10.1016/j.rse.2010.05.021

Hérault, B., Piponiot, C. (2018). Key drivers of ecosystem recovery after disturbance in a neotropical forest: Long-term lessons from the Paracou experiment, French Guiana. Forest Ecosystems, 5(2): 1-15. https://doi.org/10.1186/s40663-017-0126-7

Hermosilla, T., Wulder, M.A., White, J.C., Coops, N.C., Hobart, G.W. (2015). Regional detection, characterization, and attribution of annual forest change from 1984 to 2012 using Landsat-derived time-series metrics. Remote Sensing of Environment, 170: 121–132. https://doi.org/10.1016/j.rse.2015.09.004

Hermosilla, T., Wulder, M.A., White, J.C., Coops, N.C., Hobart, G.W., Campbell, L.B. (2016). Mass data processing of time series Landsat imagery: pixels to data products for forest monitoring. International Journal of the Digital Earth, 8947. https://doi.org/10.1080/17538947.2016.1187673

Hermosilla, T., Wulder, M.A., White, J.C., Coops, N.C., Hobart, G.W. (2017). Updating Landsat time series of surface-reflectance composites and forest change products with new observations. International Journal of Applied Earth Observation and Geoinformation, 63: 104-111. https://doi.org/10.1016/j.jag.2017.07.013

Hicke, J.A., Asner, G.P., Kasischke, E.S., French, N.H.F., Randerson, J.T., Collatz, G.J., Stocks, B.J., Tucker, C.J., Los, S.O., Field, C.B. (2003). Postfire response of North American boreal forest net primary productivity analyzed with satellite observations. Global Change Biology, 9: 1145–1157. https://doi.org/10.1046/j.1365-2486.2003.00658.x

Hicke, J.A., Allen, C.D., Desai, A.R., Dietze, M.C., Hall, R.J., Hogg, E.H., Kashian, D.M., Moore, D., Raffa, K.F., Sturrock, R.N., Vogelmann, J. (2012). Effects of biotic disturbances on forest carbon cycling in the United States and Canada. Global Change Biology 18(1): 7–34. https://doi.org/10.1111/j.1365-2486.2011.02543.x

Hirschmugl, M., Gallaun, H., Dees, M., Datta, P., Deutscher, J., Koutsias, N., Schardt, M. (2017). Methods for mapping forest disturbance and degradation from optical earth observation data: a review. Current Forestry Reports, 3(1): 32–45. https://doi.org/10.1007/s40725-017-0047-2

Hofgaard, A., Tardif, J., Bergeron, Y. (1999). Dendroclimatic response of Picea mariana and Pinus banksiana along a latitudinal gradient in the eastern Canadian boreal forest. Canadian Journal of Forest Research, 29: 1333–1346. https://doi.org/10.1139/x99-073

Holben, B. (1986). Characteristics of maximum-value composite images from temporal AVHRR data. International Journal of Remote Sensing, 7: 1417–1434. https://doi.org/10.1080/01431168608948945

Holl, K.D., Aide, T.M. (2011). When and where to actively restore ecosystems? Forest Ecology and Management, 261(10): 1558–1563. https://doi.org/10.1016/j.foreco.2010.07.004

Horler, D., Ahern, F. (1986). Forestry information content of Thematic Mapper data. International Journal of Remote Sensing, 7: 405–428. https://doi.org/10.1080/01431168608954695

Hothorn, T., Buehlmann, P., Dudoit, S., Molinaro, A., Van Der Laan, M. (2006). Survival Ensembles. Biostatistics, 7(3), 355–373. https://doi.org/10.1093/biostatistics/kxj011

Hudak, A.T., Lefsky, M.A., Cohen, W.B., Berterretche, M. (2002). Integration of lidar and Landsat ETM+ data for estimating and mapping forest canopy height. Remote Sensing of Environment, 82: 397–416. https://doi.org/10.1016/S0034-4257(02)00056-1

Ireland, G., Petropoulos, G.P. (2015). Exploring the relationships between post-fire vegetation regeneration dynamics, topography and burn severity: a case study from the Montane Cordillera Ecozones of Western Canada. Applied Geography, 56: 232–248. https://doi.org/10.1016/j.apgeog.2014.11.016

Irons, J.R., Dwyer, J.L., Barsi, J.A. (2012). The next Landsat satellite: the Landsat Data Continuity Mission. Remote Sensing of Environment, 122: 11–21. https://doi.org/10.1016/j.rse.2011.08.026

Johnstone, J., Chapin, F.S., Foote, J., Kemmett, S., Price, K., Viereck, L. (2004). Decadal observations of tree regeneration following fire in boreal forests. Canadian Journal of Forest Research, 34: 267–273. https://doi.org/10.1139/x03-183

Johnstone, J.F., Chapin, F.S. (2006). Effects of soil burn severity on post-fire tree recruitment in boreal forest. Ecosystems 9, 14–31. https://doi.org/10.1007/s10021-004-0042-x

Ju, J., Roy, D. P., Shuai, Y., and Schaaf, C. (2010). Development of an approach for generation of temporally complete daily nadir MODIS reflectance time series. Remote Sensing of Environment, 114(1): 1–20. https://doi.org/10.1016/j.rse.2009.05.022

Justice, C.O., Townshend, J.R.G.,Vermote, E.F., Masuoka, E.,Wolfe, R.E., Saleous, N., Roy, D.P., Morisette, J.T. (2002). An overview of MODIS land data processing and product status. Remote Sensing of Environment, Vol. 83: 3–15. https://doi.org/10.1016/S0034-4257(02)00084-6

Kangas, A., Astrup, R., Breidenbach, J., Fridman, J., Gobakken, T., Korhonen, K.T., Maltamo, M., Nilsson, M., Nord-Larsen, T., Næsset, E., Olsson, H. (2018). Remote sensing and forest inventories in Nordic countries – roadmap for the future. Scandinavian Journal of Forest Research, 33(4): 397–412. https://doi.org/10.1080/02827581.2017.1416666.

Kankare, V., Vauhkonen, J., Holopainen, M., Vastaranta, M., Hyyppa, J., Hyyppä, H., Alho, P. (2015). Sparse density, leaf-off airborne laser scanning data in aboveground biomass component prediction. Forests, 6(6): 1839–1857. https://doi.org/10.3390/f6061839

Kauth, R.J., Thomas, G.S. (1976). The Tasselled-Cap—A Graphic Description of the Spectral-Temporal Development of Agricultural Crops as Seen by Landsat. Proceedings, Symposium on Machine Processing of Remotely Sensed Data, Purdue University, West Lafayette, IN, 29 June-1 July 1976, 41-51.

Kennedy, R.E., Cohen, W.B., Schroeder, T.A. (2007). Trajectory-based change detection for automated characterization of forest disturbance dynamics. Remote Sensing of Environment, 110: 370–386. https://doi.org/10.1016/j.rse.2007.03.010

Kennedy, R.E., Yang, Z., Cohen,W.B. (2010). Detecting trends in forest disturbance and recovery using yearly Landsat time series: 1. LandTrendr — Temporal segmentation algorithms. Remote Sensing of Environment, 114, 2897–2910. https://doi.org/10.1016/j.rse.2010.07.008

Kennedy, R.E., Yang, Z., Cohen, W.B., Pfaff, E., Braaten, J., Nelson, P. (2012). Spatial and temporal patterns of forest disturbance and regrowth within the area of the Northwest Forest Plan. Remote Sensing of Environment, 122: 117–133. https://doi.org/10.1016/j.rse.2011.09.024

Kennedy, R.E., Andréfouët, S., Cohen, W.B., Gómez, C., Griffiths, P., Hais, M., Healey, S.P. ... Zhe, Z. (2014). Bringing an ecological view of change to Landsat-based remote sensing. Frontiers and Ecology and the Environment, 12(6): 339–346. https://doi.org/10.1890/130066.

Keogh, E., Chu, S., Hart, D., Pazzani, M. (2001). An online algorithm for segmenting time series. Proceedings IEEE International Conference on Data Mining, November 29–Dec 2, 2001. ICDM 2001, 289–296. https://doi.org/10.1109/ICDM.2001.989531

Key, C.H., Benson, N.C. (1999). Measuring and remote sensing of burn severity. In L. F. Neuenschwander, & K. C. Ryan (Eds.), Proceedings Joint Fire Science Conference and Workshop, vol. II (p. 284). Moscow, ID: University of Idaho and International Association of Wildland Fire.
https://www.researchgate.net/publication/241687936_Measuring_and_remote_sensing_of_burn_severity_the_CBI_and_NBR

Key, C.H., Benson, N.C. (2006). Landscape Assessment (LA). FIREMON: Fire effects monitoringand inventory system. In: Lutes, D.C., Keane, R.E., Carati, J.F., Key, C.H., Benson, N.C., Gangi, L.J. (Eds.), General technical report RMRS-GTR-164-CD (pp. LA−1-55). USDA Forest Service, Rocky Mountains Research Station, Fort Collins, CO. https://doi.org/10.2737/RMRS-GTR-164

Kimes, D.S., Nelson, R.F., Skole, D.L., Salas, W.A. (1998). Accuracies in mapping secondary tropical forest age from sequential satellite imagery. Remote Sensing of Environment, 65: 112–120. https://doi.org/10.1016/S0034-4257(98)00021-2

Koch, B. (2010). Status and future of laser scanning, synthetic aperture radar and hyperspectral remote sensing data for forest biomass assessment. ISPRS Journal of Photogrammetry and Remote Sensing, 65(6): 581–590.
https://doi.org/10.1016/j.isprsjprs.2010.09.001

Korhonen, L., Pippuri, I., Packalén, P., Heikkinen, V., Maltamo, M., Heikkilä, J. (2013). Detection of the need for seedling stand tending using high-resolution remote sensing data. Silva Fennica, 47(2): 1–20. https://doi.org/10.14214/sf.952

Kotivuori, E., Korhonen, L., Packalen, P. (2016). Nationwide airborne laser scanning based models for volume, biomass and dominant height in Finland. Silva Fennica, 50(4): 1–28. https://doi.org/10.14214/sf.1567

Kuuluvainen, T., Gauthier, S. (2018) Young and old forest in the boreal: critical stages of ecosystem dynamics and management under global change. Forest Ecosystems, 5:26. https://doi.org/10.1186/s40663-018-0142-2

Kurz, W.A., Dymond, C.C., White, T.M., Stinson, G., Shaw, C.H., Rampley, G.J., Smyth, C., Simpson, B.N., Neilson, E.T., Trofymow, J.A., Metsaranta, J., and Apps, M.J. (2009). CBMCFS3: A model of carbon dynamics in forestry and land-use change implementing

IPCC standards. Ecological Modelling, 220: 480–504.
https://doi.org/10.1016/j.ecolmodel.2008.10.018

Lawrence, R.L., Ripple, W.J. (1999). Calculating change curves for multitemporal satellite imagery: Mount St. Helens 1980–1995. Remote Sensing of Environment, 67: 309–319.
https://doi.org/10.1016/S0034-4257(98)00092-3

Leckie, D.G., Gillis, M.D. (1995). Forest inventory in Canada with an emphasis on map production. The Forestry Chronicle, 71(1): 74–88. https://doi.org/10.5558/tfc71074-1

Lewis, A., Oliver, S., Lymburner, L., Evans, B., Wyborn, L., Mueller, N., Wang, L.W. (2017). The Australian Geoscience Data Cube–Foundations and lessons learned. Remote Sensing of Environment, 202: 276–292. https://doi.org/10.1016/j.rse.2017.03.015

Lehmann, E.A.,Wallace, J.F., Caccetta, P.A., Furby, S.L., Zdunic, K. (2012). Forest cover trends from time series Landsat data for the Australian continent. International Journal of Applied Earth Observation and Geoinformatics, 21: 453–462.
https://doi.org/10.1016/j.jag.2012.06.005

Liaw, A., Wiener, M. (2002). Classification and Regression by randomForest. R News, 2: 18–22. https://www.r-project.org/doc/Rnews/Rnews_2002-3.pdf [Cited August 31, 2018].

Liaw, A., Wiener, M. (2018). Randomforest, R package version 4.6-14; R Core Team: Vienna, Austria, 2018.

Lindquist, E. J., Hansen, M. C., Roy, D. P., and Justice, C. O. (2008). The suitability of decadal image data sets for mapping tropical forest cover change in the Democratic Republic of Congo: implications for the global land survey. International Journal of Remote Sensing, Vol. 29: pp. 7269–7275. https://doi.org/10.1080/01431160802275890

Lu, D., Mausel, P., Brondizio, E., Moran, E. (2004). Change detection techniques. International Journal of Remote Sensing, 25(12): 2365–2407.
https://doi.org/10.1080/0143116031000139863

Lunetta, R. S., D. M. Johnson, J. G. Lyon, Crotwell, J. (2004). Impacts of imagery temporal frequency on land-cover change detection monitoring. Remote Sensing of Environment, 89(4): 444–454. https://doi.org/10.1016/j.rse.2003.10.022

MacDicken, K.G. (2015). Global Forest Resources Assesment 2015: What, why, and how? Forest Ecology and Management, 352: 3–8. https://doi.org/10.1016/j.foreco.2015.02.006

Madoui, A., Gauthier, S., Leduc, A., Bergeron, Y., Valeria, O. (2015). Monitoring forest recovery following wildfire and harvest in boreal forests using satellite imagery. Forests, 6: 4105–4134. https://doi.org/10.3390/f6114105

Magnussen, S., Wulder, M.A. (2012). Post-fire canopy height recovery in Canada's boreal forests using airborne laser scanner (ALS). Remote Sensing, 4: 1600–1616.
https://doi.org/10.3390/rs4061600

Majasalmi, T., Eisner, S., Astrup, R., Fridman, J., Bright, R.M. (2018). An enhanced forest classification scheme for modeling vegetation-climate interactions based on national forest inventory data. Biogeosciences, 15(2): 399–412. https://doi.org/10.5194/bg-15-399-2018

Maltamo, M., Packalén, P., Suvanto, A., Korhonen, K.T., Mehtätalo, L., Hyvönen, P. (2009). Combining ALS and NFI training data for forest management planning: A case study in Kuortane, Western Finland. European Journal of Forest Research, 128(3): 305–317. https://doi.org/10.1007/s10342-009-0266-6

Markham, B.L., Helder, D.L. (2012). Forty-year calibrated record of earth-reflected radiance from Landsat: a review. Remote Sensing of Environment, 122: 30–40. https://doi.org/10.1016/j.rse.2011.06.026

Masek, J.G., Vermote, E.F., Saleous, N., Wolfe, R., Hall, F.G., Huemmrich, F., Gao, F., Kutler, J., Lim, T.K. (2006). A Landsat surface reflectance data set for North America, 1990–2000. IEEE Geoscience and Remote Sensing Letters, 3(1): 68–72. https://doi.org/10.1109/LGRS.2005.857030

Masek, J.G., Huang, C., Wolfe, R., Cohen, W., Hall, F., Kutler, J., Nelson, P. (2008). North American forest disturbance mapped from a decadal Landsat record. Remote Sensing of Environment, 112: 2914–2926. https://doi.org/10.1016/j.rse.2008.02.010

Masek, J.G., Cohen,W.B., Leckie, D., Wulder, M.A., Vargas, R., de Jong, B., Healey, S., Law, B., Birdsey, R., Houghton, R.A., Mildrexler, D., Goward, S., Smith,W.B. (2011). Recent rates of forest harvest and conversion in North America. Journal of Geophysical Research: Biogeosciences, 116: G00K03. https://doi.org/10.1029/2010JG001471

Matasci, G., Hermosilla, T., Wulder, M.A., White, J.C., Coops, N.C., Hobart, G.W., Zald, H.S. (2018a). Large-area mapping of Canadian boreal forest cover, height, biomass and other structural attributes using Landsat composites and lidar plots. Remote Sensing of Environment, 209: 90–106. https://doi.org/10.1016/j.rse.2017.12.020

Matasci, G., Hermosilla, T., Wulder, M.A., White, J.C., Coops, N.C., Hobart, G.W., Bolton, D.K., Tompalski, P., Bater, C.W. (2018b).Three decades of forest structural dynamics over Canada's forested ecosystems using Landsat time-series and lidar plots. Remote Sensing of Environment, 216:697–714. https://doi.org/10.1016/j.rse.2018.07.024

McDonald, A. J., Gemmell, F.M., and Lewis, P.E. (1998). Investigation of the utility of spectral vegetation indices for determining information on coniferous forests. Remote Sensing of Environment, 66, 250–272. https://doi.org/10.1016/S0034-4257(98)00057-1

McKenney, D., Pedlar, J.H., Papadopol, P., and Hutchinson, M.F. (2006). The development of 1901-2000 historical monthly climate models for Canada and the United States. Agricultural and Forest Meterology, 138(1–4): 69–81. https://doi.org/10.1016/j.agrformet.2006.03.012

Meijer, J.R., Huijbegts, M.A.J., Schotten, C.G.J. and Schipper, A.M. (2018): Global patterns of current and future road infrastructure. Environmental Research Letters, 13-064006. https://doi.org/10.1088/1748-9326/aabd42

Miina, J., Turunen, J., Korhonen, K.T., Strandström, M., Ahola, A. (2018). Predicting the need for tending of conifer seedling stands in southern Finland, 33(7): 641–649. https://doi.org/10.1080/02827581.2018.1447681

Myneni, R.B., Asrar, G. (1994) Atmospheric effects and spectral vegetation induces. Remote Sensing of Environment, 47, 390–402. https://doi.org/10.1016/0034-4257(94)90106-6

Natural Resources Canada. (2013). The State of Canada's Forests Annual Report 2013. Canadian Forest Service, Ottawa, Ontario. https://cfs.nrcan.gc.ca/publications?id=35191 [Cited January 15, 2014].

Natural Resources Canada. (2018). The State of Canada's Forests Annual Report 2018. Canadian Forest Service, Ottawa, Ontario. http://cfs.nrcan.gc.ca/pubwarehouse/pdfs/39336.pdf [Cited November 1, 2018].

Natural Resources Institute of Finland. (2015). The multi-source national forest inventory raster maps of 2013. Available at. http://kartta.luke.fi/index-en.html, Accessed date: 1 June 2017.

Natural Resources Institute of Finland. (2017). Finland's forests 2017. Available online: https://www.luke.fi/wp-content/uploads/2017/06/finlands-forests-facts-2017-www.pdf

Neuenschwander, A., Pitts, K. (2019). The ATL08 land and vegetation product for the ICESat-2 Mission. Remote Sensing of Environment, 221: 247–259. https://doi.org/10.1016/j.rse.2018.11.005

Nilsson, U., Luoranen, J., Kolström, T., Örlander, G., Puttonen, P. (2010). Reforestation with planting in northern Europe. Scandinavian Journal of Forest Research, 25: 283–294. https://doi.org/10.1080/02827581.2010.498384

Nilson, T., Peterson, U. (1994). Age dependence of forest reflectance: analysis of main driving factors. Remote Sensing of Environment, 48: 319–331. https://doi.org/10.1016/0034-4257(94)90006-X

Oliver, C.D., Larson, B.C. (1996). Forest Stand Dynamics (Updated Edition). New York: John Wiley.

Olofsson, P., Foody, G.M., Herold, M., Stehman, S.V., Woodcock, C.E., Wulder, M.A., (2014). Good practices for estimating area and assessing accuracy of land change. Remote Sensing of Environment, 148: 42–57. https://doi.org/10.1016/j.rse.2014.02.015

Olsson, H. (2009). A method for using Landsat time series for monitoring young plantations in boreal forests. International Journal of Remote Sensing, 30(19): 5117–5131. https://doi.org/10.1080/01431160903022993

Ørka, H.O., Gobakken, T., Næsset, E. (2016). Predicting attributes of regeneration forests using airborne laser scanning. Canadian Journal of Remote Sensing, 42: 541–553. https://doi.org/10.1080/07038992.2016.1199269

Pan, Y., Birdsey, R.A., Fang, J., Houghton, R., Kauppi, P.E., Kurz, W.A., Phillips, O.L., Shvidenko, A., Lewis, S.L., Canadell, J.G., Ciais, P., Jackson, R.B., Pacala, S.W., McGuire, A.D., Piao, S., Rautiainen, A., Sitch, S., Hayes, D. (2011). A large and persistent carbon sink in the world's forests. Science 333, 988–93. https://10.1126/science.1201609

PEFC Finland. (2014). Criteria for PEFC forest certification. Available online. http://pefc.fi/wp-content/uploads/2016/09/PEFC_FI_1002_2014_Criteria_for_Forest_Certification_20141027.pdf [Cited August 15, 2018].

Pelletier, J., Goetz, S.J. (2015). Baseline data on forest loss and associated uncertainty: Advances in national forest monitoring. Environmental Research Letters, 10(2): 021001. https://doi.org/10.1088/1748-9326/10/2/021001

Peterson, U. (1992). Seasonal reflectance factor dynamics in boreal forest clear-cut communities. International Journal of Remote Sensing, 13:4, 753-772. https://doi.org/10.1080/01431169208904150

Pflugmacher, D., Cohen, W.B., Kennedy, R.E., Yang, Z. (2014). Using Landsat-derived disturbance and recovery history and lidar to map forest biomass dynamics. Remote Sensing of Environment, 151: 124–137. https://doi.org/10.1016/j.rse.2013.05.033

Pickell, P.D., Hermosilla, T., Frazier, R.J., Coops, N.C., Wulder, M.A. (2016). Forest recovery trends derived from Landsat time series for North American boreal forests. International Journal of Remote Sensing, 37: 138–149. https://doi.org/10.1080/2150704X.2015.1126375

Popescu, S.C., Zhou, T., Nelson, R., Neuenschwander, A., Sheridan, R., Narine, L., Walsh, K.M. (2018). Photon counting LiDAR: An adaptive ground and canopy height retrieval algorithm for ICESat-2 data. Remote Sensing of Environment, 208: 154–170. https://doi.org/10.1016/j.rse.2018.02.019

Potapov, P., Turubanova, S., Hansen, M.C. (2011). Regional-scale boreal forest cover and change mapping using Landsat data composites for European Russia. Remote Sensing of Environment, 115: 548–561. https://doi.org/10.1016/j.rse.2010.10.001

Potapov, P., Turubanova, S., Hansen, M. C., Adusei, B., Broich, M., Alstatt, A., Mane, L., Justice, C. O. (2012). Quantifying forest cover loss in Democratic Republic of the Congo, 2000-2010, with Landsat ETM+ data. Remote Sensing of Environment, 122: 106–116. https://doi.org/10.1016/j.rse.2011.08.027

Potapov, P.V., Turubanova, S.A., Tyukavina, A., Krylov, A.M., McCarty, J.L., Radeloff, V.C., Hansen, M.C. (2015). Eastern Europe's forest cover dynamics from 1985 to 2012 quantified from the full Landsat archive. Remote Sensing of Environment, 159: 28–43. https://doi.org/10.1016/j.rse.2014.11.027

Püssa, K., Liira, J., Peterson, U. (2005). The effects of successional age and forest site type on radiance of forest clearcut communities. Scandinavian Journal of Forest Research, 20(S6): 79–87. https://doi.org/10.1080/14004080510040995

Qi, W., Dubayah, R.O. (2016). Combining Tandem-X InSAR and simulated GEDI lidar observations for forest structure mapping. Remote Sensing of Environment, 2016, 187, 253–266. https://doi.org/10.1016/j.rse.2016.10.018

Qi, W., Lee, S.-K., Hancock, S., Luthcke, S., Tang, H., Armston, J., Dubayah, R. (2019). Improved forest height estimation by fusion of simulated GEDI Lidar data and TanDEM-X InSAR data. Remote Sensing of Environment, 221: 621–634. https://doi.org/10.1016/j.rse.2018.11.035

Rautianen, M., Lukes, P., Homolová, L., Hovi, A., Pisek, J., Mõttus, M. (2018). Spectral Properties of Coniferous Forests: A Review of In Situ and Laboratory Measurements. Remote Sensing, 10, 207. https://doi.org/10.3390/rs10020207.

Roy, D. P. (2000). The impact of misregistration upon composited wide field of view satellite data and implications for change detetcion. IEEE Transactions on Geoscience and Remote Sensing, 38: 2017–2032. https://doi.org/10.1109/36.851783

Roy, D. P., Ju, J., Kline, K., Scaramuzza, P. L., Kovalskyy, V., Hansen, M., Loveland, T. R., Vermote, E., and Zhang, C. (2010).Web-enabled Landsat Data (WELD): Landsat ETM+ composited mosaics of the conterminous United States. Remote Sensing of Environment, 114: 35–49. https://doi.org/10.1016/j.rse.2009.08.011

Saksa, T., Uuttera, J., Kolstöm, T., Lehikoinen, M., Pekkarinen, A., Sarvi, V. (2003). Clear-cut detection in boreal forest aided by remote sensing. Scandinavian Journal of Forest Research, 18(6): 537–546. https://doi.org/10.1080/02827580310016881

Schmidt, G. L., Jenkerson, C. B., Masek, J., Vermote, E., Gao, F. (2013). Landsat ecosystem disturbance adaptive processing system (LEDAPS) algorithm description. U.S. Geological Survey Open-File Report 2013–1057, 17 p. Available online: http://pubs.usgs.gov/of/2013/1057/

Schroeder, T.A., Cohen, W.B., Yang, Z. (2007). Patterns of forest regrowth following clearcutting in western Oregon as determined from Landsat time-series. Forest Ecology and Management, 243: 259–273. https://doi.org/10.1016/j.foreco.2007.03.019

Schroeder, T.A., Wulder, M.A., Healey, S.P., Moisen, G.G. (2011). Mapping wildfire and clearcut harvest disturbances in boreal forests with Landsat time series data. Remote Sensing Environment, 115: 1421–1433. https://doi.org/10.1016/j.rse.2011.01.022

Shaw, J., Loveland, T. (2017). No PCD summaries for KIS and FUI ground stations. Personal communication, February 1, 2017.

Slesak, R.A., Kaebisch, T. (2016) Using lidar to assess impacts of forest harvest landings on vegetation height by harvest season and the potential for recovery over time. Canadian Journal of Forest Research, 46: 869–875. https://doi.org/ 10.1139/cjfr-2015-0517

Stoker, J., Harding, D., Parrish, J.B. (2008). The need for national LiDAR data set. Photogrammetric Engineering and Remote Sensing, 74(9): 1066–1068.

Song, C., Woodcock, C.E., Seto, K.C., Lenney, M.P., Macomber, S.A. (2001). Classification and change detection using Landsat TM data: When and how to correct for atmospheric effects. Remote Sensing of Environment, 75, 230-244. https://doi.org/10.1016/S0034-4257(00)00169-3

Song, C., Woodcock, C.E., Li, X. (2002). The spectral/temporal manifestation of forest succession in optical imagery: The potential of multitemporal imagery. Remote Sensing of Environment, 82: 285–302. https://doi.org/10.1016/S0034-4257(02)00046-9

Song, C., Woodcock, C.E. (2003). Monitoring forest succession with multitemporal Landsat images: factors of uncertainty. IEEE Transactions on Geoscience and Remote Sensing, 41(11): 2557–2567. https://doi.org/10.1109/TGRS.2003.818367

Song, C., Schroeder, T.A., Cohen, W.B. (2007). Predicting temperate conifer forest successional stage distributions with multitemporal Landsat Thematic Mapper imagery. Remote Sensing of Environment, 106: 228–237. https://doi.org/10.1016/j.rse.2006.08.008

Spake, R., Ezard. T.H.G., Martin, P.A., Newton, A.C., Doncaster, C.P. (2015). A meta-analysis of functional group responses to forest recovery outside of the tropics. Conservation Biology, 29(6): 1695–1703. https://doi.org/10.1111/cobi.12548

Stinson, G., Kurz, W.A., Smyth, C.E., Neilson, E.T., Dymond, C.C., Metsaranta, J.M., Boisvenue, C., Rampley, G.J., Li, Q., White, T.M., Blain, D. (2011). An inventory-based analysis of Canada's managed forest carbon dynamics, 1990 to 2008. Global Change Biology, 17: 2227–2244. https://doi.org/10.1111/j.1365-2486.2010.02369.x

Stocks, B.J., Mason, J.A., Todd, J.B., Bosch, E.M., Wotton, B.M., Amiro, B.D., Flannigan, M.D., Hirsch, K.G., Logan, K.A., Martell, D.L., Skinner, W.R. (2002). Large forest fires in Canada, 1959–1997. Journal of Geophysical Research: Atmospheres 108: 8149. https://doi.org/10.1029/2001JD000484

Strobl, C., Boulesteix, A.L., Zeileis, A., Hothorn, T. (2007). Bias in Random Forest Variable Importance Measures: Illustrations, Sources and a Solution. BMC Bioinformatics, 8(25). https://doi.org/10.1186/1471-2105-8-25

Strobl, C., Boulesteix, A.L., Kneib, T., Augustin, T., Zeileis, A. (2008). Conditional Variable Importance for Random Forests. BMC Bioinformatics, 9(307). https://doi.org/10.1186/1471-2105-9-307

Strobl, C., Hothorn, T., Zeileis, A. (2009). Party on! A new conditional Variable Importance Measure for Random Forests Available in the party Package. Technical Report Number 050, Department of Statistics, University of Munich. 4p. https://epub.ub.uni-muenchen.de/9387/1/techreport.pdf [Cited September 5, 2018].

Storey, J., Roy, D.P., Masek, J., Gascon, F., Dwyer, J., Choate, M. (2016). A note on the temporary misregistration of Landsat-8 Operational Land Imager (OLI) and Sentinel-2 Multi Spectral Instrument (MSI) imagery. 186: 121–122. https://doi.org/10.1016/j.rse.2016.08.025

Thompson, I. D., M. R. Guariguata, K. Okabe, C. Bahamondez, R. Nasi, V. Heymell, and C. Sabogal. (2013). An operational framework for defining and monitoring forest degradation. Ecology and Society, 18(2): 20. https://www.ecologyandsociety.org/vol18/iss2/art20/

Thompson, S., Nelson, T., White, J.C., Wulder, M.A. (2016). Mapping dominant tree species over large forested areas using Landsat best-available pixel image composites. Canadian Journal of Remote Sensing, 41(3): 203–218. https://doi.org/ 10.1080/07038992.2015.1065708

Tomppo, E., Katila, M., Moilanen, J., Mäkelä, H., Peräsaari, J. (1998) Kunnittaiset metsävaratiedot 1990-94. Folia For. 4B/1998:619–839. http://dx.doi.org/10.14214/ma.6453

Tomppo, E., Olsson, H., Stahl, G., Nilsson, M., Hagner, O., Katila, M. (2008a). Combining national forest inventory field plots and remote sensing data for forest databases. Remote Sensing of Environment, 112: 1982–1999. https://doi.org/10.1016/j.rse.2007.03.032

Tomppo, E., Haakana, M., Katila, M., Peräsaari, J. (2008b). Multi-source National Forest Inventory: Methods and Applications. Springer Netherlands, 373 p. https://doi.org/10.1007/978-1-4020-8713-4

Tomppo E., Gschwantner T., Lawrence M., McRoberts R.E. (2010). National forest inventories –pathways for common reporting. Springer. 612 p. https://doi.org/10.1007/978-90-481-3233-1

Tomppo, E., Katila, M., Mäkisara, K., Peräsaari, J. (2013). The multi-source National Forest Inventory of Finland – methods and results 2009. Working Papers of the Finnish Forest Research Institute. Available online: http://www.metla.fi/julkaisut/workingpapers/2013/mwp273.htm [Cited November 1, 2018].

Tomppo E., Katila M., Mäkisara K., Peräsaari J. (2014). The multi-source national forest inventory of Finland – methods and results 2011. Working Paper of the Finnish Forest Research Institute 319. http://urn.fi/URN:ISBN:978-951-40-2516-7. [Cited February 12, 2018].

Townshend, J.R.G., Justice, C.O. (1988). Selecting the spatial resolution of satellite sensors required for global monitoring of land transformations. International Journal of Remote Sensing, 9(2): 187–236. https://doi.org/10.1080/01431168808954847

Tucker, C. J., Grant, D. M., and Dykstra, J. D. (2004). NASA's global orthorectified Landsat data set. Photogrammetric Engineering and Remote Sensing, 70: 313–322. https://doi.org/10.14358/PERS.70.3.313

Tuominen S., Pitkänen T., Balázs A., Kangas A. (2017). Improving Finnish multi-source national forest inventory by 3D aerial imaging. Silva Fennica, 51(4): 7743. https://doi.org/10.14214/ sf.7743

Turtiainen, M., Miina, J., Salo, K., Hotanen, J.-P. (2016). Modelling the coverage and annual variation in bilberry yield in Finland. Silva Fennica, 50(4): 1573. https://doi.org/10.14214/sf.1573

Urbano, A.R., Keeton, W.S. (2017). Carbon dynamics and structural development in recovering secondary forests of the northeastern U.S. Forest Ecology and Management, 392: 21–35. https://doi.org/10.1016/j.foreco.2017.02.037

USGS (United States Geologic Survey). (2012). Landsat Ecosystem Disturbance Adaptive Processing System (LEDAPS): Algorithm description document. Version 1.3, December 2012. https://landsat.usgs.gov/sites/default/files/documents/ledaps_add.pdf [Cited August 15, 2018]

USGS (United States Geologic Survey). (2018a). Product Guide: Landsat 4-7 Surface Reflectance (LEDAPS) Product, Version 8.3, March 2018. https://landsat.usgs.gov/sites/default/files/documents/ledaps_product_guide.pdf [Cited August 15, 2018]

USGS (United States Geological Survey). (2018b). Product Guide: Landsat 8 Surface Reflectance Code (LaSRC) Product. Version 4.3. March 2018: Available online: https://landsat.usgs.gov/sites/default/files/documents/lasrc_product_guide.pdf [Cited August 15, 2018]

Valkonen, S., Ruuska, J. (2003). Effect of *Betula pendula* admixture on tree growth and branch diameter in young *Pinus sylvestris* stands in Southern Finland. Scandinavian Journal of Forest Research, 18:416–426. https://doi.org/ 10.1080/02827581.2003.9610645

Valkonen, S., Siitonen, J. (2016). Tree regeneration in patch cutting in Norway spruce stands in northern Finland. Scandinavian Journal of Forest Research, 31(3): 271–278. https://doi.org/10.1080/02827581.2015.1099726

Valkonen, S., Koskinen, K., Mäkinen, J., Vanha-Majamaa, I. (2011). Natural regeneration in patch clear-cutting in *Picea abies* stands in Southern Finland. Scandinavian Journal of Forest Research, 26(6): 530–542. https://doi.org/10.1080/02827581.2011.611818

van Aardt, J., Wynne, R.H. (2001). Spectral separability among six southern tree species. Photogrammetric Engineering and Remote Sensing, 67(12): 1367–1375.

Veraverbeke, S., Gitas, I., Katagis, T., Polychronaki, A., Somers, B., Goossens, R. (2012a). Assessing post-fire vegetation recovery using red-near infrared vegetation indices: accounting for background and vegetation variability. ISPRS Journal of Photogrammetry and Remote Sensing, 68: 28–39. https://doi.org/10.1016/j.isprsjprs.2011.12.007

Veraverbeke, S., Somers, B., Gitas, I., Katagis, T., Polychronaki, A., Goossens, R. (2012b). Spectral mixture analysis to assess post-fire vegetation regeneration using Landsat Thematic Mapper imagery: accounting for soil brightness variation. International Journal of Applied Earth Observation and Geoinformation, 14: 1–11. https://doi.org/10.1016/j.jag.2011.08.004

Vermote, E.F., Tanre, D., Deuze, J.L., Herman, M., Morcette, J.-I. (1997). Second simulation of the satellite signal in the solar spectrum, 6S: An overview. IEEE Transactions on Geoscience and Remote Sensing, 35: 675–686. https://doi.org/ 10.1109/36.581987

Vermote, E.F., Justice, C., Claverie, M., Franch, B. (2016). Preliminary analysis of the performance of the Landsat 8/OLI land surface reflectance product. Remote Sensing of Environment, 185: 46–56. http://dx.doi.org/10.1016/j.rse.2016.04.008.

Viedma, O., Meliá, J., Segarra, D., García-Haro, J. (1997). Modeling rates of ecosystem recovery after fires by using Landsat TM data. Remote Sensing of Environment, 61: 383–398. https://doi.org/10.1016/S0034-4257(97)00048-5

Vila, J.P.S., Barbosa, P. (2010). Post-fire vegetation regrowth detection in the Deiva Marina region (Liguria-Italy) using Landsat TM and ETM+ data. Ecological Modeling, 221: 75–84. https://doi.org/10.1016/j.ecolmodel.2009.03.011

Vogelmann, J.E., Gallant, A.L., Shi, H., Zhu, Z. (2016). Perspectives on monitoring gradual change across the continuity of Landsat sensors using time-series data. Remote Sensing of Environment, 185: 258–270. https://doi.org/10.1016/j.rse.2016.02.060

White, J.C., Wulder, M.A. (2013). The Landsat observation record of Canada: 1972–2012. Canadian Journal of Remote Sensing, 39(6): 455–467. https://doi.org/10.5589/m13-053

White, J.C., Wulder, M.A., Gómez, C., Stenhouse, G. (2011). A history of habitat dynamics: characterizing 35 years of stand replacing disturbance. Canadian Journal of Remote Sensing, 37: 234–51. https://doi.org/10.5589/m11-034

White, J.D., Ryan, K.C., Key, C.C., Running, S. (1996). Remote sensing of forest fire severity and vegetation recovery. International Journal of Wildland Fire, 63(5): 125-136. https://doi.org/10.1071/WF9960125.

Woodcock, C. E., Allen, R., Anderson, M., Belward, A., Bindschadler, R., Cohen, W., Gao, F., Goward, S. N., Helder, D., Helmer, E., Nemani, R., Oreopoulos, L., Schott, J., Thenkabail, P. S., Vermote, E. F., Vogelmann, J., Wulder, M. A., Wynne, R. (2008). Free

access to Landsat imagery. Science, 320(5874): 1011. https://doi.org/10.1126/science.320.5879.1011a

Wolfe, R. E., Roy, D. P., Vermote, E. (1998). MODIS land data storage, gridding, and compositing methodology: Level 2 grid. IEEE Transactions on Geoscience and Remote Sensing, 36: 1324–1338. https://doi.org/10.1109/36.701082

Wulder, M.A., Kurz, W.A., Gillis, M.D. (2004). National level forest monitoring and modeling in Canada. Progress in Planning, 61: 365–381. https://doi.org/10.1016/S0305-9006(03)00069-2

Wulder, M.A., Campbell, C., White, J.C., Flannigan, M., Campbell, I.D. (2007a). National circumstances in the international circumboreal community. The Forestry Chronicle, 83(4): 539–556. https://doi.org/10.5558/tfc83539-4

Wulder, M. A., White, J. C., Magnussen, S., McDonald, S. (2007b). Validation of a large-area land cover product using purpose acquired airborne video. Remote Sensing of Environment, 106: 480–491. https://doi.org/10.1016/j.rse.2006.09.012

Wulder, M.A., White, J.C., Bater, C.W., Coops, N.C., Hopkinson, C., Chen, G. (2012). Lidar plots — a new large area data collection option: context, concepts, and case study. Canadian Journal of Remote Sensing, 38(5): 600–618. https://doi.org/10.5589/m12-049

Wulder, M.A., Hilker, T., White, J.C., Coops, N.C., Masek, J.G., Pflugmacher, D., Crevier, Y. (2015). Virtual constellations for global terrestrial monitoring. Remote Sensing of Environment,170: 62–76. https://doi.org/10.1016/j.rse.2015.09.001

Wulder M.A., White J.C., Loveland T.R., Woodcock C.E., Belward A.S., Cohen W.B., Fosnight E.A., Shaw J., Masek J.G., Roy D.P. (2016). The global Landsat archive: status, consolidation, and direction. Remote Sensing of Environment 185: 271–283. https://doi.org/10.1016/j. rse.2015.11.032

Zhu, Z., Woodcock, C.E. (2012). Object-based cloud and cloud shadow detection in Landsat imagery. Remote Sensing of Environment, 118: 83–94. https://doi.org/10.1016/j.rse.2011.10.028

Zhu, Z., Woodcock, C.E., (2014). Automated cloud, cloud shadow, and snow detection in multitemporal Landsat data: an algorithm designed specifically for monitoring landcover change. Remote Sensing of Environment, 152: 217–234. https://doi.org/10.1016/j.rse.2014.06.012

Zhu, Z., Wang, S., Woodcock, C.E. (2015). Improvement and expansion of the Fmask algorithm: cloud, cloud shadow, and snow detection for Landsats 4–7, 8, and Sentinel 2 images. Remote Sensing of Environment, 159: 269–277. https://doi.org/10.1016/j.rse.2014.12.014